To the Graduate Council:

I am submitting a dissertation written by David Post Allison entitled "Scanning Probe Microscopy: Applications for Genomic Research." I have examined the final electronic copy of this dissertation for form and content and recommend that it be accepted in partial fulfillment of the requirements for the degree of Doctor of Philosophy, with a major in Microbiology.

Jeffrey Becker

Major Professor

We have read this dissertation
and recommend its acceptance:

Pamela Small

David Joy

Steven Wilhelm

Accepted for the Council:

Carolyn Hodges

Vice Provost and Dean of the Graduate School

(Original signatures are on file with official student records)

Scanning Probe Microscopy:
Applications for Genomic Research

A dissertation
Presented for the
Doctor of Philosophy
Degree

The University of Tennessee, Knoxville

David Post Allison
May 2007

Acknowledgements

I would like to thank the members of my committee, Dr. Pamela Small, Dr. David Joy and Dr. Stephen Wilhelm for the help and support they have given me and for taking time out of there busy schedules to help me reach my goal. A very special thank you goes to my major professor Jeffery Becker and also to Stuart Riggsby for considering my unusual circumstances and facilitating my reentry into the graduate program at the University of Tennessee.

My journey in science has sometimes been frustrating, sometimes rewarding, and overall a lot of fun. I have thoroughly enjoyed the excitement of working in a laboratory, making friends all over the world, and finally completing my goal of earning a Ph.D. degree. I have many to thank along the way beginning with Dr. Richard Anderson at Michigan State University where I began my career, in the early 1960's, as a technician working on the enzymology of carbohydrate metabolism in bacteria.

Upon coming to the Biology Division of Oak Ridge National Laboratory I met my mentor in Dr. Lucien Caro, who taught me electron microscopy and opened up a world of biological imaging at the nanoscale that I have been intrigued with to this day. During my years in the biology division I had the pleasure of working with some wonderful scientists and friends that would include Howard Adler, Roy Curtiss III, Sankar Mitra, Salil Niyogi, and both Jane and Dick Setlow. While I was working in the biology division I earned the MS degree in 1971, in the Department of Microbiology, at the University of Tennessee, with Dr. Arthur Brown as my major professor.

After leaving the biology division in 1988, I joined what is now the Biosciences Division at ORNL where I worked with Tom Ferrell, Tom Thundat and Bruce Warmack, developing applications for Scanning Probe Microscopy. Today I still collaborate with people at ORNL especially with Mitchel Doktycz and Tom Thundat and I hope that we will continue to work together for many more years.

Finally, all of this would not have been possible or worth doing without the love and support of my family. Long hours in the laboratory and deadlines for abstracts, papers and proposals very often cut into quality time with the family. Sacrifices made by those I love have made reaching my goal possible so I would like to thank my grown children Susan Norrell, Dr. David Allison, and John Allison for being there for me. Currently, I would like to thank my two teenagers Addie and Martin Allison for their love and support and putting up with a preoccupied father around the house. Finally, last but by no means least I could not have accomplished this goal without the love and support of my wife Marie Rorvik.

Abstract

The inauguration of the International Human Genome Initiative in the later part of the 1980's coincided with the development of scanning probe microscopy (SPM). SPM was a good fit as one of the new technologies that might be implemented to sequence or map DNA and perhaps make a major contribution toward the goal of sequencing the entire human genome. Although the scanning tunneling microscope (STM) was invented in 1982 [Binnig 1982] and the atomic force microscope (AFM) in 1986 [Binnig 1986], it was not until 1987 that the first STM became commercially available; the AFM became available in 1989.

Our group entered this exciting new scientific adventure in genome research towards the end of 1987. An interdisciplinary team was assembled that capitalized on our expertise in the fabrication and use of scanning tunneling microscopes. Additionally, we purchased one of the first commercially available scanning tunneling microscopes. Rounding out the team was expertise in imaging biomolecules such as DNA using electron microscopy.

Our initial research focused on STM imaging and scanning tunneling spectroscopy (STS) of 1) tobacco mosaic virus adsorbed to gold surfaces [Mantovani 1990] and 2) DNA passively mounted on highly ordered pyrolytic graphite (HOPG) surfaces [Allison 1990]. Our spectroscopy results with DNA encouraged speculation that the electronic signatures of nucleotide bases might be used to sequence DNA. However, in this early work we also discovered that simply adsorbing either virus or DNA to gold or HOPG surfaces resulted in substantial amounts of the sample being removed by the STM tunneling tip.

In order to more firmly immobilize negatively charged DNA molecules onto surfaces for STM scanning, we created gold sample surfaces with positive functionality mediated by a self-assembled monolayer of 2-dimethylaminoethane thiol. Using this method, we produced the first reported images of entire genetically functional plasmid DNA molecules obtained by STM [Allison 1992$_a$, Allison 1992$_b$ Allison 1993, Bottomley 1992].

Efforts initiated by our laboratory to restriction map DNA molecules by AFM imaging were successful. This was accomplished by physically mapping the location of a mutant *Eco*RI endonuclease that binds to but does not cleave large DNA clones. Our new AFM technology was pioneered as an alternative to conventional gel-based restriction mapping; it was first demonstrated on plasmid DNA molecules [Allison 1996] and later on larger molecules including cosmid clones [Allison 1997]. This technology should prove to be more effective than conventional mapping methods because by using AFM mapping neither the number nor the proximity of restriction sites to one another is problematic.

Table of Contents

List of Figures

Figure **Page**

Chapter 1
Introduction: scanning probe microscopes and the Human Genome Program

Background and Significance

As I began to put material together and started to think about writing this Ph.D. thesis, many thoughts went through my mind. How it should be organized and presented was determined by starting with an outline and then doing a lot of writing to fill in the blanks. However, the research described in this thesis originated from the coincidence of two major scientific events that made this research possible. One was the invention of the first scanning probe microscope, namely the scanning tunneling microscope (STM) in 1982 [Binnig 1982], and its development and implementation in many laboratories over the next several years. The initial appearance of the STM was the catalyst for the development of other scanning probe microscopes, most notably the atomic force microscope (AFM) in 1986 [Binnig 1986_a]. The other major scientific event was the onset of the Human Genome Initiative in 1987. Funding opportunities for DNA research were offered by the Human Genome Program of the U. S. Department of Energy's Office of Health and Environmental Research. These two events moved me from the Biology Division of Oak Ridge National Laboratory (ORNL) to the Health and Safety Research Division, later Life Sciences Division, and now the Biosciences Division of ORNL to work with Drs. Thomas Ferrell and Robert (Bruce) Warmack.

Tom and Bruce, both physicists, had built a vacuum-based and a tabletop STM and needed a biologist to work with them. Early in 1987 they gave a seminar in the Biology Division of ORNL describing this new microscope. Until that seminar I believe that no one in the Division was aware that such a new research tool even existed. They described how the STM was an instrument without lenses that sensed surfaces by moving a conducting metallic tip over a conducting

surface and detecting changes in tunneling current. They claimed this instrument could be operated in any environment, including liquid. Unlike conventional microscopes that require fixation and staining for obtaining image contrast, this instrument had the potential to image untreated samples. In addition, the microscope had incredible resolution, capable of imaging at the atomic scale.

I was very interested in the talk they gave because I had been working with the electron microscope for many years imaging biological samples, primarily DNA and DNA-protein complexes. My samples required either staining or shadowing with evaporated metal in order to achieve image contrast. After their talk, I approached them with more questions and we discovered that we had mutual interests: they needed someone to help them with biological specimen preparation, which they knew nothing about, and I would need their help if I was to use the microscope they had built. So I started collaborating with Tom and Bruce in late 1987.

When I started working with them, only thirteen papers had been published on imaging biological material with the STM. That year the Nanoscope I (Digital Instruments, Santa Barbara, CA) became the first commercially available STM. Our group purchased a Nanoscope I; it was labeled with serial number "5".

Early images with the STM

Early attempts to image biological molecules with the STM were frustrating for us and for others who were entering the field. All of the instruments were primitive by today's standards. Images were generally recorded on oscilloscopes. With the Nanoscope I, the image was produced after the scan was made — not imaged in real time, as is the case today. For instance, an imaging session devoted to looking for DNA on highly ordered pyrolytic graphite (HOPG) surface consisted of moving the STM tip to an unexplored area of the surface. After engaging the tip and waiting for two or three minutes while the surface was scanned, the image was brought up on the computer. If you were lucky, you would view something other than an image of the HOPG surface. This procedure

was repeated over and over, until you either got an image of DNA, or got tired of trying. Nevertheless, we were able to produce images of what we thought had to be DNA. This was accomplished by placing a drop of relaxed circular pBR 322 plasmid DNA, suspended at a concentration of 2 μg/ml in 0.01 M potassium chloride, on freshly cleaved HOPG and letting it air dry. These images and an image of the HOPG surface showing the atomic structure of the graphite are shown in Fig. 1-1.

Human Genome Program of U. S. Department of Energy

As our new group was getting into biological imaging with the STM, the Human Genome Program of the U. S. Department of Energy (DOE) Office of Health and Environmental Research (OHER) was beginning a major initiative to sequence the human genome. The 3 billion base pairs in the human genome would have to be sequenced, and accomplishing that goal would require a combination of efforts. The approach that DOE would embark on would include efforts on physical mapping, sequencing, and informatics. Physical mapping would be directed toward disassembly of individual chromosomes into clonable sized fragments that could be propagated in yeast or bacteria. These clones would then be mapped and assembled into the minimum tiling group that could be used to reassemble the chromosome. This would allow for a minimum amount of sequencing effort per chromosome. Informatics and data base management would collect and assemble the sequencing information.

It was recognized in the OHER approach that only a few technologies existed to accomplish this goal. Therefore, from the onset, this ambitious new initiative welcomed new approaches that might enhance sequencing, mapping, or informatics efforts.

Our group, very likely due to the images presented in Fig.1-1, became one of the earliest grantees of the DOE human genome initiative. We attended, see the

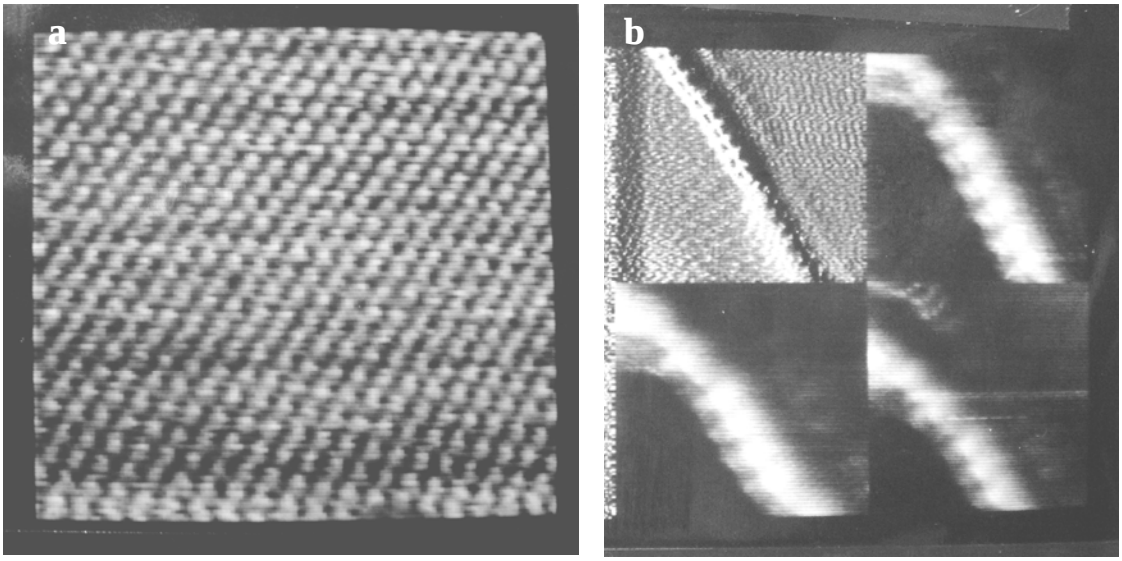

Figure 1-1. First STM images of DNA and an image of HOPG. The ability of the STM to image surfaces at the atomic scale opened up the possibility that this instrument might be developed to sequence DNA. Fig. 1a is an image of the atomic structure of HOPG taken with the Nanoscope I STM with a bias voltage of +50 mV and a tunneling current of 1.0 nA. The scan size is 5 nm. In Fig. 1b several images of structures believed to be pBR 322 DNA adsorbed on graphite are shown. In three of the images a helical structure is present that might be expected in a DNA molecule The scan size for each of the panels is 50 nm and the data was collected at a bias of +50 mV with a tunneling current of 1.0 nA.

program cover Fig. 1.2, of the first workshop for grantees of the Human Genome Program held in Santa Fe, New Mexico, November 4-5, 1989. Fig. 1-3, is the abstract that we wrote for that first meeting. As you can see the abstract was quite vague — two physicists and a biologist were just getting started on a new and exciting adventure in science.

The Scanning Probe Microscope

Twenty five years ago Gerd Binnig and Heinrich Rohrer at the IBM research facility in Zürich, Switzerland, published the first images taken with a scanning probe microscope [Binnig 1982]. Their new microscope, called a scanning tunneling microscope (STM), was able to resolve atomic structure on a conductive crystalline surface by raster-scanning a conductive probe over the sample and recording changes in the tunneling current between the probe and the sample. Although these images were of poor quality by today's standards, they clearly resolved the atomic structure of the silicon (111) surface.

This new high-resolution instrument was greeted with great enthusiasm within the scientific community. Just four years latter, in 1986, Gerd Binnig, Heinrich Rohrer and Ernst Ruska, the inventor of the electron microscope, were awarded the Nobel Prize in physics for their contributions. In 1986 the atomic force microscope (AFM) was invented by Gerd Binnig, Calvin Quate and Christoph Gerber [Binnig 1986$_a$]. Although a number of scanning probe instruments have been described that allow recording a variety of surface properties, the STM and AFM are still by far the most common of these instruments in use today.

Scanning probe microscopes are a family of microscopes

Scanning probe microscopes (SPM) comprise a family of instruments that are designed to measure properties of surfaces. All operate by placing a sensitive element over a surface and recording some property of that surface.

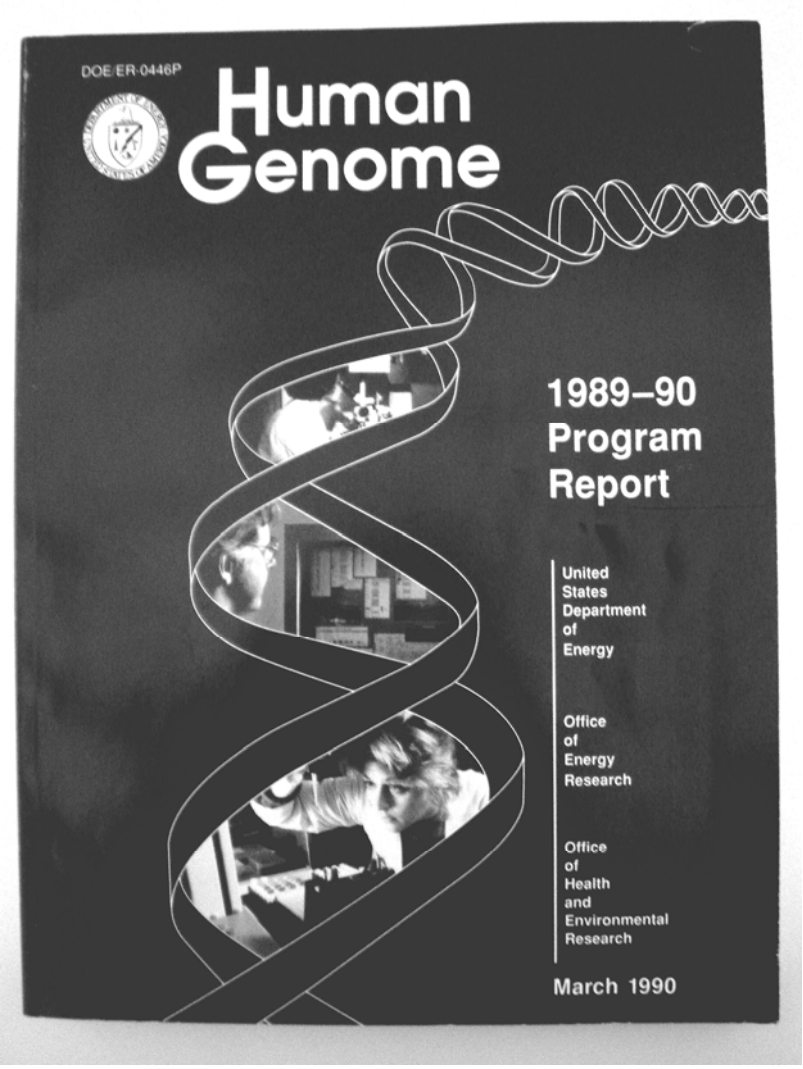

Figure 1-2. Cover of program report first DOE Human Genome Program. The first grantee workshop was held November 4-5, 1989, in Santa Fe, New Mexico. Our group was privileged to be one of the grantees as a potential new technology that would contribute toward sequencing the human genome.

Scanning Tunneling Microscopy

T. L. Ferrell, **R. J. Warmack**, and Dave Allison
Health and Safety Research Division, Oak Ridge National Laboratory,
Oak Ridge, TN 37831
(615) 574-6214, FTS 624-6214

This project includes the operation and continued development of scanning tunneling microscopes for basic physics research related to health and environmental problems. The primary focus of this research is the use of scanning tunneling microscopes in sequencing the human genome. A scanning tunneling microscope with single-atom resolution is used to image atomic structure on surfaces, to alter atomic positions, and to probe the dynamical phenomena caused by collective electron motion and motion of ions. Development includes extending capabilities to a wider range of materials, to identification of atomic species, and to studies of biological samples. Methodologies are developed for atom-by-atom studies of biological molecules important in understanding the human genome and in providing other applications in surface science.

Figure 1-3. Our abstract presented at the first DOE Human Genome Program. Our group had just begun working on applications for either sequencing or mapping the human genome. At this point in time it was not unreasonable to speculate that given the resolution of the STM, methodology could be implemented to sequence DNA directly using this instrument.

This is accomplished by either raster-scanning the surface-sensitive probe over the surface, or by scanning the surface beneath a fixed surface-sensitive probe Fig. 1-4. The scanning mechanism is usually a cylindrical piezo-ceramic configured to raster-scan in the X Y domains while recording information in the Z or height domain.

Instruments that qualify as scanning probe microscopes would include the scanning tunneling microscope (STM), atomic force microscope (AFM), scanning capacitance microscope (SCM)[Williams 1989], magnetic force microscope (MFM) [Martin 1987], scanning ion conductance microscope (SICM) [Hansma 1989], scanning electrochemical microscope(SECM) [Bard 1991], and the scanning near-field optical microscope (SNOM)[Pohl 1988]. All of these instruments are capable of resolution from the nanometer to the micron range. The STM and AFM are capable of atomic resolution on crystalline surfaces.

STM and AFM general characteristics

This thesis will primarily be concerned with work accomplished using both the STM and AFM. It is important to understand how the STM paved the way for probe microscope applications designed to solve specific biological problems. Both the STM and AFM operate in a similar fashion to obtain a topographical profile of the sample. They differ from optical or electron microscopes by not requiring waves or lenses to generate an image. This advantage was quickly recognized by biologists for it would not be necessary to use conventional fixatives, stains, or other contrasting material in order to obtain an image. With probe microscopes, biological molecules and surfaces of cells could be imaged free of chemical additives.

Fig. 1-5 illustrates the essential elements of both the STM and AFM. The STM is illustrated in the so called “device scanning” configuration that is often referred to as top down scanning: the piezoelectric scanning mechanism is mounted in a scanning head and the sample is simply placed beneath the scanner and imaged.

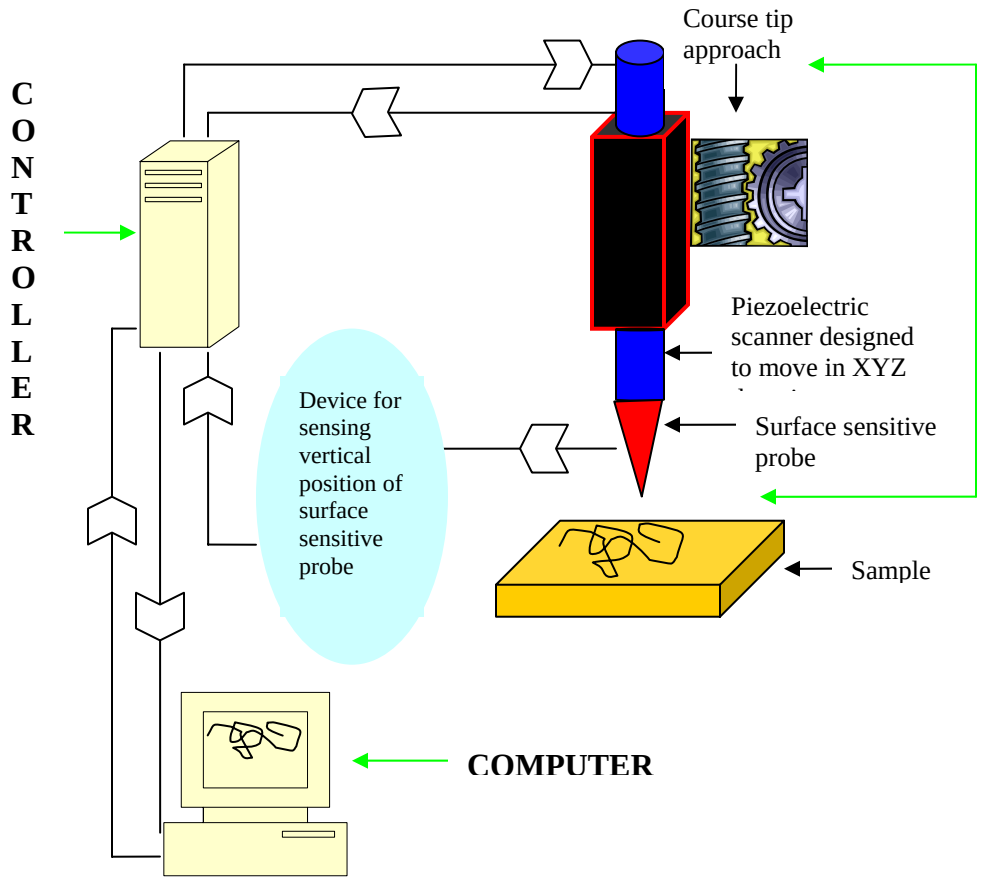

Figure 1-4. The scanning probe microscope. The SPM consists of three major components: the microscope, a controller and a computer. The microscope is composed of a piezoelectric scanner that raster-scans a surface and gathers information in the vertical domain. The device for sensing the vertical position of the surface sensitive probe is usually built into the microscope. The computer runs the SPM via the system software and records images. The controller is the interface between the computer and the microscope. It supplies voltages for scanning surfaces and processing signals between the microscope and the computer. Course approach is handled by stepper motors that mechanically advance the probe to the surface. Once proximity to the surface is reached, the electronics take over and maintain distance between the probe and sample.

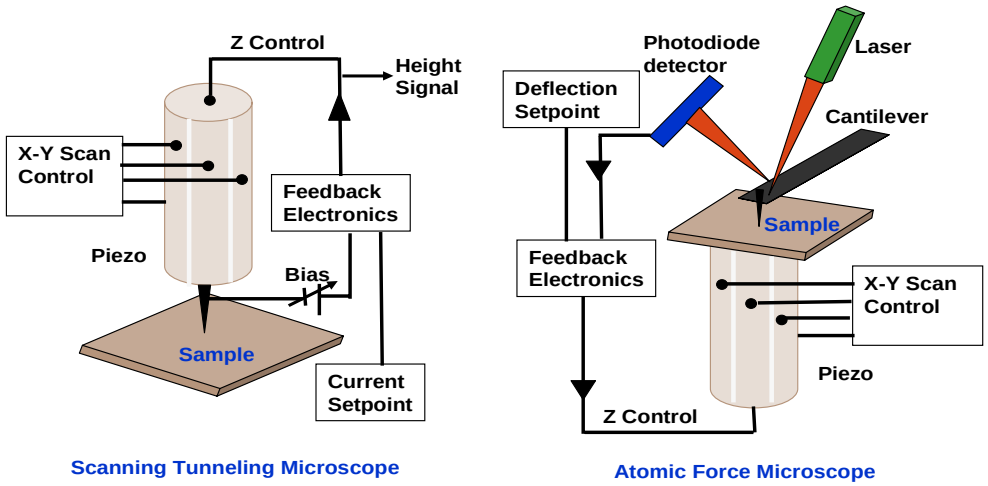

Figure 1-5. The scanning tunneling and atomic force microscopes. The STM and AFM differ primarily in the manner in which they sense proximity to the surface. The STM senses changes in surface topography electronically by monitoring a tunneling current as the surface is scanned. The AFM senses the surface by contacting or near contacting a surface with a sharp tip on the end of a microcantilever. Both instruments use the same control electronics so that only the scanning mechanism is different. This allows for the instrument to be operated as either an STM or AFM.

The AFM is illustrated in the “sample scanning” configuration: the cantilever is fixed and the sample is placed on the piezo and scanned beneath the cantilever. It is important to note that the AFM can also be configured to the top down scanning operation by incorporating the piezo, laser, and photodiode detector into a scanning module. In this configuration the cantilever is then placed on the end of the piezoelectric scanner.

Device scanning is the configuration that is best adapted to biological imaging because it offers more options for the variety of sample shapes and sizes that can be placed beneath the scanner. For example, cultured cells in petri dishes can easily be scanned using device scanning simply because there is room and the sample is easily immobilized. However, if a Petri dish of cultured cells is placed on the piezo and scanned beneath a fixed cantilever there is not only problems with room but also with the weight and bulk of the sample on the fragile piezo element. This configuration would also cause serious problems if the sample leaked allowing liquid to interact with the high voltage applied to the scanning piezo.

The scanning mechanism for the STM and AFM are the same. A cylindrical piezoelectric ceramic configured to move in three directions (X,Y,Z) is implemented to raster scan the surface taking a series of voltage points for each scan line in the X direction and scanning an equal number scan lines in the Y direction. This is user-defined and is generally influenced by the level of resolution one wishes to obtain. Higher resolution is obtained by scans where more voltage points are taken. For example, by taking 128 voltage points per scan line in the X direction with 128 scan lines in the Y direction, the result would be a two dimensional map of the surface composed of 128 X 128 points having both X and Y voltage coordinates. Options for multiples of 128 points of 256, 512, 1024, can be selected such that a 512 X 512 voltage point image will offer a higher resolution than a 128 X 128 image but will take longer to scan.

What has been described so far creates a flat two dimensional image of a surface when entered into the computer. What is needed to create a meaningful

computer generated image of the surface is Z (height) voltage input for each of the X, Y positions.

The scanning tunneling microscope

The STM is an instrument that obtains height information derived from the electronic tunneling current. This is the current generated between a sharp conductive tip and a conductive sample when a difference in potential is applied between the tip and the surface. Tips are usually made from 2 millimeter (mm) diameter tungsten or platinum/iridium wire by simply cutting the wire at an angle. The tip is then placed into a holder at the end of the piezoelectric scanner and mechanically brought into near contact with the sample surface by the action of stepper motors. As the tip is brought within a nanometer (nm) of the surface the wave functions of electrons on the tip interact with the electron wave functions of the sample. By applying a difference in potential between the tip and sample, tunneling current can be measured.

The tunneling current is especially sensitive to changes in the gap between the tip and sample with changes of 0.1 nm being reflected by changes of an order of magnitude in the tunneling current. This strong gap-dependent current effectively concentrates the current to a very small region of the tip that is only 0.1-0.5 nm wide. In practical terms, on crystalline surfaces the tip will have an atomically sharp appendage that will first interact electronically with the surface allowing for atomic resolution of the surface. On surfaces that are not atomically flat, nanometer deviations in flatness will cause switching of the tunneling current to other areas of the tip. This tip switching causes the profile of the tip to influence resolution to the extent that atomic resolution is no longer possible and resolution is limited to the nanoscale.

Creating an image in what is called constant current mode is accomplished by applying a bias voltage between the tip and sample and maintaining a constant tunneling current as the tip is raster-scanned over the surface. The constant tunneling current is maintained by a feedback loop that responds to changes in

surface topography. A change in surface height in the positive direction will close the gap between the tip and surface and the tunneling current will increase. The feedback circuit responds by applying a voltage to the Z piezo that raises the tip in order to maintain a constant tunneling current. This voltage is the Z or height input at that particular XY coordinate. Conversely, if the tip encounters a trough in the surface, the tunneling current drops off and the feedback loop compensates by applying a voltage to lower the tip. Therefore, voltages applied to the Z piezo to raise or lower the tip to maintain a constant tunneling current, that thereby keep the tip at a constant height above the surface, are the height input for each of the XY voltage points used to create a computer image. This is the usual mode of operating the STM.

Alternatively, on very flat surfaces, usually atomically flat surfaces, the tip can be scanned over the surface at a constant height and fluctuations in tunneling current, caused by height or charge differences at the atomic scale, are converted to voltages that serve as the height input. This is referred as constant height imaging.

The key issue with the STM is that it requires electrical conductivity between the tip and surface in order to create an image. Therefore, it is severely limited for non-conducting biological applications.

The atomic force microscope

Following its development and commercialization in 1989, the AFM has proven to be the most successful and popular offspring of the STM. Instead of sensing surfaces electronically, the AFM mechanically interacts with the surface. This interaction defines the most important feature of AFM in that the instrument is capable of interacting with and creating an image of any surface, including insulating surfaces, making the instrument especially attractive for biological applications. As has already been pointed out, the scanning mechanism of the AFM is identical to the STM with the only difference being how each instrument senses the surface.

Contact mode AFM

Imaging with the AFM is accomplished by bringing a sharpened tip on the end of a microcantilever into contact with the sample surface and allowing the tip to interact with the surface. The tip is either raster-scanned over the surface or the surface is scanned beneath a fixed cantilever. Commercial cantilevers are silicon or silicon nitride structures with a tip at one end that typically has a radius of curvature of 10 nm. This results in a broadening of the image so that 2 nm wide DNA molecule imaged with a tip having a radius of curvature of 10 nm will be imaged with a diameter of 10 nm or perhaps somewhat greater. Although the AFM is capable of atomic resolution on atomically flat surfaces, the radius of curvature of the tip limits resolution to the nanoscale on other than atomically flat surfaces.

The cantilever can be rectangular shaped or triangular as shown in Fig. 1-6. Typically the cantilevers are from 10-200 microns (μ) in length with spring constants of 0.01-3.0 Newtons/meter (N/m). The method of choice for monitoring the position of the cantilever relative to the surface is to reflect a laser beam off the back side of the cantilever into a split photodiode detector having an upper and lower quadrant. As the cantilever tip is brought into contact or near-contact with the surface, the cantilever will deflect causing the spot where the laser beam contacts the photodiode to change. This results in a change in the voltage output of the photodiode. The feedback loop senses this change and responds by raising or lowering the tip to bring the output of the photodiode back to the setpoint voltage. The voltage that is applied to the Z piezo to raise or lower the tip serves at the voltage input for the individual XY voltages. By applying a voltage to raster-scan the surface, as we have already described, Z or height information is collected for each of the XY points. This information is then used to create a topographic image of the surface. If the AFM is operated in contact mode, the cantilever is actually in physical contact with the surface.

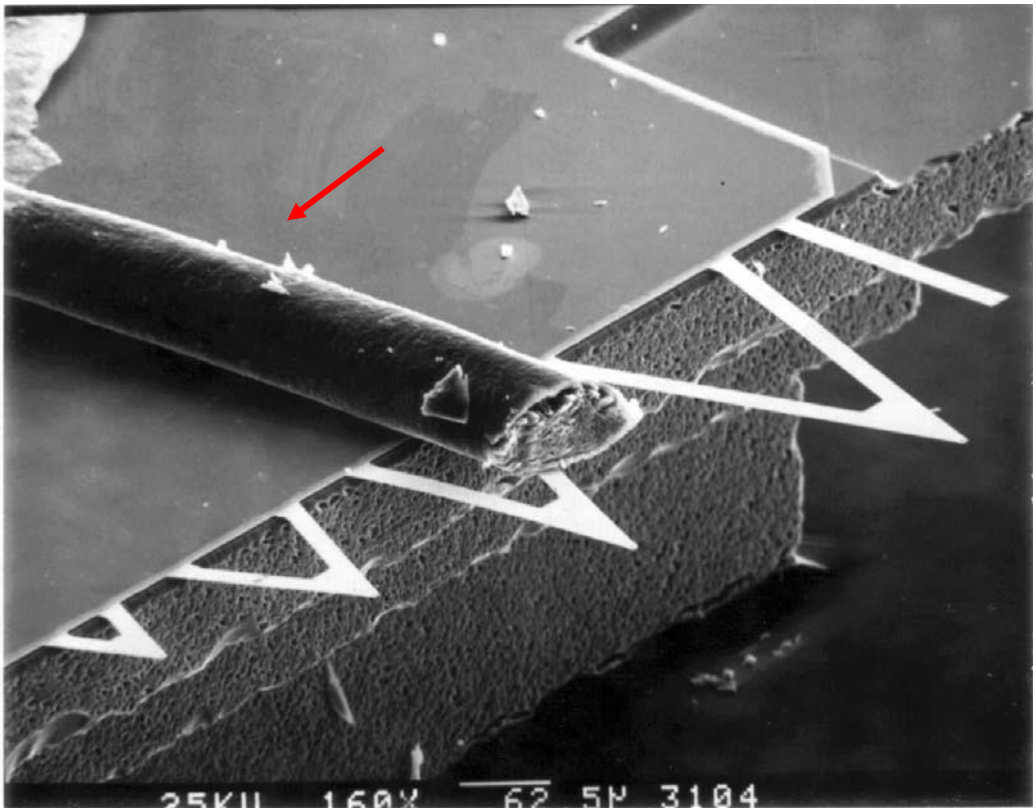

Figure 1-6. AFM cantilever chip with 5 cantilevers. Sensing the surface with the AFM requires a light touch in order to avoid destroying the sample. This silicon nitride chip supports 5 cantilevers with spring constants ranging from 0.01 to 0.5 N/m. A sharpened tip on the underside and at the very end of the cantilever either contacts or comes in near contact with the surface. Monitoring the position of this tip relative to changes in surface topography is used to create an image. There is a human hair (arrow) sitting on the top of the chip to give one an idea of the size of these cantilevers (imaged by scanning electron microscopy).

Intermittent contact AFM

The AFM can also be operated in an intermittent contact mode where contact of the tip with the surface is not constant. Operating in this mode requires that the cantilever be oscillated at its resonant frequency. This is usually accomplished by an acoustic transducer attached to the cantilever mounting that essentially shakes the cantilever into oscillation with oscillation amplitude of approximately 100 nm. Imaging is accomplished by identifying dampening of the cantilever oscillation, caused by surface forces such as van der Waals and electrostatic forces, as the tip nears the surface. Dampening of oscillation detected by the feedback system is a signal to apply voltage to the Z piezo to move the cantilever away from the surface in order for the cantilever to return to free oscillation. The point where the cantilever oscillation was dampened is considered the Z voltage input at that particular XY coordinate. This process is repeated for all of the voltage points taken in a raster-scan of the surface and generating a computer image using the XYZ information is accomplished as previously described. This mode of operation results in smaller forces being applied to the sample during imaging, but resolution is not quite as good as with contact mode. This is most commonly called "tapping mode" when the cantilever is oscillated acoustically by shaking the cantilever housing [Hansma 1994]. Alternatively, by coating the back side of the cantilever with a magnetic material and applying an alternating magnetic field the cantilever can be induced to oscillate at its resonant frequency. This results in better control of oscillation with the amplitude of oscillation of the free cantilever being about 5 nm. This is true non-contact imaging with the long range van der Waals attractive forces between the tip and sample producing the dampening effect on the cantilever [Lanz 1994, Han 1996].

Development of STM and AFM applications

In this thesis I will report on our early work to image tobacco mosaic virus (TMV) and DNA. This work was accomplished on the Nanoscope I and is reported in Chapter 2. Approximately two years after the STM became

commercially available as the Nanoscope I, the Nanoscope II became commercially available combining both STM an AFM imaging capabilities. In chapter 3 and 4 imaging was accomplished using the Nanoscope II. In chapter 3, I report on methodology our group developed to immobilize and image for the first time entire genetically functional plasmid DNA molecules with the STM. In Chapter 4, I report on our group's pioneering efforts to demonstrate restriction mapping of plasmids and the development of AFM mapping technology to map cosmid-sized DNA clones. In chapter 5, I discuss the accomplishments reported in this thesis and the evolution of scanning probe microscope technology that have allowed these instruments to attain a prominent role in research today.

Chapter 2
Imaging biological samples with the scanning tunneling microscope

Background and Significance

Beginning with the first atomic resolution images of silicon [Binnig 1982] the scanning tunneling microscope (STM) ushered in an exciting new era for surface imaging. Images of metals and semiconductors have contributed to material science, condensed matter physics, and surface physics in general [Binnig 1986$_b$, Hansma 1987]. The demonstrated resolving power of the STM and the ability to use this new research tool in air or liquid [Sonnenfeld 1986] made this an attractive instrument for biological imaging. Potentially, biological samples could be viewed in their native environment without any image contrasting measures that would alter the native ultrastructure. The poor conductivity of biological material would likely present major problems. If the full potential of nanometer-scale and perhaps even atomic scale resolution were to be realized, however, samples would have to be examined in their native state.

Preliminary reports confirmed that native biological molecules, untreated with any agents to increase their conductivity, could be imaged by STM. Native bacteriophage *ø 29* [Baro 1985], phosphorylase-kinase [Edstrom 1989,1990], and untreated polypeptide structures [McMaster 1990$_a$] have been imaged by STM. It was the report by Baro *et al.* that encouraged us to pursue techniques for imaging native biological samples. In addition to our primary goal of imaging DNA, we chose to look at tobacco mosaic virus (TMV), a stable well characterized entity, and our initial sample for the STM.

TMV is a rod shaped virus 18 nm in diameter. It has a monomeric length of 300 nm, but can attain much greater lengths through end-to-end dimerization. The protein subunits in the TMV protein coat are arranged in a helix with a pitch spacing of 2.3 nm, thereby providing an optimal sample with distinct nanoscale features [Klug 1960]. The characteristic size and shape of the virus could be

easily identified by STM, while the pitch and spacing of the protein subunits would allow a good test of instrument resolution.

As our research group and others began to use the STM as an imaging tool, there were not a lot of background papers to reference. The result was that everyone was pretty much left up to their own devices to try to understand how samples might be prepared and how images should be interpreted. The driving force for STM imaging resided in the fact that this was an instrument capable of atomic resolution of native biomolecules. This led to speculation that STM could be used to sequence DNA. Could a way be found to place lengths of single strand DNA on an atomically flat surface and then scan the polymer length at atomic resolution to identify the individual bases? This speculation was fed by reports where liquid crystals had been imaged [McMaster 1990$_b$], and a report where thymine and adenine were placed on an HOPG surface and the single ring structure of thymine could be differentiated from the double ring structure of adenine [Allen 1991]. Furthermore, the instrument could scan samples at such a rapid rate that sequencing by STM would make conventional sequencing efforts obsolete. This is the arena that we found ourselves in as we began our efforts to become players in the exciting new technology of STM imaging.

Materials and Methods

TMV and DNA

TMV was isolated from tobacco plants 10-14 days after infection using standard procedures [Gooding 1967], purified by sucrose density centrifugation [Reddick 1989], pelleted and suspended in 0.03 M phosphate buffer pH 7.0 at a concentration of 1 mg/ml. TMV was provided by Dr. Brad Reddick, Dept. of Entomology and Plant Biology, University of Tennessee. The plasmid DNA used in the study was PZ 189 obtained from Dr. Frank Larimer, Biology Division, Oak Ridge National Laboratory, Oak Ridge Tennessee. The plasmid was subjected to

70,000 rads of X-ray in order to single-strand nick the DNA molecules and thereby produce relaxed circular DNA molecules.

Coating Pd/Au surfaces with tobacco mosaic virus

Microdroplets of virus diluted 1/20 in dd-H_2O were sprayed onto mica surfaces, which were either sputter-coated with platinum/gold (Pd/Au) or coated with Pd/Au by thermal evaporation. Spraying was done with a glass nebulizer held 5 cm from the Pd/Au surface. The Pd/Au surfaces were heated to 55 ^oC prior to spraying 5 squirts of the TMV from the nebulizer onto the heated surface. Sputter-coated surfaces were made by depositing Pd/Au in an argon atmosphere onto freshly cleaved mica placed in the Hummer VI sputter-coating system (Anatech Ltd, Alexandria, VA). Thermal evaporated gold was prepared by evaporating, at 2.3-2.6 x 10^{-6} Torr, 15 mm of 0.2 mm diameter Pd/Au wire wound around a tungsten filament placed 14 cm directly above the mica surface. Both a Ladd evaporator (Ladd Research Industries, Burlington, VT) and an evaporator constructed in our laboratory were used for the thermal evaporation. Both the evaporated and sputter-coated surfaces were required to be over 12 nm in thickness in order to maintain sufficient conductivity for STM imaging.

DNA sample preparation

A 20 μl droplet of PZ 189 circular plasmid DNA was diluted to 40 μg/ml in 0.01 M Tris + 0.001 M EDTA at pH 7.5 (TE) was deposited onto a freshly cleaved HOPG surface. Electro-deposition was accomplished by contacting the DNA droplet with a platinum electrode that was DC biased 2-4 volts with respect to the graphite surface. This contact was maintained for 1-2 minutes. The unbound DNA was removed by touching the droplet to 200 μl of TE followed by two rinses by touching the surface to dd-H_2O. Excess liquid was removed by wicking with filter paper. After drying, the sample was imaged in the STM.

Scanning Tunneling Microscopy

STM images were taken in air using a commercial STM Nanoscope I (Digital Instruments, Santa Barbara, CA) interfaced with a computer to digitally control the raster-scanning and to process the image data. The instrument feedback circuit controlled tip height to keep a constant tunneling current. The raster, XY scan was calibrated to better than 10 % using images taken on the instrument of the atomic structure of graphite. Data were generally taken with a tunneling current of 0.25-1.0 nanoAmperes (nA), with a tip direct current (dc) bias of $^{+}$30-50 milliVolt (mV). The polarity of the bias voltage did not seem to affect any of the results. The tip height signal from the Z piezo was integrated into the XY raster scan voltage points and processed as a topographic image. In some experiments spectroscopic images were simultaneously obtained with topographic images. This was accomplished by injecting a small high frequency alternating current (ac) bias (7 mV rms at 100 kilo Hertz [kH]) onto the dc bias. The resulting ac tunneling current signal was recorded with a single-channel lock-in amplifier. The high frequency was necessary to avoid interference with the STM feedback circuit in order to avoid interference with the normal constant-current image acquisition. The spectroscopic images were recorded at -90 degrees with respect to the phase of the signal maximum. The resulting output signal roughly corresponds to the negative of the local differential conductivity, i.e. $-dI/dV$. Thus in the spectroscopic image the high points are shaded white and represent points of low conductivity.

Results: STM of TMV on Pd/Au surfaces

Evaluation of Pd/Au surfaces on mica

One of the problems associated with imaging biological molecules on HOPG or gold surfaces concerns the forces exerted on the molecules by the tip. Surfaces with atomic flatness are ideal and necessary for imaging biological molecules, such as DNA or proteins, but generally lack sites that might anchor molecules to

the surface. For imaging TMV we used either sputter-coated or evaporated gold surfaces composed of Pd/Au nodules with apparent diameters of 10-15 nm and a surface roughness of 1-2.5 nm Fig. 2-1. Since TMV is much larger than DNA or proteins, the problem of STM tip forces sweeping molecules off the surface might be reduced because the Pd/Au is rougher than an atomically flat surface. Prior to mounting a TMV sample, the Pd/Au surface was routinely imaged in order to evaluate the quality of the surface. Deviations from the image in Fig. 2-1 in either the height or the diameter of the Pd/Au nodules would be viewed as an unsatisfactory mounting surface, while image noise or poor quality of the image would indicate problems with the tunneling tip.

STM images of TMV sprayed on Pd/Au films

STM images of TMV sprayed onto evaporated Pd/Au substrates showed the TMV to be above the background substrate Fig.2-2$_a$, while images of TMV sprayed onto sputter-coated mica surfaces Fig.2-3$_a$, showed the virus to be below the substrate surface. Cross-sectional line scans through TMV on both the evaporated and sputter-coated images showed the virus in Fig. 2-2$_b$, and in Fig.2-3$_b$, to have viral widths between 70-100 nm. This is considerably larger than the known 18 nm width of TMV. In the vertical domain the line scans showed that the tip moves up and over the virus mounted on the evaporated Pd/Au surface in Fig. 2-2$_b$, while on the sputter-coated surface in Fig.2-3$_b$, the tip clearly moves 13-20 nanometers down relative to the surface as the tip passes over the virus. When TMV was sprayed directly onto a freshly cleaved mica surface and covered with sputter-coated Pd/Au, the STM image and line data results were essentially the same as TMV mounted on evaporated Pd/Au substrates. Similarly, when TMV mounted on sputter-coated Pd/Au were overcoated with evaporated platinum/carbon (Pt/C), both the viral images in Fig. 2-4$_a$, and the cross-sectional line scan data in Fig. 2-4$_b$, showed viral widths of 70-100 nm. The virus was imaged as being above the mounting surface, in agreement with what was found on the evaporated substrates.

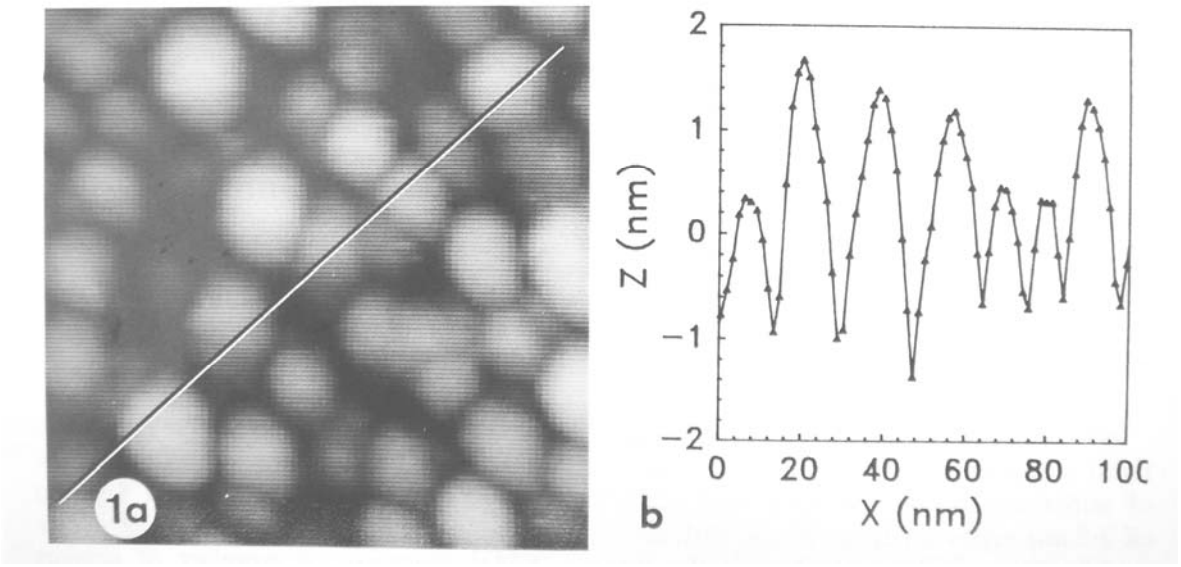

Figure 2-1. STM image of sputter coated Pd/Au mica surface. The image presented is an STM image of a 20 nm thick Pd/Au sputter-coated substrate deposited on a freshly cleaved mica surface. The STM image (a) showed the substrate composed of a confluent bed of Pd/Au nodules. From the line scan data (b) the nodules were seen to have diameters of 10-15 nm, with vertical heights of 1-2.5 nm.

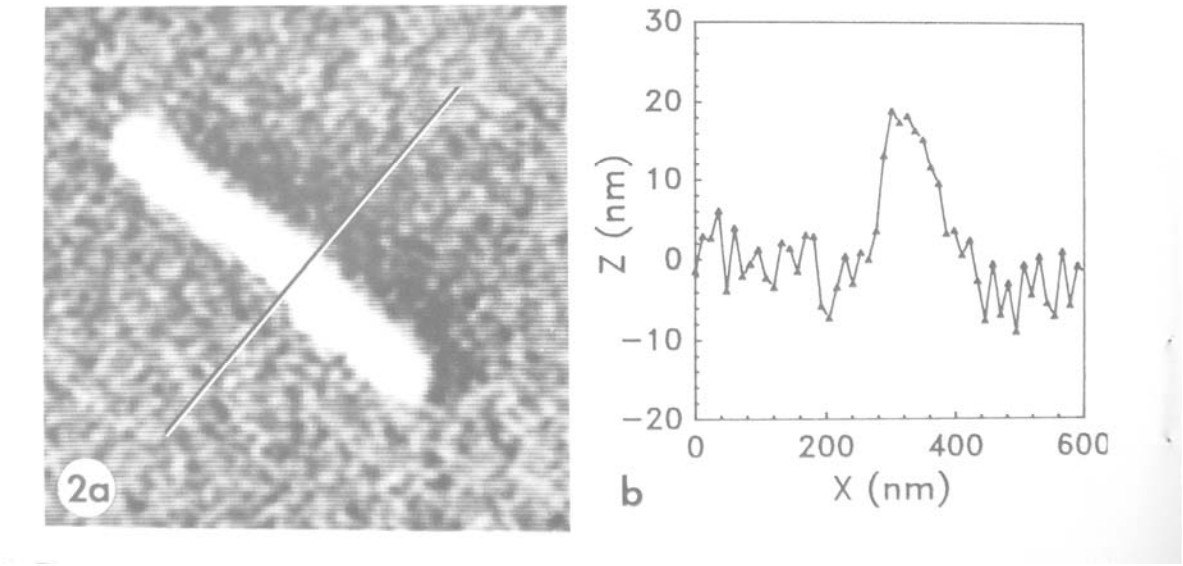

Figure 2-2. An STM image of tobacco mosaic virus on an evaporated Pd/Au substrate. An STM image (a) of cylindrical TMV prepared by spraying microdroplets of virus onto a Pd/Au substrate thermally evaporated onto a freshly cleaved mica surface. From the line scan data (b) the virus was seen to have a diameter of 100 nm and a height above the surface of 20 nm. The monomer length of TMV is 300 nm, although multiples of the unit length are common through end-to-end association. The virus imaged was a dimer.

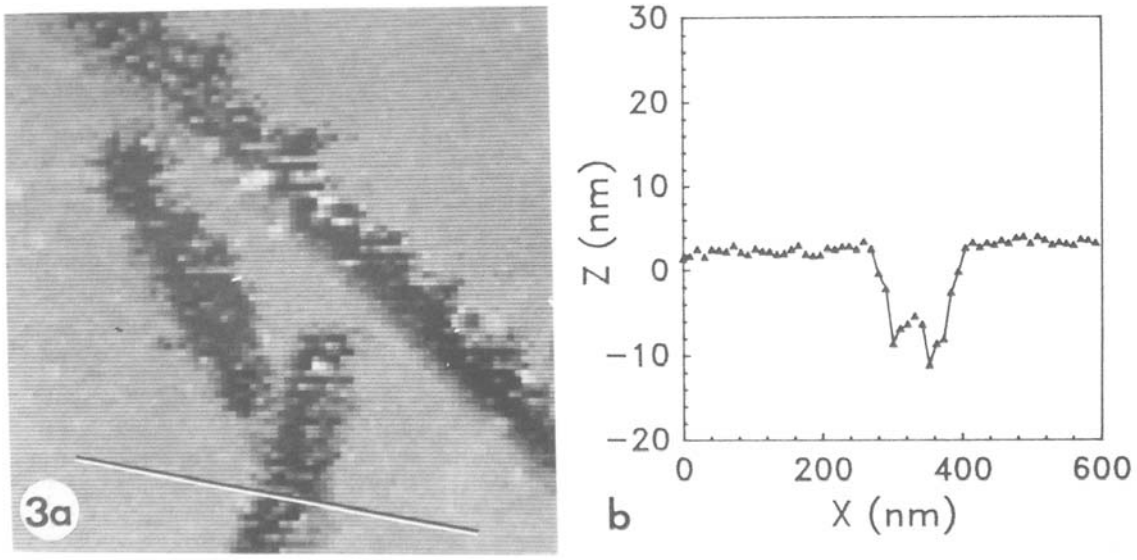

Figure 2-3. An STM image of tobacco mosaic virus on a sputter-coated Pd/Au substrate. The STM image (a) showed several TMV viruses of different lengths immobilized on a 20 nm sputter-coated Pd/Au substrate supported on a freshly cleaved mica surface. The sample was prepared by using a glass nebulizer to spray microdroplets of the virus onto the Pd/Au surface. The line scan data (b) through the virus showed a diameter of 100 nm with the vertical dimension of the virus appearing to be 13 nm below the Pd/Au substrate.

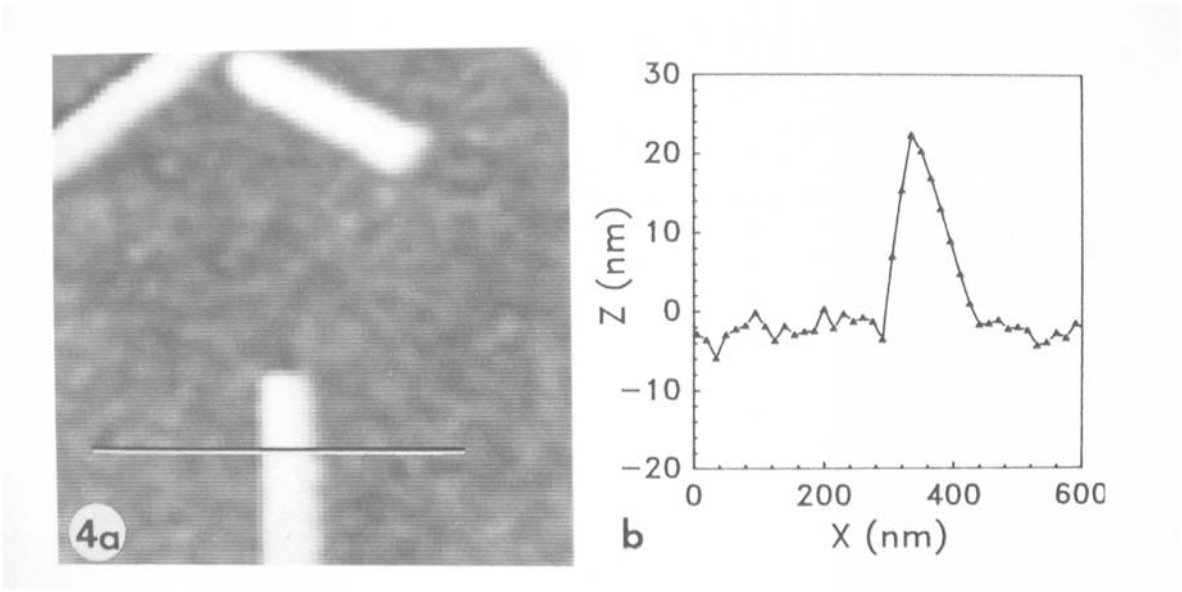

Figure 2-4. An STM image of tobacco mosaic virus on a sputter-coated Pd/Au substrate with a Pt/C overcoat. Sample preparation for the STM image of TMV (a) involved spraying microdroplets of the virus onto 20 nm Pd/Au sputter-coated substrates supported on freshly cleaved mica surfaces. After the virus was immobilized on the Pd/Au substrate, it was lightly overcoated with Pt/C. This image was quite similar to the STM image of virus shown in Fig.2-2$_{a,}$ where the virus was immobilized on a thermal evaporated Pd/Au surface. Line scan data showed the virus to be 100 nm in diameter with a positive vertical dimension of 22 nm.

High-resolution image of TMV

The image in Fig. 2-5 was taken from a storage oscilloscope while operating the STM in the analog mode. Although the TMV was sprayed onto an evaporated Pd/Au surface, unlike other virus sprayed onto such a surface this image was positive, with a diameter of 16-17 nm which is comparable to the known diameter of TMV. As can be seen in this figure, there was a substructure that correlated well with the 2.3 nm protein subunit structure reported from x-ray diffraction experiments [Klug 1960]. A number of images similar to this were observed in this experiment but could not be duplicated in subsequent experiments.

Results: STM of DNA on graphite surface

STM of DNA on graphite surfaces

In all experiments where imaging was used to identify DNA on highly ordered pyrolytic graphite (HOPG) surfaces, a Nanoscope I scanning tunneling microscope was used. This is an interesting point to note because the Nanoscope I STM did not yet have the option for AFM.

In Fig. 2-6, topographic STM images of HOPG showed different features found on graphite surfaces. These structures were recorded on graphite that was tape stripped only without further treatment, and on graphite treated with TE buffer with and without DNA that had been exposed to the electro-deposition immobilization procedure. In Fig. 2-6a, a structure on the surface treated with DNA in TE showed a structure with a nodal period of 2.3 nm, with the widths of each of the apparent strands being 2.0 nm. This agreed with the known width of B-form DNA. However, the helical period of B-form DNA is 3.4 nm not 2.3 nm. Similar structures were seen where the periodicities varied between 2.0 and 4.7 nm and with widths from 2.0 to 4.0 nm. These strands were most often observed in lateral associations and rarely in unassociated single strands.

Contrary to what might be expected from the amount of DNA applied to the surface, DNA coverage was much less dense than expected. Features that

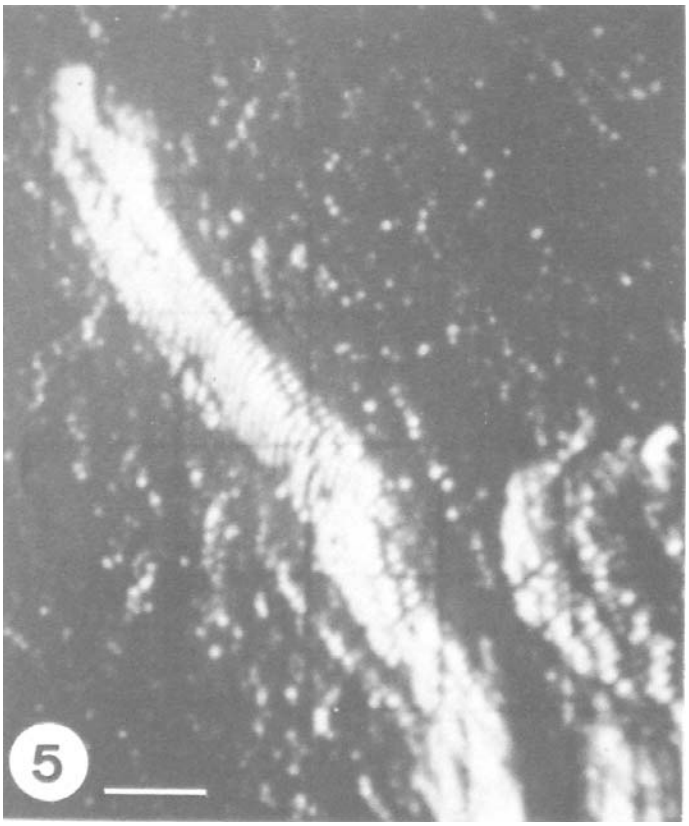

Figure 2-5. Analog STM image of TMV taken from an oscilloscope. The analog STM image of a single TMV was taken from a storage oscilloscope. The virus was mounted onto the Pd/Au substrate supported on a freshly cleaved mica surface by spraying the virus on the surface. Favorable tip geometry, indicated by the measured diameter, allowed imaging the virus with a width of 16-17 nm, in good agreement with the known viral width of 18 nm. Due to unusual conductivity, that we fail to understand, a diagonal array of subunits were imaged with an axial separation of 2.4 nm that is in good agreement with the known subunit ultrastructure [Klug 1960]. Although several images were taken in this experiment showing positive images of TMV with well defined ultrastructure we were not able to repeat these results in subsequent experiments. The scale bar is equal to 20 nm.

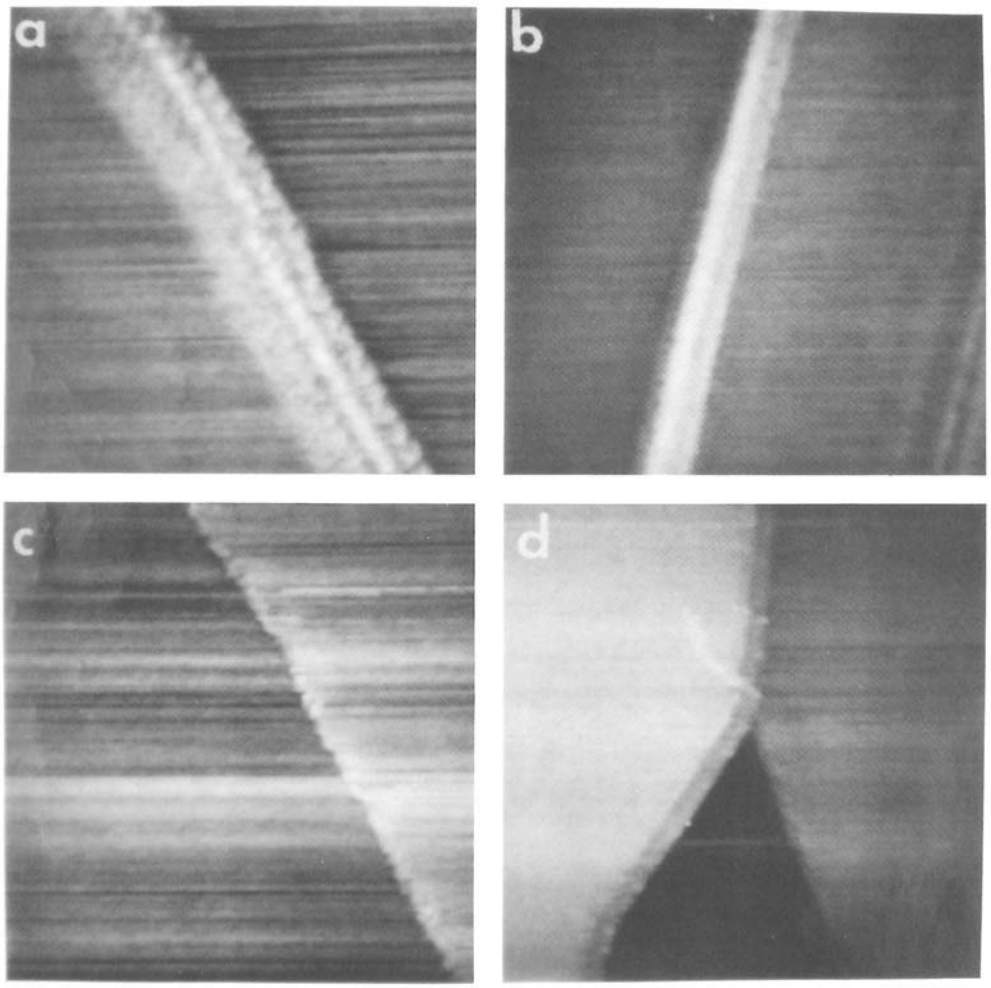

Figure 2-6. STM images of features on HOPG surfaces. Gray scale STM images of features on graphite shaded from black (lowest) to white (highest): (a) DNA in TE buffer, electro-eluted to the surface with a height range of 2.9 nm and a field width of 50 nm. (b) Feature found on untreated graphite with a height range of 6.4 nm and a field width of 100 nm. (c) Monoatomic planar step on untreated HOPG with a height range of 2.2 nm and a field width of 100 nm. (d) Single and multiple step edges on HOPG treated with TE buffer with height range of 2.1 nm and field width of 200 nm.

appeared to be ridges or trenches were also seen on untreated HOPG that had only been tape stripped without further treatment. In Fig. 2-6b, an example of a ridged structure that was double-stranded but without periodicity was seen. This structure was 2.0 nm in height and each of the strands was 4.0 nm in width.

Other structures that appear to be single or multiple steps in the crystal structure were often imaged. In Fig. 2-6c, a single atomic step was seen in the untreated graphite. In Fig. 2-6d, multiple steps associated with three distinct crystal planes could be seen in this sample of HOPG that was treated with buffer and electro-deposition.

Collectively, these images represent the unusual structures that were found on graphite during imaging sessions. These images were relatively rare in that the usual image of graphite taken during these experiments showed only the atomically flat surface.

Spectroscopic Images

The spectroscopic images ($-dI/dV$) that corresponded to and were taken simultaneously with the topographic images are shown in Fig. 2-7. The high points in the images shown in white corresponded to points where the differential conductivity was low. This meant that a strong $-dI/dV$ signal over a DNA molecule in Fig. 2-7a identified a profound difference in conductivity between the DNA and the HOPG surface. Although the nodal periodicity in the DNA molecules were seen in this image, the point-to-point resolution was not as good as that seen in the corresponding topographic image of Fig. 2-6a, and the 2.3 nm periodicity was not resolved.

The spectroscopic image of the anomalous double-strand structure in Fig. 2-7b and the step edge in Fig. 2-7c of graphite that was only tape stripped, and the image of multiple step edges in Fig. 2-7d of graphite treated with TE and electro-deposition both show significantly less $-dI/dV$ response than the DNA image shown in Fig. 2-7a. In Fig. 2-8, the spectroscopic signal from a line arbitrarily drawn through each of the images in Fig. 2-7 was plotted using the same scale for

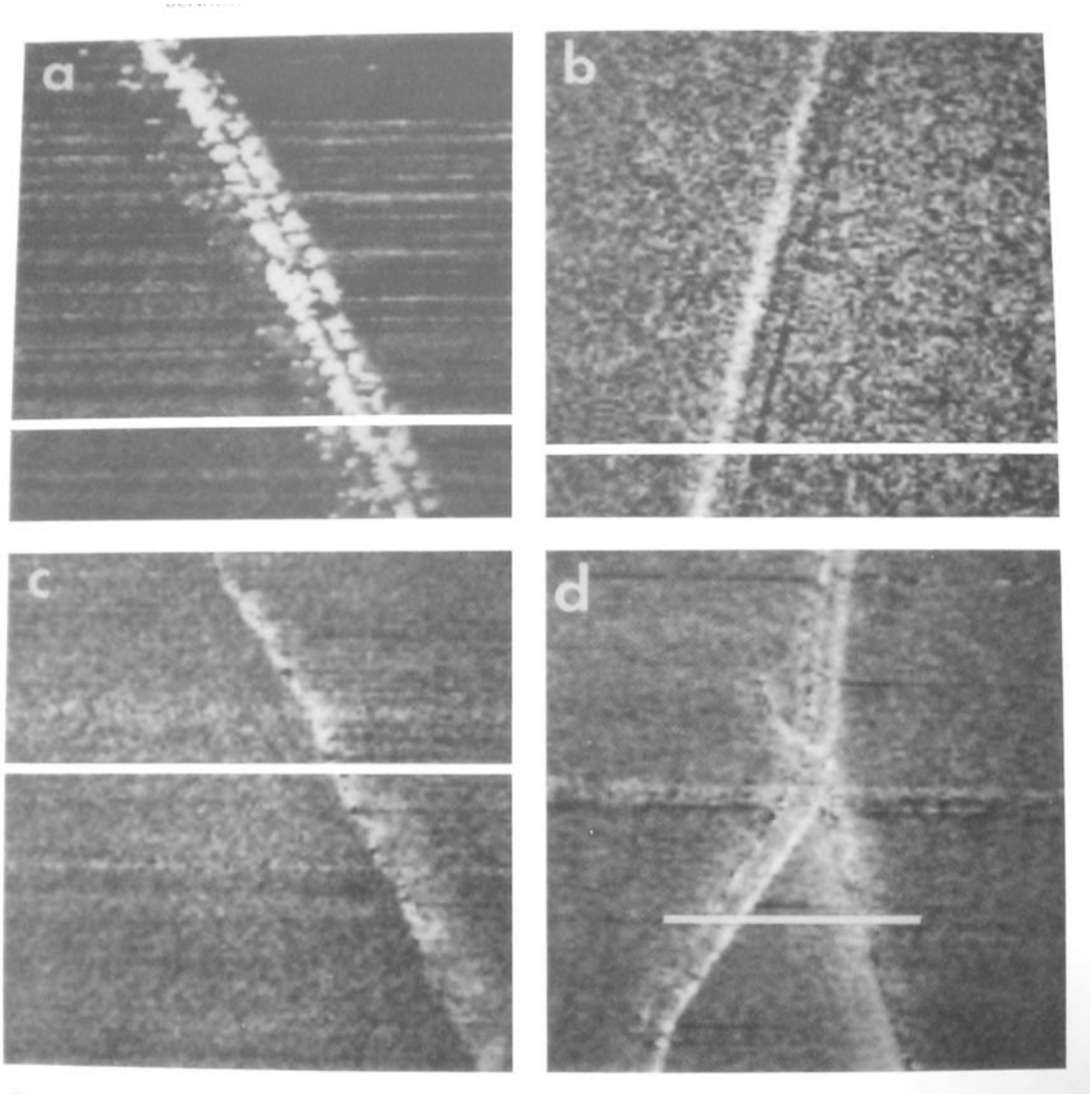

Figure 2-7. STM spectroscopic images of features on HOPG surfaces. The spectroscopic images were recorded simultaneously with the topographic STM images shown in Fig. 2-6. White features indicated decreased differential conductivity and were displayed at varying range scales to allow significant features to be viewed.

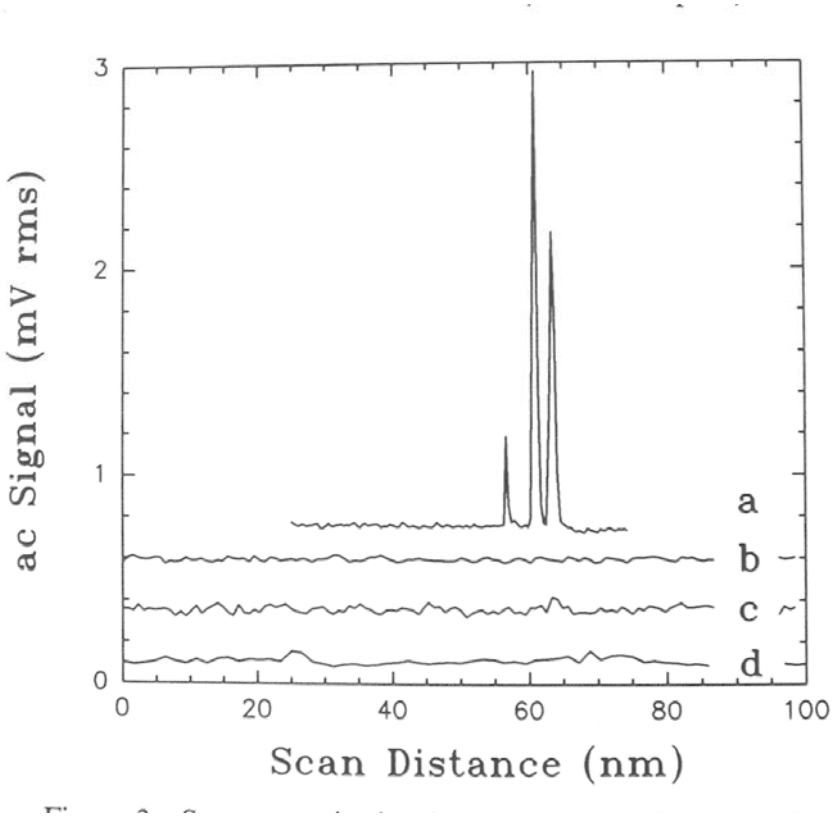

Figure 2-8. Spectroscopic signal amplitude for line scans in Fig. 2-7. The horizontal line scans were taken from the positions indicated in Fig. 2-7 were shown as spectroscopic amplitude. The ac bias on the STM tip was the same in all of the scans at 7 mV rms. For clarity the curves were shown with an arbitrary shift in the vertical position. A strong ac signal indicates low conductivity.

all the images. This clearly showed a marked difference in conductivity over DNA molecules when compared to the step edges and other apparent imperfections observed on the graphite.

Discussion

Our primary objective in this study was to evaluate potential substrates for STM imaging of native biological samples. We chose to image larger TMV on a moderately rough Pd/Au surface, while DNA was imaged on an atomically flat HOPG surface.

Imaging TMV on Pd/Au surfaces

TMV was successfully imaged on mica surfaces that were prepared by both thermal evaporation and sputter-coating the surface with a 12 nm thick coating of Pd/Au in order to make the surface conductive. On the thermally evaporated surfaces, TMV images were routinely obtained, while on the sputter-coated surfaces images of TMV were only occasionally recorded. This observation could be explained in two ways: either the virus was not sticking when it was sprayed onto the sputter-coated surface; or forces exerted by the STM tip were removing the virus during scanning. The latter explanation was supported by the application of a conductive coating of Pt/C to samples of TMV prepared on sputter-coated mica surfaces and finding that the virus could be routinely imaged by this method.

Perhaps the two most important observations made while imaging TMV on Pd/Au surfaces concern 1) the greater width of the STM images of the virus compared to the known width of TMV; and 2) the conflicting height data of TMV located above the surface on evaporated Pd/Au surfaces and below the surface on sputter-coated Pd/Au surfaces.

The observed TMV widths of 70-100 nm recorded in our STM images as opposed to the known 18 nm width of the virus might be explained by drying

effects and or sample mounting conditions; but perhaps a better explanation resides in the tunneling tip geometry. Depending on the degree of surface roughness, the tunneling current may not be confined to the very small region at the end of the tip as is the case when imaging atomically flat surfaces. If the surface is atomically flat, tunneling is confined to a 0.1-0.5 nm region of the tip and the possibility of atomic resolution is possible. However, if there is nanometer vertical roughness in the surface, then the effective diameter of the tip can change due to switching of the tunneling current across the tip as the object is encountered [Warmack 1988]. This could account for the broadening of the TMV images in observed on both the evaporated and sputter-coated surfaces.

Others have applied a thin coating of conductive material Pt/C to samples prepared for STM imaging [Amerin 1988, Traviglini 1988]. We were not able to identify TMV subunits using this technique, but we were able to drastically change the height profile of virus immobilized on sputter-coated Pd/Au surfaces. Prior to coating with Pt/C, the imaged virus appeared to be below the substrate surface. After coating, the virus was imaged above the substrate surface. This was similar to what was found with TMV on evaporated Pd/Au surfaces.

The remarkable differences in the height of TMV imaged on evaporated surfaces as opposed to sputter-coated substrates could be caused during sample preparation when the virus on evaporated surfaces could become coated with Pd/Au. This explanation is supported by the observation that TMV on evaporated surfaces behaved as good conductors with the STM tip accurately recording the viral height as 18 nm as it rode up and over the virus during scanning.

In contrast, images of naked virus on sputter-coated Pd/AU surfaces appeared to be below the level of the surface. This can be explained by the poor conductivity of the virus causing the tunneling tip to move closer to the surface in order to maintain a constant tunneling current. It is of interest to note that the tunneling tip appeared to move 13-20 nm below the surface, which is close to the 18 nm width of the virus. However, in reality the tunneling tip maintains a constant tunneling current and scans the surface on the order of 1 nm above the

surface; it would seem to be impossible for the tip to move down without destroying the virus.

These observations could be explained by collective elastic deformation of the tip and substrate, as illustrated in Fig. 2-9 as the tip exerts increased force on the nonconductive virus [Coombs 1986, Durig 1986]. The extra force exerted by the tip might also flatten the cylindrical virus onto the sputter-coated surface. This could produce the 70-100 nm width of the virus observed. However, this same 70-100 nm width was observed on the conductive virus, indicating that other factors may be responsible for the increase in TMV width over the known 18 nm. Also, by applying a conductive coating of Pt/C to the sputter-coated virus surface, the negative image of the virus can be reversed to positive with the tip moving up and over the virus.

The high-resolution image shown in Fig. 2-5 is an image from an experiment that could not be repeated. Although this image was prepared on an evaporated Pd/Au substrate, it did not become coated with Pd/Au nodules. The width of the image is comparable to the known width of TMV and the height is positive with respect to the substrate. The nanoscale substructure observed in the image agrees with what have been described as the protein subunits of the viral coat [Klug 1960]. This image could be the product of an exceptional tunneling tip in combination with superior viral conductivity.

STM of DNA on graphite surfaces

From experiments using electro-deposition to deposit plasmid DNA onto graphite surfaces which were rinsed with water and dried prior to imaging, we were confident that the surface was adequately covered with plenty of DNA molecules for STM imaging. This was confirmed by our quantitative experiments using ^{32}P radio-labeled plasmid DNA. Even after vigorous rinsing in H_2O, the graphite surface remained covered with DNA [Allison 1992]. However, imaging experiments with STM detect a smaller number of DNA molecules than expected. Therefore, either the DNA on the HOPG surface is invisible to STM, or not

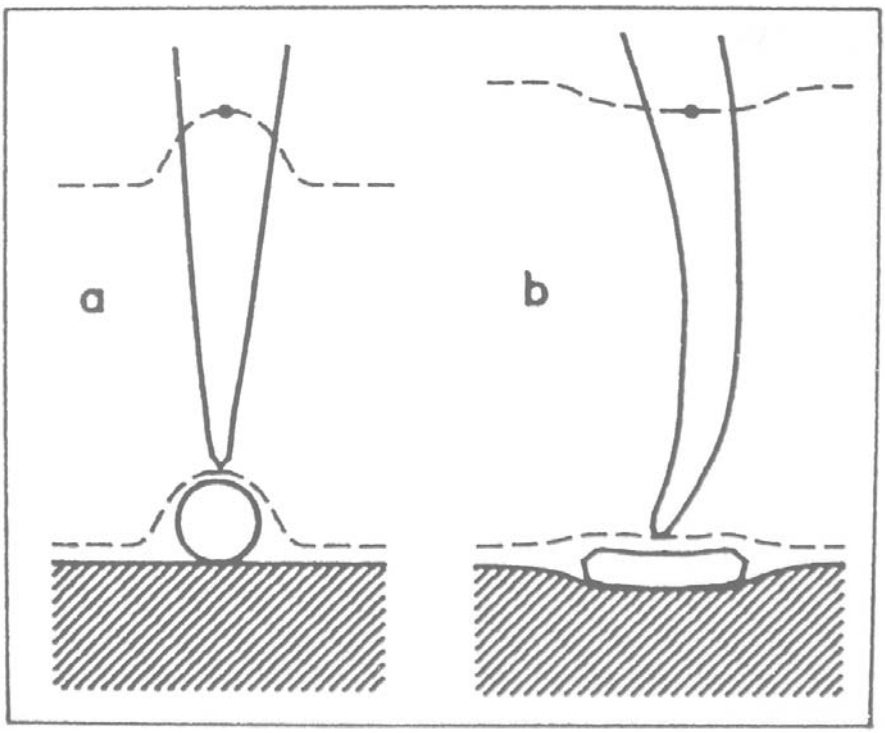

Figure 2-9. Elastic deformation of STM tip and mounting surface. If both the sample and substrate surface are good conductors (a) the STM tip will maintain a constant distance above the surface. If the sample is a poor conductor the tip must move toward the surface in order to maintain a constant tunneling current. This results in the tip applying extra force to the sample, the substrate surface, and also to the tip. This force may flatten the sample and or cause elastic deformation to the tip, sample, and substrate (b) which will be recorded by the STM as an exaggerated downward movement of the tip. Even though the tip has to move up and over the sample (lower dashed line) in order not to destroy it, the piezoelectric crystal associated with recording height (upper dashed line) may indicate a different contour height.

present in the regions imaged, or is removed by the STM tip. This last explanation is most likely. Our results and the results of others [Travaglini 1987, Arscott 1989, Beebe 1989, Lee 1989, Keller 1989] have demonstrated that some DNA structure was visible when it was trapped in what appeared to be dried buffer deposits, or in step edges or other imperfections on the graphite. These structures were assumed to be DNA although in many ways they were not what one might expect DNA to look like. For instance, images of DNA taken with the electron microscope show the DNA polymer to be a thread like structure that coils and bends like a length of string dropped on a flat surface. All of our DNA images and most of the images presented by other laboratories of DNA on graphite were similar to the image presented in Fig. 2-6a. The DNA appears as a straight seemingly rigid structure that does not bend. Also, the 2.3 nm helical repeat we observed does not agree with the expected repeat of 3.4 nm of B-form DNA. These variations in the helical repeat might be explained by the electro-deposition method used to deposit DNA and the forces exerted on the DNA molecules during deposition. Also, the atomically flat graphite surface might affect the way DNA adheres to the surface, influencing both the configuration the molecule assumes by either stretching or compressing the helix of the molecule.

It would appear from our initial attempts to image DNA passively mounted on HOPG that better immobilization procedures need to be implemented. Otherwise, the researcher is presented with the problem of imaging occasional structure associated with step edges, or molecules embedded in what appears to be buffer salts, or objects that are inherent to graphite yet have some structure similar to DNA.

When first proposed by Binnig and Rohrer [Binnig 1982] the STM was developed as an instrument to investigate both the topographic and spectroscopic properties of conductors. Scanning tunneling spectroscopy (STS) has been used on both metal and semiconductor surfaces, at the atomic level, for identifying different densities of state [Binnig 1983, Becker 1985$_a$, de Lozanne 1985, Becker 1985$_b$] and in combination with topographic information as a means to gain a

better understanding of structures. Travaglini *et al.* published the first high-resolution STS image of DNA employing *dI/dS* as a way to enhance structural aspects of the DNA molecule [Travaglini 1987]. In a similar experiment Lindsay *et al.* used *dI/dS* spectroscopy in liquid to image adsorbate patches of DNA electrochemically deposited on atomically flat gold surfaces.

In our studies we used STS as a means to qualitatively identify DNA from the HOPG substrate, and as a means to further distinguish structures inherent to graphite that could be confused with DNA molecules. In our experiment we used *dI/dV* spectroscopy to investigate graphite surfaces that were only tape stripped, those that were tape stripped and subjected to electro-deposition with buffer only, and those that were subjected to electro-deposition with DNA in the buffer. Since in bulk DNA is an insulator, the lower differential conductivity observed in the STS image over the DNA molecule is expected Fig 2-7$_a$. Similar results have been reported by others [Lindsay 1988$_b$]. In our experiments where we imaged tobacco mosaic virus [Mantovani 1990], we also used STS and found a similar sharp decrease in the differential conductivity (*dI/dV*), although this data was not published.

Important for this study, the STS mode provided a means for simultaneously identifying qualitative differences in conductivity that are not identifiable in the constant current topographic imaging mode. The spectroscopic image in Fig. 2-7$_a$ clearly identifies the poorly conductive DNA molecules from the step edges in Fig. 2-7$_c$ and in Fig. 2-7$_d$, as well as from the unknown structure on untreated HOPG in Fig. 2-7$_b$ that could be confused with DNA. Perhaps when reliable methods are developed for routinely attaching DNA to surfaces, STS may evolve into that missing tool for identifying individual nucleotide bases by their electronic signature, allowing for rapid DNA sequencing.

Chapter 3
Imaging DNA with the scanning tunneling microscope

Background and Significance

With the invention of the scanning tunneling microscope (STM) a powerful new tool with demonstrated ability to image crystalline surfaces at atomic resolution[Binnig 1982,] was realized. This invention coincided well with the international commitment to sequence the human genome as a new technology with expectations that this new tool might be developed to sequence DNA. Many features of the STM, including the potential for using this instrument in any environment including biologically relevant liquid medium held great promise for applications of this instrument in genomic research. However, there are two significant problems that need to be addressed in order to reap the full benefits of STM for imaging biomolecules more specifically DNA. These problems result from the forces exerted by the tip and the poor conductivity of biological samples.

The instrument is a topographic tool where a sharpened tip is scanned over a conductive surface and the electronic interaction between the tip and surface is used to create the image. This creates a certain force on the sample and when imaging biomolecules passively mounted on atomically flat surfaces, such as highly ordered pyrolytic graphite (HOPG) or crystalline gold, samples are rarely seen. In our experiments where we imaged tobacco mosaic virus on sputter-coated gold surfaces, we recognized that tip forces were responsible for removing virus from the surface making imaging erratic and unpredictable [Mantovani 1990]. Our group [Allison 1990] and others have recorded fragments of both natural and synthetic DNA on HOPG [Arscott 1989, Binnig 1984, Beebe 1989, Lee 1989, Keller 1989, Dunlap 1989, Driscoll 1990, Bendixen 1990] and gold surfaces [Lindsay 1989, Cricenti 1989]. Although atomic resolution of DNA has not been realized, highly resolved images claiming to identify the helical repeat, major and minor groves [Beebe 1989], base paring [Driscoll 1990], and individual bases [Dunlap 1989] have been reported. However, in all cases only

fragments of DNA molecules have been imaged and usually these images show the molecules trapped in lattice defects or perhaps aggregates of dried material on the surface.

Although biological molecules are insulators in bulk there is little known about conductivity through individual molecules. DNA although infrequently imaged has nevertheless been imaged on graphite and gold surfaces. Preliminary reports have confirmed that native biological molecules, not treated with any agents that would increase their conductivity, can be imaged by STM. Images of native bacteriophage *ø 29* [Baro 1985], Phosphorylase-kinase [Edstrom 1989,1990], and polypeptide structures [McMaster 1990_a] untreated with agents or coatings to increase conductivity have been imaged by STM. Nevertheless, the heterogeneity of a biomolecule on a conductive surface, unless it is removed by the scanning tip, should provide image contrast.

At this juncture it became obvious that if the STM could become a practical tool for imaging DNA there would have to be an immobilization strategy developed that would allow for routine imaging of DNA molecules. Although successful attempts to image DNA have been reported using electrochemical [Lindsay 1988_a, Brown 1991] and covalent [Lyubchenko 1991, Cricenti 1991] immobilization techniques only fragments of molecules have been imaged. Recently we presented results of successful coulostatic immobilization of DNA onto chemically modified epitaxial gold surfaces [Allison 1992]. This approach involved the anchoring of polarizable pendant groups to clean gold surfaces mediated through the reaction of thiols with the gold surface. This was followed by reaction with and immobilization of polyanionic DNA by ion exchange. By monitoring the uptake of radiolabeled DNA on various treated surfaces we were able to quickly evaluate the efficacy of each treated surface. Using a gold surface chemically modified with 2-dimethylaminoethanethiol we reported reproducible imaging of DNA and for the first time imaging of entire circular plasmid DNA molecules.

Materials and Methods

DNA used in Experiments

Plasmid DNA (3204 bp, pBS$^+$ Stratagene, LaJolla, CA) was subjected to cesium chloride-ethidium bromide equilibrium centrifugation to enrich for the supercoiled form. After two ethanol precipitations the sample was suspended to a concentration of 500 μg/ml in 2.4 ml of TE buffer (10 mM Tris-HCl, 0.01 mM EDTA in dd-H_2O at pH 7.5). Relaxed circular DNA was prepared from the supercoiled DNA by subjecting 0.5 ml of the sample to X-ray (70,000 rad) mediated single-strand nicking. Agarose gel electrophoresis was used to differentiate between supercoiled and relaxed circular plasmid DNA to determine the degree of single strand nicking.

Preparation of radiolabeled DNA

Radiolabeled DNA was prepared by nick translation of the relaxed circular plasmid DNA using the following reaction mixture: 35 μl DNA (500 μg/ml), 5 μl 10 X NT buffer (500 mM Tris-HCl, pH 7.5, 50 mM $MgCl_2$, 100 mM 2-mercaptoethanol, 1 mg/ml of nuclease-free bovine serum albumin), 4 μl dTAG (50 μM dTTP, 50 μM dATP, 50 μM dGTP), 5 μl [a-^{32}P]dCTP (3000 Ci/mmol, 10 μCi/μl), and 1 μl *E. coli* DNA polymerase I (10 units/μl) [Sambrook 1989]. After the sample was incubated for 40 min at 14 ^{o}C, it was diluted with 150 ml of dd-H_2O and 25 μl of 3 M sodium acetate. After extraction with phenol-chloroform (1:1) the sample was ethanol-precipitated twice and suspended in 35 μl of TE. In experiments where it was necessary to use exclusively relaxed circular DNA the radiolabeled DNA was size fractionated by agarose gel electrophoresis, extracted from the gel using the glass powder procedure [Vogelstein 1979], and resuspended in TE.

Glass powder procedure

The relaxed circular DNA band was carefully excised from the gel using a sharp razor blade, weighed in a micro-centrifuge tube and 3 volumes of NaI solution per gram of gel was added. The solution was incubated at 37-50 ^{o}C with mixing until the agarose dissolved. DNA was then added to the well mixed glass milk solution in a ratio of 1 μg of DNA to 1 μl glass milk, Incubated on ice for 5-10 minutes with occasional mixing, followed by centrifugation at 12,000 xg for 1-2 minutes in a micro-centrifuge. The glass pellet was rinsed with 250 μl of NaI solution, micro-centrifuge 1-2 minutes and the pellet suspend in ethanol. This step was repeated 3 times followed by drying the pellet and suspending the pellet in 20 μl TE at 50 ^{o}C for 10 minutes to elute the DNA. The solution was then centrifuge for 1 minute at 12,000 xg in the micro-centrifuge and the DNA in the supernatant collected.

The recipes for the NaI solution and for glass milk are as follows. For NaI solution dissolve 90.8 gm NaI + 1.5 gm Na_2SO_4 in 100 ml dd-H_2O, filter through whatman # 1.0 paper into a foil wrapped bottle, containing 0.5 gm Na_2SO_4 in dialysis bag, for storage at 4 ^{o}C . For glass milk use powdered silica, not fumed, (Sigma, St. Louis MO) and suspend 40 g of powder in 80 ml dd-H_2O, stir for 60 minutes, remove stirring allowing particles to settle for 90 minutes to remove large particles. Remove supernatant and centrifuge at 6000 xg for 10 minutes to pellet glass (6000 rpm in a Sorvall GSA rotor). Resuspend pellet in 20-30 ml dd-H_2O, add equal volume of concentrated nitric acid, bring close to a boil in fume hood for 5 minutes, and cool to room temperature. Pellet and wash glass 4-6 times in dd-H_2O as described above. Store the glass milk-H_2O solution as a 50% slurry divided into 1.7 ml micro-centrifuge tubes. The working solution can be stored at 4 ^{o}C while stock solutions are stored at -80^{o}C.

Preparation of crystalline gold surfaces

Gold (111) surfaces 120 nm thick were prepared in a vacuum evaporator at 2.0 x 10^{-6} Torr by electron-beam evaporation of 99.999% pure gold (Cerac Inc.,

Milwaukee, WI) onto freshly cleaved mica surfaces (5 X 3 cm) heated to and maintained at a temperature of 480 ^{o}C during evaporation. After evaporation the gold surfaces were allowed to cool to room temperature under vacuum [DeRose 1991]. The mica was placed gold side down in a hole punch that offered a selection of different diameter holes that could be selected (Ralmike's tool-A-Rama, Plainfield, NJ). For our experiments we punched out 3/16 diameter disks which were stored in a dessicator with silica gel to maintain a dry environment.

Passively mounting DNA on Gold surfaces

pBS^{+} at a concentration of 5.0 μg/ml in 0.01 ammonium acetate pH7.0 was sprayed, using a nebulizer, onto an untreated gold surface maintained at 55 ^{o}C to volatize the ammonium acetate solution Fig. 3-1.

Chemical modification of gold surfaces

Chemical modification of the gold surfaces was accomplished by emersion of the disks for up to 24 hours in 0.005 M aqueous or ethanol solutions of the modifier to be tested. The modifiers tested with positively charged head groups were 2-dimethylaminoethanethiol and 2-mercaptoethylamine, while the modifier with a negative head groups tested was 3,3/ dithiodipropionic acid. Also, included in the testing was 2-mercaptoethanol.

DNA uptake on modified gold surfaces

After modification the disks were rinsed thoroughly in dd-H_2O and air dried prior to using. DNA uptake on the chemically modified surfaces was measured by floating the modified disks, gold side down, on 1.2 ml solutions of 0.04 to 0.06 μg/ml relaxed circular pBS^{+} DNA in 0.01 ammonium acetate adjusted to pH 5.0, 7.0, 8.0, or 9.8. Each solution to be tested was placed in a well of a 9 well porcelain spot plate and 3-5 disks added to each well. After 2 hours at room temperature the disks were thoroughly rinsed by plunging each disk 10 times into 4 beakers of dd-H_2O. After rinsing, each disk was placed in scintillation vial

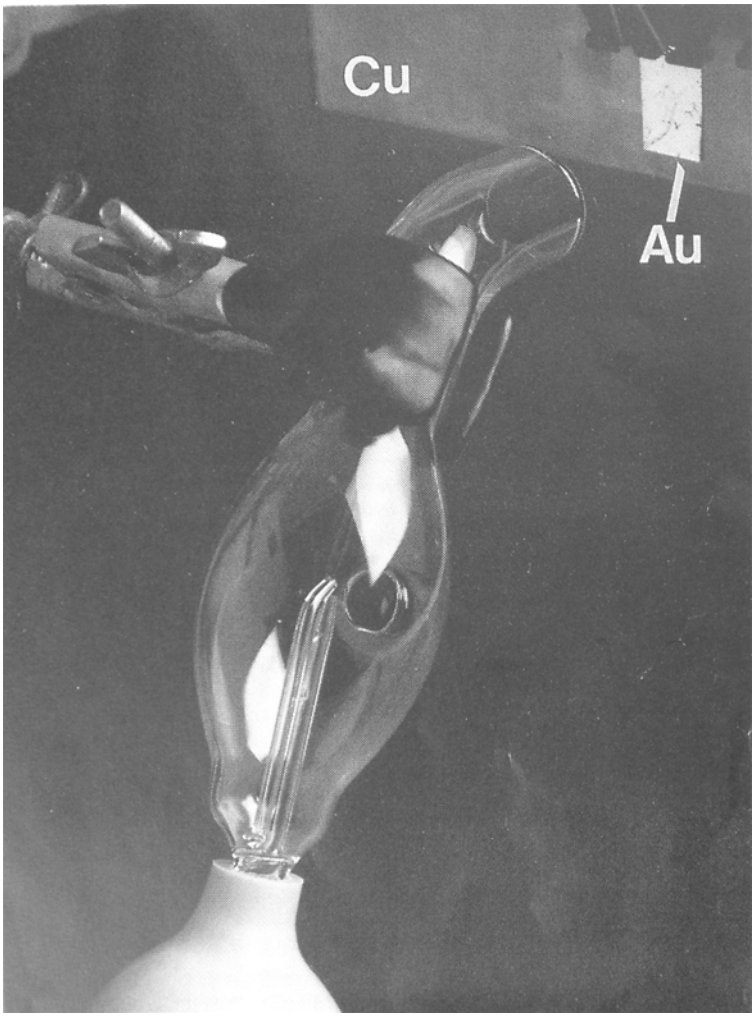

Figure 3-1. Glass nebulizer for spray mounting DNA on surfaces. A glass nebulizer was used to passively apply pBS^{+} plasmid DNA to untreated gold surfaces. Using the nebulizer a DNA solution at a concentration of 5.0 μg/ml in 0.01 M ammonium acetate was sprayed onto a untreated crystalline gold surface supported on a mica substrate. The surface was place on a piece of copper attached to a soldering iron that could be voltage controlled by a variable transformer. The DNA was sprayed onto the surface with the surface maintained at 55 C.

containing 5 ml of Insta Gel XF scintillation fluid (Packard Instruments Inc., Downers Grove, IL) and counted for 2 minutes (each vial) in a Beckmann LS6001C scintillation counter (Beckmann Instruments Inc., Fullerton, CA). Autoradiographic analysis of disks was done over a time course of 0.5 to 30 hours in order to obtain information related to the pattern of uptake. After incubating the modified surface for a given length of time the disk was rinsed as described, dried and either glued or immobilized with double-stick tape mica side down onto a sheet of paper. The disks were then exposed to x-ray film (Kodak Inc., Rochester, NY).

Scanning tunneling microscopy

STM images were obtained with the Nanoscope II (Digital Instruments, Santa Barbara, CA) operating in the constant current mode with the substrate biased 100-1000 mV positive with respect to the platinum/Iridium (Pt/Ir) tip and at a tunneling current of 0.2-1.0 nA. Most images were recorded at a tunneling current of 0.4 nA and a bias of 500 mV with a scan rate of 4.7 Hz or less.

Results: DNA Immobilization on gold surfaces

STM of DNA on gold surfaces

All of the experiments concerning the immobilization and STM imaging of DNA on gold surfaces were recorded on a Nanoscope II scanning probe microscope that could be operated as either a STM or AFM. Our initial attempts to immobilize DNA on gold surfaces and image relaxed circular pBS^+ plasmid DNA was done by spraying DNA onto a gold surface heated to 55 ^oC. By dissolving the DNA in ammonium acetate and heating, the volatile buffer is removed so that only the DNA molecules should be left on the surface. The results in this experiment are shown in Fig. 3-2. The amount of DNA used in these experiments was sufficient to cover the surface of the gold to the extent that images of DNA should occur with every scan of the surface. The sequence of

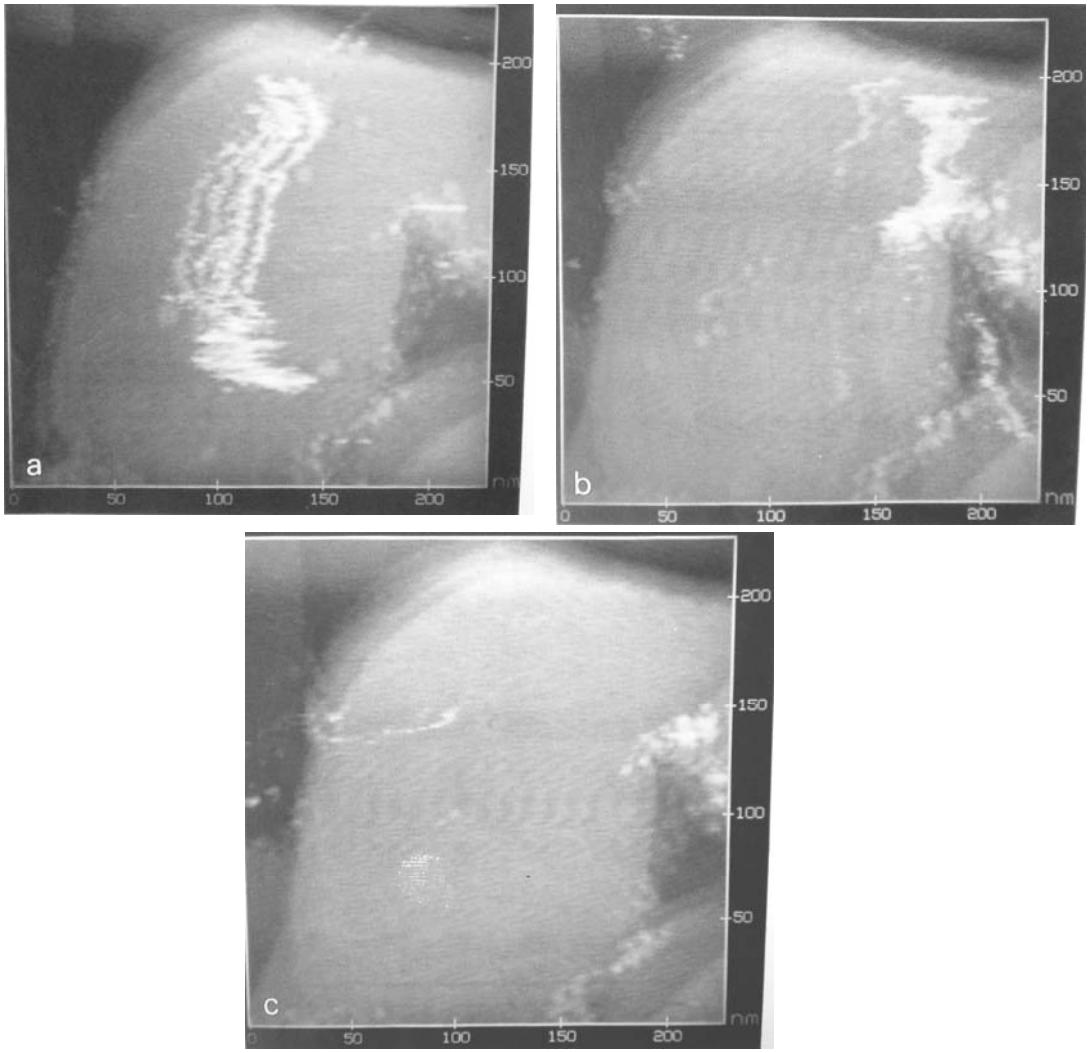

Figure 3-2. DNA mounted on gold by spraying microdroplets. Microdroplets of pBS$^+$ at a concentration of 5.0 μg/ml in 0.01 ammonium acetate pH7.0 were sprayed, using a nebulizer, onto an untreated gold surface maintained at 55 ^{o}C to volatize the ammonium acetate. A sequence of three scans of the same area shows that an aggregate of at least 4 strands (a) are present in the first scan. In the second scan (b) the aggregate has been lost and the DNA displaced while in the third scan (c) a single fragment not present in the first two scans is evident.

images presented in Fig. 3-2, clearly illustrate that DNA bundles of plasmid DNA imaged in the first scan are removed or displaced in subsequent scans. This is the result that we consistently found when imaging DNA mounted on gold surfaces using this technique.

Quantifying DNA binding to gold surfaces

The modification of electrode surfaces by chemical means has been an active area of investigation [Murray 1984]. The adsorption of alkanethiols and alkanedisulfides from solution to gold surfaces by the formation of Au-S-C bonds has been demonstrated by Whitesides and co-workers [Bain 1989]. Long chain alkanethiols have been shown to adsorb to gold surfaces resulting in a self-assembled densely packed oriented monolayer of material. This allows for the derivation of gold surfaces as an efficacious way for introducing functionality to the gold/solution interface. Using alkanethiols with both positive and negative charged head groups we have derivitized gold surfaces and developed an assay to determine if these surfaces can be used to immobilize DNA molecules [Allison 1992]. The assay involves taking 3-5 disks that have been functionalized with a test alkanethiol and floating the disks gold side down on a solution of radiolabeled pBS^+ plasmid DNA Fig 3-3.

After a period of time the disks were removed rinsed in dd-H2O, dried and counted in a scintillation counter. The assay is quantitative in two different ways. First, the gold surfaces on the 3/16 inch diameter disks used in the assay are uniform in size so that when they are functionalized and floated on a solution of radiolabeled DNA multiple disks floated on the same solution display a close grouping of counts. Floating the disks on the solution is important since our results with immersing the disks in the radiolabeled DNA resulted in a wide range of counts. This is very likely due to partially open cleavage planes in the disks that result from shock associated with the process for punching out the disks. Radiolabeled DNA can wick into the disks to varying degrees grossly affecting the counts. Second, since both the concentration of radiolabeled DNA is

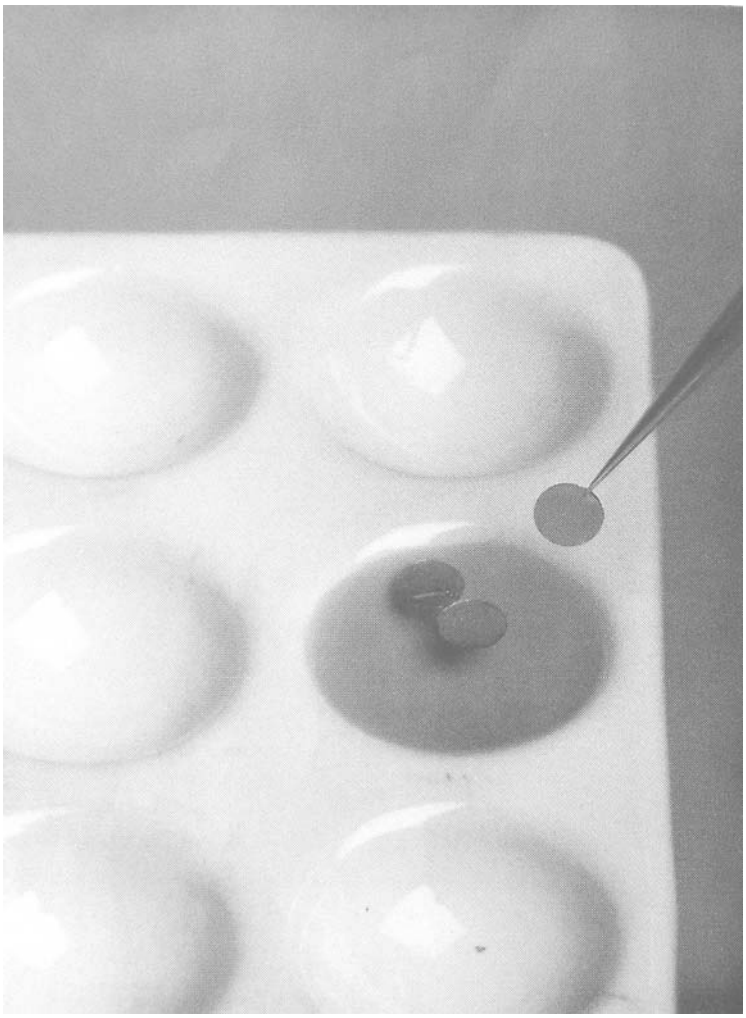

Figure 3-3. Immobilization of DNA on gold disks. In the figure, part of a 9 well spot plate is shown where either untreated gold surfaces or gold surfaces treated with 2-dimethylaminoethanethiol are floated on a solution of DNA. If radiolabeled DNA is used the quantity of DNA bound to the surface can be determined. The films are removed from the surface with tweezers and rinsed vigorously in dd-H_2O prior to using.

known and the molecular weight of the plasmid is known by knowing the counts on a disk the number of DNA molecules that should be on a treated disk can be calculated.

The utility of the assay to evaluate binding of DNA to gold surfaces functionalized with alkanethiol compounds with either positive ($N(CH_3)_2$ or NH_2) or negative (COOH) charge to the interface between water and the monolayer was demonstrated at various solution pH. The results of our experiment to determine the efficacy of the assay is illustrated in Fig. 3-4. Disks incubated in water prior to incubation in radiolabeled DNA served as the benchmark control in the experiment and are included to illustrate passive adsorption instead of affinity DNA binding. Surfaces functionalized with alkanethiol compounds that bind DNA better than the water control are assumed to be actively binding DNA. These chemicals would be candidates for further consideration in determining the optimal conditions for binding prior to STM imaging. Conversely, surfaces that show a lower affinity to bind DNA than the water control would be eliminated from further consideration. Binding results for the chemicals tested correlate quite well with the results recorded in Fig. 3-4, relative to the solution pH used in the experiment. For example the pK_a of 2-mercaptoethylamine is 8.27. From Fig. 3-4, it can be seen that at a lower pH the protonated amino group attracted the negatively charged DNA molecules while at higher pH the amino group is not protonated and will not attract DNA. In similar fashion the gold surfaces functionalized with 3-mercaptoproponic acid did not attract DNA at any pH and at higher pH actually repeled DNA as the carboxyl group becomes deprotonated. Because surfaces derivitized with the 2-mercaptoethanol behave much the same as the water control this compound does not merit further consideration. This is also true for the 3-mercaptoproponic acid treated gold surface where this compound actually repeled DNA. The compound that was chosen for further study was 2-dimethylaminoethanethiol with two methyl groups on the nitrogen head group. This chemical has a pK_a of 10.8 and remains protonated through all three of the solution pH tested in the experiment. At pH

Modified Surface[b]	pH of the DNA Solution[c] 5.0	7.0	9.85
	350 ± 4	255 ± 20	252 ± 13
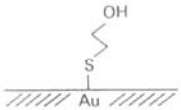	277 ± 25	182 ± 17	124 ± 23
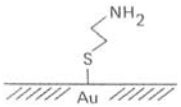	416 ± 30	288 ± 32	204 ± 21
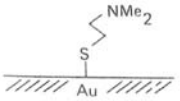	403 ± 18	428 ± 20	458 ± 28
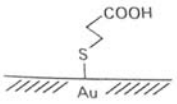	177 ± 3	142 ± 33	126 ± 11

Figure 3-4. Radioscintillographic results. The figure demonstrates the affinity of radiolabeled pBS+ plasmid DNA, suspended in 0.01 M ammonium acetate at the pH values listed, for chemically modified gold substrates on mica surfaces. The values listed are mean disintegrations per minute for at least 3 disks per surface treatment plus or minus the standard deviation. Surfaces were pretreated with 5 mM solutions of the chemical modifier for 24 hours prior to exposure to DNA solution. Solutions of the following chemicals were used H_2O, 2-mercaptoethanol (in toluene), 2-mercaptoethylamine (in H_2O), 2-dimethylaminoethanethiol (in H_2O) and 3,3/ dithiodipropionic acid (in ethanol).

5.0 it behaves much the same as 2-mercaptoethylamine that is also protonated at pH 5.0 but at higher pH it is superior.

Autoradiographic analysis of radiolabeled DNA incorporation

In another experiment the binding of radiolabeled pBS^+ to gold surfaces was investigated using autoradiography. When it was found that floating disks as opposed to immersing disks in the solution was important in order to maintain accuracy of the scintillation counting it was decided to check the hypothesis that radiolabeled DNA was leaching into cleavage planes on the edge of the disks. This was done by using autoradiography where the water control gold surface disks and disks treated with 2-dimethylaminoethanethiol were incubated on a solution of ^{32}P radiolabeled pBS^+ plasmid DNA (0.4 μg/ml in 0.01 ammonium acetate at pH 7.0) using a time course of 0.5 to 30 hours. The results of this experiment are shown in Fig. 3-5. From the half hour time point through the rest of the experiment it is clear that disks derivitized with 2-dimethylaminoethanethiol are adsorbing DNA uniformly over the entire disk surface. Conversely, the water control disks appear to be adsorbing very little DNA on the disk surface and at the 3 hour time point the disks are obviously incorporating radiolabeled DNA through cleavage planes on their edges. At later time points in the control sample this donut shaped incorporation of DNA from the edge is much more apparent. This is also happening with the 2-dimethylaminoethanethiol treated disks but is masked by the incorporation of DNA on the surface of the disk.

Time dependent immobilization of DNA on functionalized gold surfaces

The binding of the negatively charged radiolabeled DNA onto the positively charged surfaced mediated by 2-dimethylaminoethanethiol was found to be time dependent. Fig. 3-6, shows the results that were obtained when the water control and the 2-dimethylaminoethanethiol were incubated on ^{32}P plasmid labeled DNA and uptake was determined by scintillation counts. The amount of DNA adsorbed

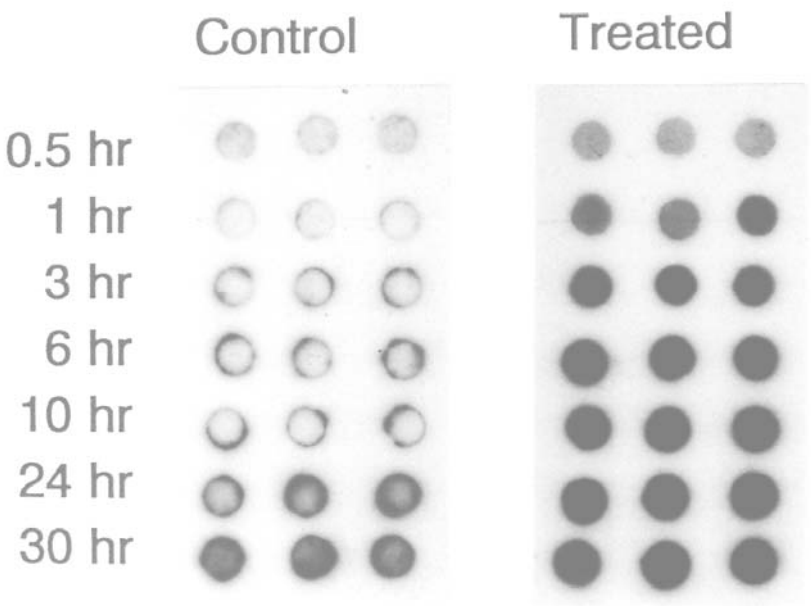

Figure 3-5. Autoradiogram of radiolabeled DNA on gold disks. Gold coated mica disks either untreated or treated with 2-dimethylaminoethanethiol were incubated on ^{32}P radiolabeled pBS^{+} plasmid DNA for the times indicated. After thorough rinsing the disks were dried, placed on a sheet of paper with double stick tape, and exposed to x-ray film.

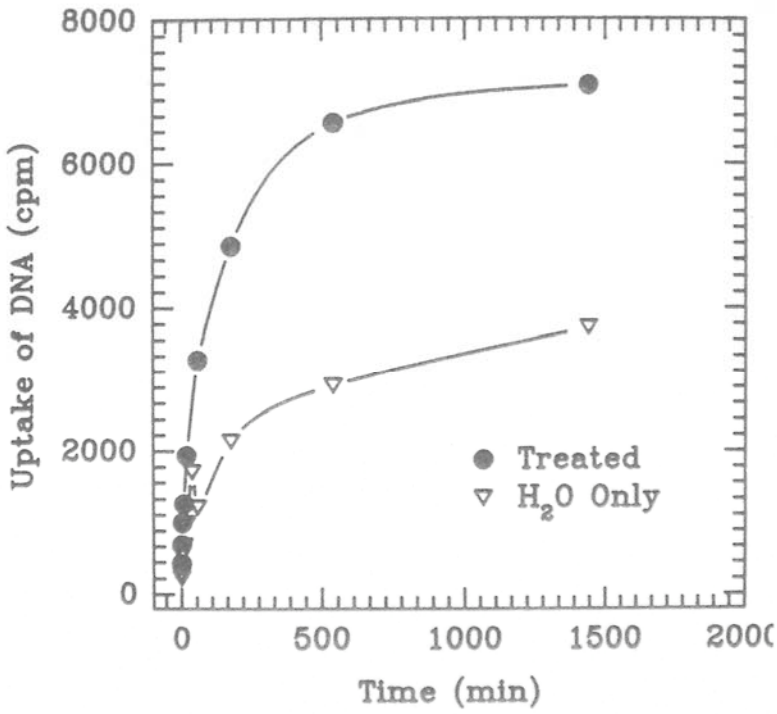

Figure 3-6. Time dependence of radiolabeled DNA onto gold surfaces. The time dependent incorporation of DNA onto treated and untreated gold surfaces was determined by measuring the uptake on gold surfaces, floated on a 0.4 μg/ml solution of radiolabeled pBS^+ in 0.01 M ammonium acetate at pH 7.0. The water-treated (untreated) gold surfaces are represented as open triangles, while gold surfaces

by both the control and treated disks increased with time. However, at all time points the affinity of DNA for the amine modified disks was at least twice that as for the water treated control disks. After about six hours the rate of DNA uptake for both the treated and control disks was comparable. This would indicate that incorporation after 6 hours is primarily due to DNA leaching into the lattice defects in the cleavage planes.

Results STM of DNA immobilized on gold surfaces

DNA on STM of DNA on chemical modified gold surfaces

In our first experiments directed toward immobilizing DNA on surfaces treated with 2-dimethylaminoethanethiol, pBS^+ plasmid at a concentration of 5.0 μg/ml in 0.01 M ammonium acetate buffer at pH 7.0. was placed on the derivitized surface. After six hours the sample disk was removed from the DNA solution, rinsed thoroughly in distilled water, dried and imaged by STM. The image showed a heavy adsorbate on the surface (data not shown) that indicated that the DNA concentration was too high. When the concentration of DNA solution was reduced to 0.25 μg/ml and the amino derivitized gold surface incubated for 3 instead of 6 hours isolated plasmid DNA molecules were imaged by STM [Bottomley 1992, Allison 1992]. The DNA molecules Fig. 3-7, are clearly circular and appear to be evenly distributed over the surface and do not appear to congregate either to the flat terraces or to the step edges. The DNA can also be seen to cross step edges without any apparent effect on the DNA or on the image.

It is also interesting to note that the images of DNA are negative meaning that the molecules are imaged as being below the surface of the gold. This was also found to be the case in previous work that we reported on imaging tobacco mosaic virus (TMV) on sputter coated cold surfaces with the scanning tunneling microscope [Mantovani 1990]. In the course of these studies it was apparent that image contrast and reproducibility was independent of the sign or magnitude of the bias voltage [Allison 1993]. In Fig. 3-7, the circular plasmid molecules are

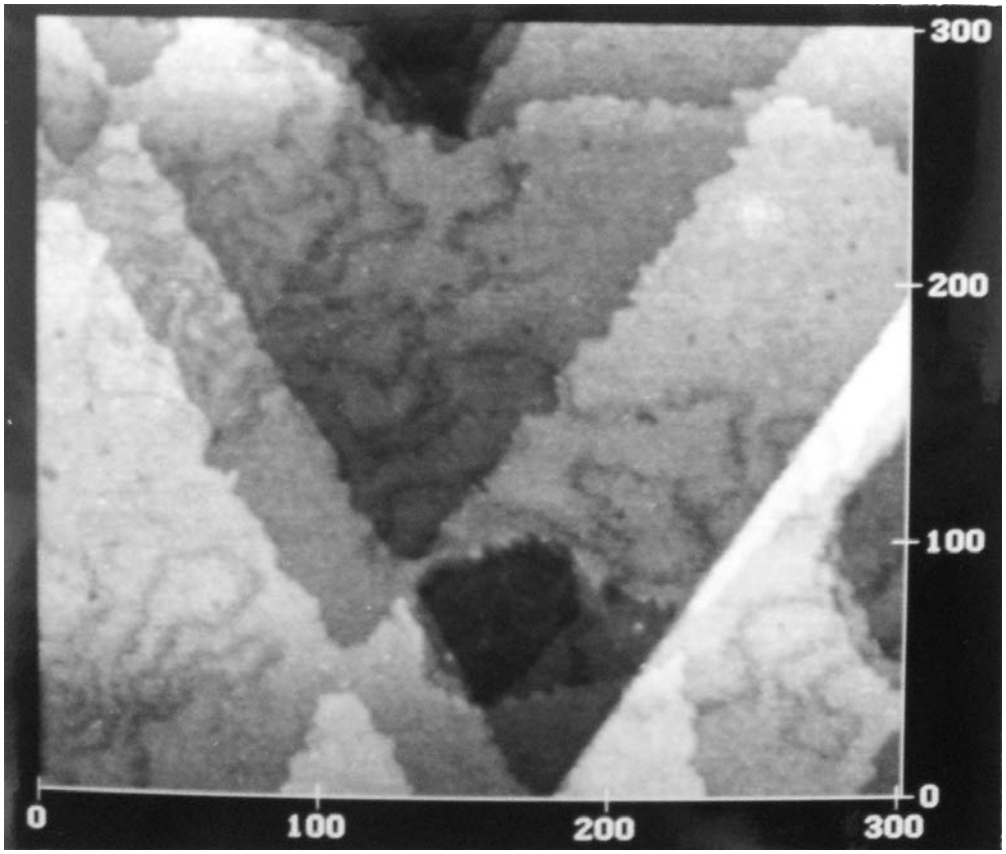

Figure 3-7. pBS⁺ plasmid adsorbed on treated gold not impeded by step edges. Plasmid DNA adsorbed to gold due to the positively charged amino group on 2-dimethylaminoethanethiol attracting the negatively charged DNA molecule. Note that the DNA fibers pass freely over step edges in the crystalline gold surface. Image was recorded at a bias voltage of 400 mV and a tunneling current of 0.4 nA. The Z height range in the image is 5 nm.

clearly imaged as being below the surface. The triangular morphology of the gold (111) surface and the multiplicity of crystal planes does not affect the contrast of the DNA as it passes over step edges nor does encountering a step edge seem to affect the alignment or contrast of the DNA in any way.

Fig. 3-8, is a higher resolution image of a single circular plasmid DNA molecule with a measured contour length of 0.94 μm. Since the pBS^+ plasmid used in this work has exactly 3204 base pairs if the plasmid was in the A form of DNA the contour length should be 0.815 μm with a helical pitch of 2.8 nm per 11 base pairs. If the plasmid was in the B form of DNA the contour length should be 1.08 μm with a helical pitch of 3.4 nm per 10 base pairs [Watson 1987]. Since this molecule is circular and of the correct size we propose that our images are the first STM images of a genetically functional DNA molecule. Repeated imaging of this molecule did not enlist either conformational or positional changes in the molecules thus further supporting the utility of the coulostatic immobilization technique.

In Fig. 3-9, the circular plasmid molecule, shown at a vertical scale of 10 nm, is clearly imaged as negatively contrasted structure. A line trace through the plasmid shows this molecule to be a negative image with the tip moving down ~ 1.5 nm as it passes over strands of DNA.

Although most of the images that we have recorded are negative images, occasionally we see positive images where the DNA is 0.7 to 1.4 nm above the surface. This is shown in Fig. 3-10, where the positive image in Fig.$3\text{-}10_a$ changed in the following scan Fig. $3\text{-}10_b$ to a negative image [Allison 1992]. Overall our results with imaging DNA molecules immobilized onto 2-dimethylaminoethanethiol derivitized atomically flat gold surfaces show that the majority of molecules imaged are negatively contrasted. Although we consistently use the same method to prepare samples for imaging, during scanning sessions molecules are seen approximately half the time. Image contrast is also variable where molecules can be barely seen while at other times the molecules are very distinct. This is made even more puzzling when contrast can

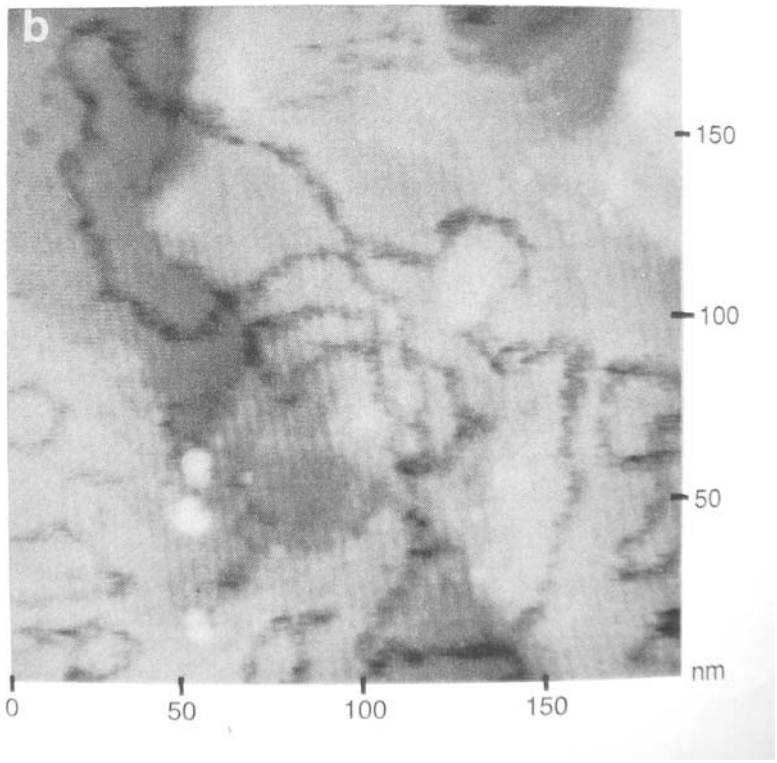

Figure 3-8. STM image of Relaxed Circular pBS$^+$ on a treated gold surface. An individual pBS$^+$ plasmid electrostatically bound to a 2-dimethylaminoethanethiol treated gold surface. The plasmid was measured and found to be slightly smaller than 1.0 μm in length which would be expected for this 3204 base pair plasmid. The image was taken at a bias voltage of 400 mV and a tunneling current of 0.4 nA. The gray scale Z range was set to 10 nm.

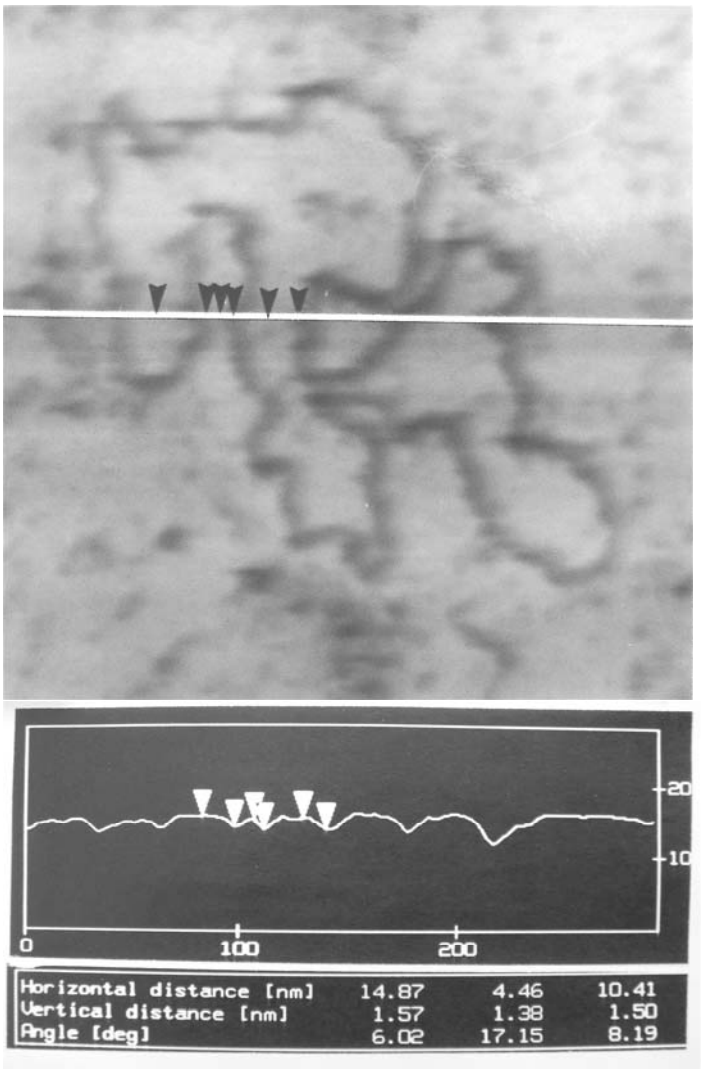

Figure 3-9. Line scan through a relaxed pBS$^+$ plasmid showing negative contrast. A high-contrast negative image of a complete relaxed circular DNA plasmid. The line scan through the plasmid molecule shows several heights of the gold surface marked with arrows along with several depths of the DNA molecule in the gold surface marked with arrows. Note that the vertical depth over three different places in the DNA molecule measured 1.57, 1.38, and 1.50 nm in the negative direction in respect to the substrate surface. The gray scale Z range is 10 nm and the image was taken with a bias voltage of 500 mV and a set point tunneling current of 0.2 nA.

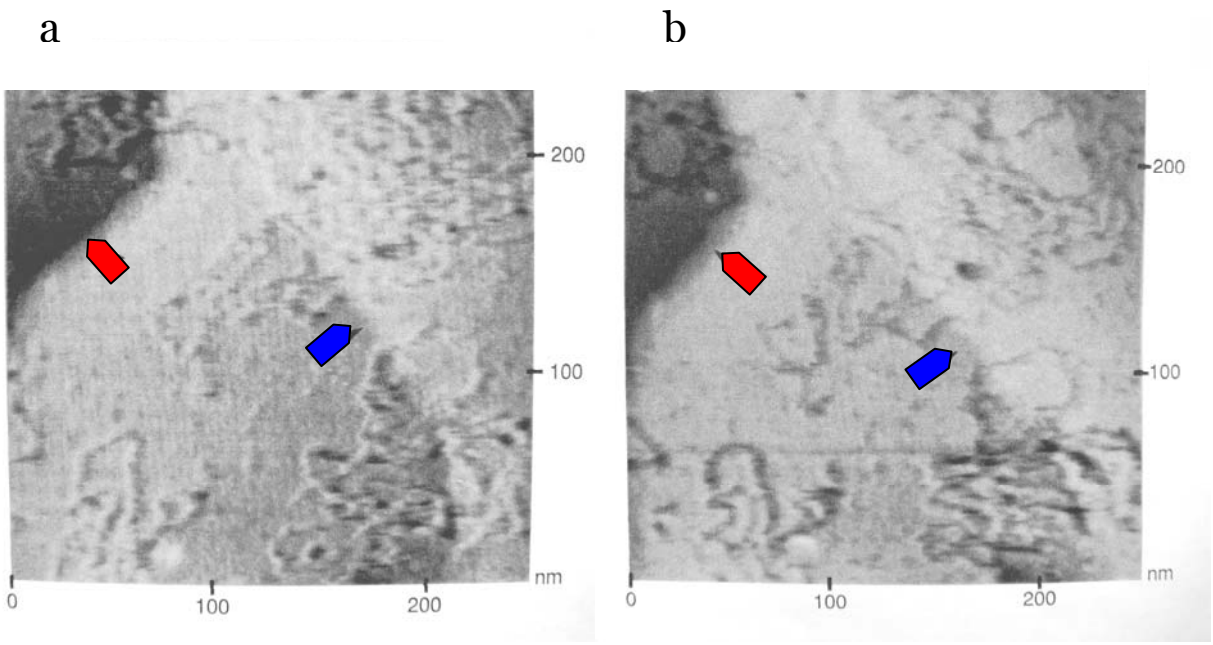

Figure 3-10. DNA switching from positive to negative contrast. Successive scans show the image of plasmid DNA switching from positive (a) to negative (b) contrast. This switching was spontaneous since no imaging operating parameters were changed. The step edges indicated by the (blue arrows) do not change contrast and remain at 1.27 nm in height while the step edges indicated by the (red arrow) remains at 2.64 nm in height. Images were obtained at a voltage bias of 500 mV and a tunneling current of 0.4 nA with a scan rate of 4.34 Hz.

change during a scanning session from good to bad negative contrast or occasionally even switch from negative to positive contrast.

Discussion

STM of DNA on gold surface

Spraying droplets of DNA contained in a volatile buffer onto the surface, where the temperature is a maintained at 55 ^{o}C, has shown that the surface coverage should be adequate to consistently image DNA molecules with the STM. However, our results, as indicated in Fig. 3-2, have shown that passive application of DNA on gold surfaces does not result in consistent imaging of DNA molecules. Our observations of passive application of DNA to both gold and graphite surfaces, supported by our studies using radio-labeled ^{32}P pBS^{+} plasmid DNA [Allison 1992], have shown that surfaces are covered with DNA adequately to insure consistent imaging but only occasional images of DNA are recorded. These observations have been supported by others who have reported adequate coverage of DNA on graphite surfaces but with infrequent STM images of DNA. The obvious conclusion that we and others have reached is that DNA molecules are removed by forces exerted by the tip during scanning [Travaglini 1987, Beebe 1989, Lee 1989, Keller 1989, Allison 1990]. Fig 3-2, illustrates this point where the sequence of images show that the plasmid DNA on the surface is sequentially removed during repeated scanning. Very likely DNA is generally removed on the initial scan thereby explaining why imaging of molecules is infrequent given the concentration of molecules known to be on the surface. Another characteristic of the image of DNA shown in Fig. 3-2$_a$, is that the DNA appears more natural in that it is not rigid as is seen in graphite images of DNA molecules. Also, the strands of DNA appear to be of the correct width but the molecules cannot be identified as circular plasmid DNA.

Quantifying DNA binding to gold surfaces

Our experience with trying to image DNA molecules on graphite and gold surfaces using techniques that passively decorate the surface with adequate coverage for consistent STM imaging produced frustrating results. Forces exerted on molecules by the STM tip clearly are responsible for removing adsorbed DNA molecules. The solution to this problem obviously depends on developing a technique for actively attaching DNA to surfaces.

Although atomically flat gold surfaces are more difficult and more expensive to prepare by employing thiol chemistry these surfaces can easily be functionalized. A plethora of thiol compounds with different functional head groups are commercially available (Sigma, Saint Louis, Mo) and not very expensive. Therefore, serious attention was given to epitaxial gold surfaces for the active immobilization of DNA.

Collectively the experiments described in the results have clearly demonstrated the active adsorption of DNA to the gold surface mediated by the positive charge on the head group of the alkane thiol compound. The data in Fig. 3-4, identifies 2-mercaptoethylamine and 2-dimethylaminoethanethiol as compounds that when allowed to form self-assembled monolayers on atomically flat gold surfaces attract DNA to the surface. The data in this figure also identifies the nature of the immobilization as being due to charge differences between the gold surface and the DNA molecules. Since 2-mercaptoethylamine has a pK_a of 8.27 as opposed to the pK_a of 10.8 for 2-dimethylaminoethanethiol it only stays protonated at the lower pH and becomes progressively unprotonated at higher pH. In contrast, 2-dimethylaminoethanethiol with the higher pK_a value stays protonated through all the solution pH values tested. DNA is a negatively charged polymer due to the phosphate linkage between the deoxyribose molecules that form the polymer backbone [Watson 1987]. Therefore, at lower pH the positively charged 2-mercaptoethylamine attracts the negatively charged DNA while at higher pH it loses its positive charge and no longer is effective. The

2-dimethylaminoethanethiol is positively charged throughout the pH values tested and, as seen in the figure, effectively immobilizes DNA in all of the test solutions.

The autoradiographic experiment shown in Fig. 3-5, graphically shows what happens when untreated and treated gold surfaces derivitized with a self-assembled monolayer of 2-dimethylaminoethanethiol were placed on an pH 7.0 ammonium acetate solution of ^{32}P radio-labeled plasmid DNA. From the very early time point taken at 0.5 hour it can be seen that DNA has diffused to and has been actively adsorbed to the surface on the 2-dimethylaminoethanethiol treated disks. Active adsorption continues for approximately 6 hours, as shown in Fig. 3-6, but at any time during the time course a disk could be taken for STM imaging and hopefully good results obtained. The control disks in Fig. 3-5, clearly show that the radio-labeled DNA leaks into the mica disk from lattice defects in the edges. This also happens with the treated disks but is masked by the active adsorption of the radio-labeled DNA that covers the entire surface beginning with the earliest time point. Mica is a nonconductive surface that is atomically flat, much like HOPG, in that pristine surfaces can be prepared by tape stripping. Because mica is a layered surface the sheer effect caused by punching the gold coated mica disks out using the hole punch disrupts the lattice edge and likely cleaves planes within the disk allowing radio-labeled DNA to leach into the disk. Although it is a slow process, as can be seen from Fig. 3-5, it is a continuous process that eventually involves the entire interior of the disk. For our experiments with imaging DNA 2-dimethylaminoethanethiol was used to form a self-assembled monolayer on the surface to capitalize on charge differences between the negatively charged DNA molecules and the positive amino head group of 2-dimethylaminoethanethiol to actively immobilize DNA for STM imaging.

STM of DNA on chemical modified gold surfaces

The instability of passively adsorbed DNA on gold surfaces has shown that forces exerted by the STM tip during imaging actively remove DNA molecules. By treating surfaces with 2-dimethylaminoethanethiol and allowing a self-assembled monolayer to form on the surface we have introduced positive functionality to the surface and have demonstrated affinity binding of negatively charged DNA molecules to this surface. In Fig. 3-7, when the concentration of the DNA solution is appropriate isolated plasmid DNA molecules can be imaged by STM. The triangular morphology of the gold (111) surface and the multiple step edges does not appear to have any effect on either the image contrast or on the alignment of the molecules as they pass over step edges. These images were the first STM images of entire circular plasmids and the first images of entire genetically functional DNA molecules. Fig. 3-8, is a high-resolution image where the contour length of one plasmid molecule can be followed without being confused with another molecule. By measuring this molecule we have determined that the molecular contour length of 0.94 is very close to the 1.04 contour length of B form pBS^+ with a helical repeat of 3.4 nm [Bottomley 1992, Allison 1992]. Because these molecules are circular and of the correct size they are obviously DNA molecules and not surface related artifacts as might be the case with the DNA molecules observed on HOPG surfaces. However, they are imaged as negative molecules in that they appear to be below the gold surface.

In Fig. 3-9, a line scan through the DNA molecule identifies the strands of DNA as being on the order of 1.5 nm below the surface roughly equivalent to the known 2.0 nm diameter of DNA. Perhaps the simplest explanation for the observed negative contrast would be that the tip is removing the DNA much the same as was observed in images where the molecules were passively mounted on the gold surface. The negative image could then be explained by the DNA associated with either all or part of the alkanethiol monolayer being removed leaving a gap or imprint in the self assembled monolayer. This argument would not seem likely since the negative contrast has been reported by our group on

images of tobacco mosaic virus deposited on sputter coated gold surfaces that have not been decorated with a self-assembled monolayer [Mantovani 1990]. Our present results would also discount this possibility since we have found that when DNA molecules are found to cross over one another the point where the molecules cross is always more negative than the rest of the molecule. These observations would seem to support the idea that when the tip encounters the poorly conducting DNA molecule an additional tunneling barrier is presented that must be overcome by moving the tip down in order to establish a constant tunneling current. This downward movement must be compensated by the system flexing since in our experiments the tip is scanned over the surface only about 1 nm above the surface and the tip must rise up and over the DNA otherwise the DNA would be destroyed or removed from the surface. We have already shown with the tobacco mosaic virus work that flexibility of the tip and system can be as much as 20 nm [Matovani 1990].

Although flexing of the system is the most logical explanation for negative contrast it is difficult to understand. The question of how structural elements of the STM, the tip, self-assembled alkanethiol monolayer, and the gold surface would be the elements involved in flexing while the DNA molecule remains apparently intact remain unanswered.

Even more puzzling are our observations of positive images. Positive and negative contrast images of DNA have been observed in the AFM and are associated with changes in ambient humidity [Thundat 1992$_a$, Thundat 1992$_b$, Vesenka 1992]. Our results with AFM indicate that conditions of low humidity produce the least amount of force between the tip and surface resulting in positive images. Conversely, when the humidity is high a high capillary force exists between the cantilever tip and surface that causes buckling of the cantilever resulting in negative images [Thundat 1992$_b$]. However, the mechanism of tunneling through insulators and how contrast can be either negative or positive is not well understood. Guckenberger *et al.* [Guckenberger 1991], imaged DNA molecules using very high tunnel gap impedances (large gap between tip and

surface) attributed negative or positive images due to tip sharpness. Lindsay *et al.* [Lindsay 1988$_b$], proposed that the pressure of the tip required to establish tunneling through insulators also depends on the geometry of the tip making measurements of insulator heights unreliable. However, our results have shown spontaneous reversal of contrast from positive to negative in consecutive scans of the same area Fig. 3-10, which would seem to rule out mechanical properties of the tip being responsible.

Chapter 4
Mapping DNA with the atomic force microscope

Background and Significance

A major focus of the Human Genome Initiative has been directed toward physical mapping of cloned DNA. The overall idea is to isolate fragments from a particular chromosome; clone the fragments; and propagate the cloned fragments in either yeast as yeast artificial chromosomes (YAC'S), or in bacteria as bacterial artificial chromosomes (BAC'S). Physical mapping employs a methodology that can precisely locate a number of targets on each of the clones. Since many of the clones isolated would be duplicates or near duplicates, the goal of mapping would be to identify the clones that have minimum overlap from clone A to B, to C to D, etc. In the end, physically mapping a chromosome identifies the minimum number of overlapping clones that would be required to recreate the chromosome. In this fashion these clones could be sequenced with the minimum amount of redundancy.

Restriction endonucleases are enzymes traditionally used for physically mapping DNA. These enzymes recognize specific base sequences in DNA molecules, bind to these sequences, and cleave the DNA at that point. The frequency at which these enzymes bind and cleave a DNA molecule is determined both by the number and the order of nucleotides in the recognition site. If DNA nucleotide sequence is considered to be random (there are four nucleotides: adenine, guanine, cytosine, and thymine), each position in the sequence has an equal chance of being occupied by one of the four nucleotides. Therefore, an endonuclease that cleaves a particular sequence of three nucleotides has a probability of cleaving DNA every 64 base pairs, while an endonuclease that cleaves a specific sequence of six nucleotides would cleave DNA every 4098 base pairs. In terms of mapping a 50 kilo base (kb) clone there would be a variable number of sites depending on the clone, but on the average there should be roughly 10 sites where a specific six nucleotide sequence would be present. Since

the restriction sites for any given endonuclease are site-specific, these sites of attachment can serve as physical mapping points along the length of the DNA molecule.

Conventional methods for locating restriction sites for a particular endonuclease on a particular DNA molecule require cutting the DNA into fragments, using that endonuclease, and by various techniques determining the proper arrangement for reordering fragments that would allow for reconstruction of the DNA molecule. This is accomplished by a combination of molecular biological techniques that include multiple partial digestions of the DNA molecules, gel fractionation, hybridization with labeled end probes, and Southern blot analysis [Watson 1998]. As the size of the clone to be restriction mapped increases, the number of likely restriction sites are also increases, making the ordering of the restriction sites more complicated. For example on a 100 kb clone, locating roughly 20 restriction sites for an endonucleases that cleaves a specific 6 nucleotide sequences, such as *Eco*RI or *Bam*HI, is a difficult process. Locating these sites using conventional technologies would require roughly a month's work assuming that there aren't any problems with rapidly cleaved recognition sites.

One alternative to fragment analysis for identifying restriction endonuclease sites on cloned DNA molecules would be to use AFM to image restriction enzymes bound to restriction sites on the DNA molecule. This method for directly mapping molecules would not be compromised by the number of sites or by problems with rapidly cleaved restriction sites. Enzymes such as wild-type *Eco*RI endonuclease [Niu 1993], RNA polymerase [Bustamante 1992, Zenhauseren 1992, Hansma 1993], and other proteins [Erie 1994] have been imaged bound to DNA molecules. Imaging DNA with the AFM has rapidly advanced as methods have been developed to produce both positive functionality to mica surfaces using divalent cations [Vesenka 1992, Bustamante 1992], and amino functionality using aminopropyltriethoxysilane [Lyubchenko 1992] to immobilize negatively charged DNA to the positively charged mica surface.

Mapping DNA by imaging relatively small restriction enzymes bound to DNA molecules is a challenge because the small size of the enzyme allows it to be confused with background noise. This might be especially problematic when large areas are scanned in an attempt to map cloned molecules.

*Eco*RI is a dimeric globular protein with a molecular weight of 62,000 that recognizes the six nucleotide base sequence GAATTC with the two monomeric subunits of the dimeric protein binding to this site and the complementary site on the double-stranded DNA molecule [Green 1981, Newman 1981, McLarin 1986]. In order to identify *Eco*RI sites on intact DNA molecules the enzyme needs to bind to the DNA molecule but not cleave the DNA molecule. This can be accomplished by using a mutant, Gln 111, *Eco*RI endonuclease that binds to DNA with an affinity 1000 times greater than the wild-type endonuclease but does not cleave the DNA molecule [Wright 1989]. Using this enzyme we have done proof-of-principle experiments by identifying through AFM imaging *Eco*RI binding sites on linearized plasmids having either one or two binding sites. Furthermore, we have scaled up the technique and demonstrated the precision of the technique by mapping the five *Eco*RI sites on 48,502 bp lambda DNA. We have further demonstrated the application of the technique by mapping mouse cosmid clones.

Materials and Methods

DNA Samples used

The plasmids used in our study were 3204 base pair pBS$^+$ (Stratagene, La Jolla, CA) that has a single *Eco*RI site; and 4933 base pair pGEM-*luc* (Promega, Madison, WI) and 6821 base pair pSV-ß-galactosidase (Promega, Madison, WI) both which have two *Eco*RI sites. The three plasmids were linearized with *Sca*I (Live Technologies, Gaithersburg, MD) using the protocol recommended by the manufacturer, phenol chloroform extracted, ethanol precipitated, and suspended in 10 mM Tris-HCl + 1.0 mM EDTA (TE) at pH 7.5 to a final concentration of 200-400 µg/ml [Sambrook 1989]. The two larger DNA samples used in this study

were bacterial phage lambda DNA with 48,502 base pairs (Sigma, St. Louis, MO) and 35,000 base pair cosmids isolated from mouse chromosome 7 provided by the Mammalian Genetics Group (Oak Ridge National Laboratory, Oak Ridge, TN).

*Eco*RI restriction endonucleases

The endonucleases used in the study were wild type *Eco*RI endonuclease (Life Technologies, Gaithersburg, MD) and a mutant *Eco*RI (Gln-111), having Gln substituted for Glu at position 111 in the peptide sequence, with a binding site specificity 1000 times greater than wild type but with cleavage rates reduced by a factor of 10^4 from the wild type enzyme [Terry 1985, Wright 1989]. The Gln-111 enzyme was graciously supplied by Dr. Paul Modrich, Duke University, Durham, NC.

Assay used to evaluate Gln-111 mutant binding to DNA

Evaluating binding of the *Eco*RI (Gln-111) mutant was accomplished using the following assay. A 20-50 fold molar excess of the Gln-111 mutant was incubated at 37 ^{o}C with 0.1-0.2 μg of pBS^{+} that had been linearized with *Sca*I in a buffer that we optimized for maximum protection of *Eco*RI sites by the Gln-111 enzyme. The buffer constituents, pH, incubation time and enzyme-to-plasmid ratio were all evaluated to determine the optimal conditions for binding the mutant to the plasmid. In the assay the Gln-111 mutant would be incubated with pBS^{+} plasmid (one *Eco*RI site) for a given length of time followed by a 50 fold excess of wild type *Eco*RI. If Gln-111 was in the *Eco*RI binding site the addition of wild type *Eco*RI endonuclease would have no effect. Results were then analyzed on 1.2 % agarose gel with ethidium bromide Fig. 4-1.

AFM of Plasmid DNA

The plasmid + Glln-111 sample that was used for AFM imaging was made up in 20 μl volume and diluted 1:5, 1:10 and 1:20 in binding buffer; 25 μl aliquots

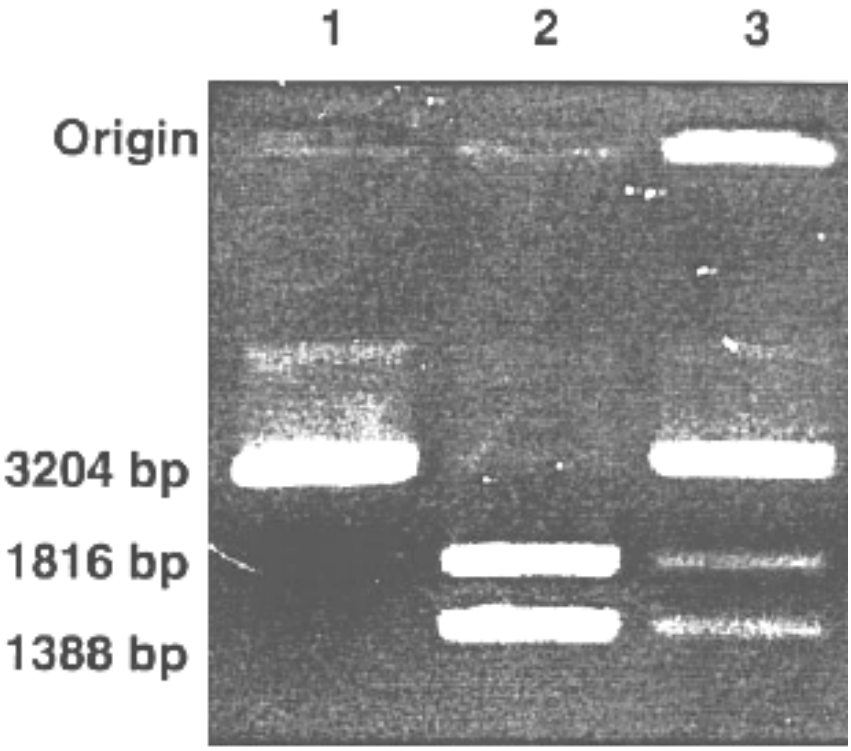

Figure 4-1. Site protection assay. The assay to determine the protective effect of the Gln-111 mutant *Eco*RI endonuclease bound to *Eco*RI sites on DNA molecules when challenged by wild type *Eco*RI is as follows. The assay typically uses pBS$^+$ plasmid, having one *Eco*RI site, linearized with *Sca*I as the test DNA molecule; and gel electrophoresis as the test system. Lane (1) shows the linearized pBS$^+$ DNA only, lane (2) DNA + wild type *Eco*RI, and lane (3) DNA incubated with Gln-111 followed by wild type *Eco*RI. In lane (3) total protection, or degree of protection, by Gln-111, will be determined by cleavage of pBS$^+$.

were applied to freshly cleaved 3/8 inch diameter mica surfaces. After 5 minutes of allowing the sample to adsorb to the mica surface, the sample was rinsed by plunging 10 times into dd-H_2O, further rinsed by plunging 10 times in 1:1 dd-H_2O/100 % ethanol, followed by final rinsing by plunging 10 times in 100 % ethanol. The sample, in ethanol, was placed into the critical point dryer and critical-point-dried [Thundat 1994]. Critical point drying is a technique where samples pass through a "critical point" transition from the liquid to the gas phase where the densities of the liquid and gas phases are equal and there is no phase boundary. This transition occurs in the critical point dryer when the sample in alcohol or acetone placed in the dryer is replaced by a transitional fluid, liquid carbon dioxide, under pressure. As the temperature is increased the pressure also increases until the "critical point" is reached and the vapor phase is exhausted from the sample. This allows DNA on surfaces to be dried without meniscus drying and results in a much cleaner sample for imaging in the AFM imaging. This step, similar to results obtained with the electron microscope [Bibel 1972], does not affect imaging DNA-protein complexes and greatly reduces surface contamination making AFM imaging of unobstructed DNA molecules routine.

AFM imaging lambda and cosmid DNA

Samples of bacteriophage lambda DNA and mouse cosmid DNA site-specifically labeled with the *Eco*RI Gln-111 mutant were prepared for AFM imaging using the methodology that was developed by our group for imaging plasmid DNA Gln 111 complexes [Allison 1996]. Either phage or cosmid DNA was incubated in 0.15 μg of DNA in 0.01M potassium phosphate + 0.15 M sodium chloride + 0.01 M magnesium acetate at pH 7.5 with a 20-fold excess of Gln-111 *Eco*RI mutant added. After 30 minute incubation at 37 ^{o}C, 27 μl of sample was placed on the 3/8 inch cleaved mica disk and the rinsing and critical point drying was carried out as described above.

Atomic force Microscopy

After critical point drying, the samples were imaged in a Nanoscope II SPM operating as an AFM (Digital Instruments, Santa Barbara, CA). Imaging was accomplished in contact mode using 200 μm silicon nitride cantilevers with spring constants of 0.12 N/m (Nanoprobes, Digital Instruments, Santa Barbara, CA). Images were acquired at a scan rate of 2.85 Hz with an information density of 400 X 400 points. Since both contrast and imaged sample width are affected by friction and relative humidity, the direction of scan was often rotated to minimize friction [Thundat 1992_b]. To minimize the effects of humidity the AFM was placed in an environmental chamber where the humidity could be controlled and maintained below 15% by purging the chamber with dry nitrogen gas. All of the images presented have been first-order flattened. The microscope was calibrated with a calibration grating supplied by the manufacturer. This allowed making accurate measurements from DNA images using the digital analysis software, NIHIMAGE, National Institutes of Health.

Results: Developing the *Eco*RI Site protection assay

Imaging biological molecules with the STM requires conductivity to obtain images consistently. Although we demonstrated that it is feasible to image entire plasmids by immobilizing DNA to alkanethiol derivitized gold surfaces, we are not confident that we solved the problems that would allow the STM to be routinely used as a research tool. Alternatively, DNA can be adsorbed to mica surfaces and imaged by AFM [Thundat 1992_a, Allison 1992]. However, sample preparation for this method ultimately results in images of DNA molecules that are super-twisted by drying stress to the point that accurate measurements of contour lengths are not possible.

Treatment of freshly cleaved mica surfaces with magnesium [Vesenka 1992]. barium [Thundat 1993], or cobalt [Thundat 1992] allows DNA to be applied to mica surfaces resulting in stabilized molecules where contour lengths can be

accurately measured. Recently, it was found that including magnesium in the buffer with the DNA prior to adsorption to the mica surface allows the DNA molecules to attach to the surface, thereby producing good imaging results. In addition, adding the divalent cation nickel to the mounting buffer permits DNA to adhere to the mica surface with sufficient strength to allow AFM imaging in liquid [Bezanilla 1994].

*Eco*RI Site protection assay

As a first step toward developing a methodology for mapping DNA using the Gln-111 mutant *Eco*RI endonuclease that site-specifically binds to but does not cleave DNA, our efforts were put toward developing the optimal conditions for binding. This required developing an assay that would allow assessment of binding of the mutant endonuclease to DNA. Fig 4-1 (see Materials and Methods) shows the three gel lanes required for the assay. The first lane has only the *Sca*I linearized plasmid and shows just one band on the gel. The second lane shows the effect of incubating *Sca*I with excess wild type *Eco*RI for 20 minutes. The third lane shows the protective effect of the Gln mutant when it is incubated with the DNA for 15 minutes prior to adding wild type *Eco*RI, followed by 20 minutes incubation, prior to gel electrophoresis. It is clear that in lane 3 the mutant occupying the binding site prevents the wild type enzyme from binding and cleaving the DNA.

Using this rationale for our assay, we evaluated binding parameters by incubating Gln-111 with linearized pBS^+ in the buffer that we eventually worked out to produce the best results. This buffer was 100 mM sodium chloride + 10 mM magnesium acetate + 10 mM potassium phosphate at pH 7.5. This assay was then used to evaluate other parameters including optimal pH for binding Gln-111 to DNA, the minimum incubation time for binding the mutant to DNA, concentration of sodium chloride, concentration of magnesium acetate, and the concentration of Gln-111 necessary for optimal results.

In addition to finding the optimal conditions for binding the Gln-111 mutant to the single binding site on pBS+ plasmid, AFM image quality was evaluated for other buffers. Because the AFM acquires images by mechanically tracing the surface, any substance on the surface can contribute to the image. As a result adsorbates either on the sample or contaminating the mica surface will be imaged and have the potential to introduce error into our results. Therefore, our efforts were concentrated on selecting sample mounting solutions that minimized buffer salt contamination of both the sample and substrate. For example, using calcium as the divalent cation in place of magnesium was a disaster; even at mM concentrations our images showed significant calcium phosphate contamination.

Our results indicated that in terms of clarity of the image and lack of contamination there was not a better buffer than phosphate based buffer. We found that TE buffer with magnesium acetate could be substituted in the assay for the phosphate, but the images with the phosphate buffer were generally superior. This held true for all the buffer conditions we evaluated.

Results: Restriction mapping plasmids by AFM imaging

AFM imaging of pBS+ with Gln-111 mutant

Fig 4-2 shows the results obtained by incubating the Gln-111 mutant pBS+ in 100 mM sodium chloride + 10 mM magnesium acetate + 10 mM potassium phosphate buffer at pH 7.5 followed by placing an aliquot of the sample on freshly cleaved mica, thoroughly rinsing in dd-H_2O, rinsing in 1:1 dd-H_2O and ethanol, followed by rinsing in ethanol and critical point drying. In this image of a field of *Sca*I linearized pBS+ plasmid DNA molecules, it is apparent that three of the DNA molecules show the Gln-111 endonuclease bound in the correct spot, i.e. about in the middle of the molecule. One other plasmid molecule has the enzyme bound nonspecifically, a condition that was not often observed.

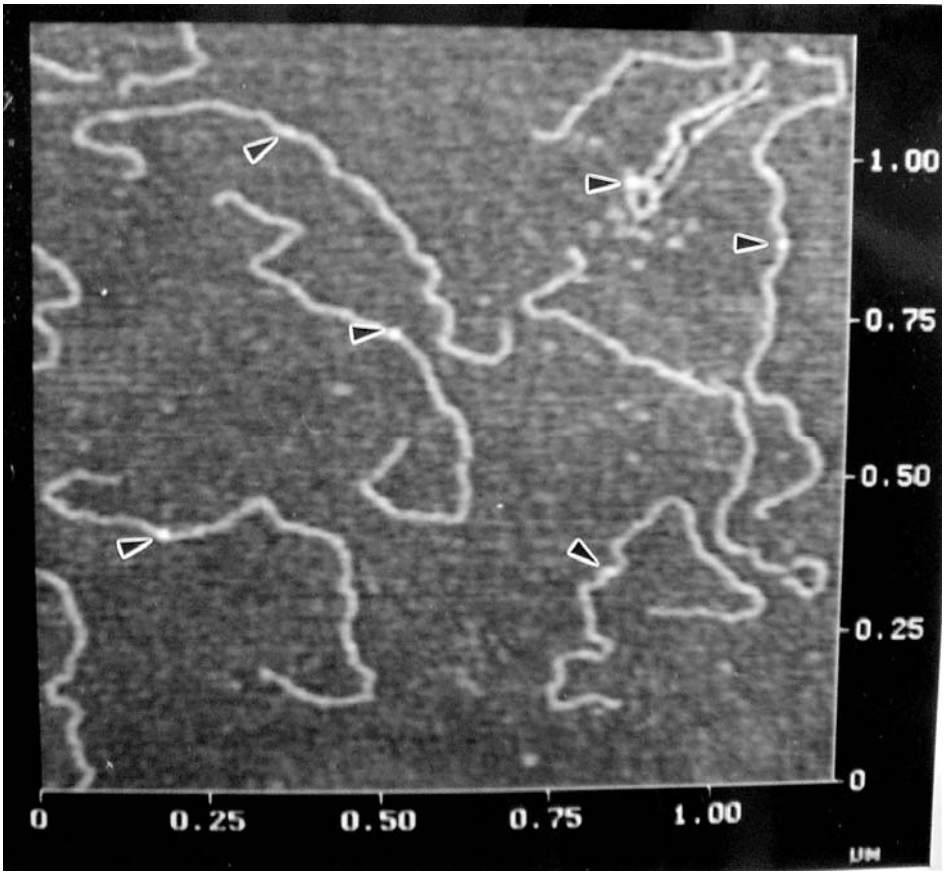

Figure 4-2. A field of pBS⁺ plasmid with Gln-111 mutant site-specifically bound to *Eco*RI site. A field of pBS⁺ plasmids with Gln-111 mutant *Eco*RI nuclease site-specifically bound to the centrally located *Eco*RI restriction site on the molecule (arrow heads). This is the beginning of a project to use AFM imaging to map genomic DNA by AFM imaging the Gln-111 mutant endonuclease specifically bound to all the *Eco*RI sites on DNA molecules.

AFM mapping plasmids

In order to evaluate this new technique as a potential application for physically mapping DNA by AFM imaging, our next experiments concentrated on using two other plasmids, pGEM-*luc* and pSV-ß-galactosidase both of which have two *Eco*RI binding sites. All of the plasmids pBS$^+$, pGEM-*luc* and pSV-ß-galactosidase used in this study are well characterized with respect to molecular length and position of restriction enzyme sites. The three plasmids were also chosen according to their degree of complexity.

Fig. 4-3$_a$ shows plasmid pBS$^+$ the smallest and therefore the simplest with 3204 base pairs and only one *Eco*RI binding site identified by Gln-111 site-specifically bound. Fig. 4-3$_b$ shows pGEM-*luc* with 4933 base pairs and two *Eco*RI binding sites occupied by the Gln-111 mutant endonuclease. Fig. 4-3$_c$ shows pSV-ß-galactosidase, the largest and therefore the most complex plasmid, with 6821 base pairs and two *Eco*RI endonuclease sites identified by the presence of Gln-111 in the *Eco*RI sites. All of the images were taken at the same height scale, as shown in Fig. 4-3$_a$, where the color scale height is a gradient from 0 to 4 nm with yellow being low and black being high.

In all of the images the DNA molecules are above the mica surface that appears as yellow-orange in the color gradient. The DNA molecules appear in the orange-red region of the gradient while bound Gln-111 endonuclease due to the added height appears as a black dot. This color gradient can be exploited for the easy separation and therefore identification of the bound enzyme (dark spot) which is higher than the orange-red DNA molecules.

In Fig.4-4 the maps of all three plasmids linearized with *Sca*I are shown with the position of *Eco*RI sites identified along with molecular lengths both in base pairs and in nanometers. These maps are constructed assuming that the molecules are in B-form DNA with 0.34 nm interbase distance [Watson 1988]. In Fig. 4-4 the values in parentheses are the experimental values of measurements made using NIHIMAGE on at least 20 molecules from each plasmid. Using standard deviation criteria, these results show that AFM mapping of the

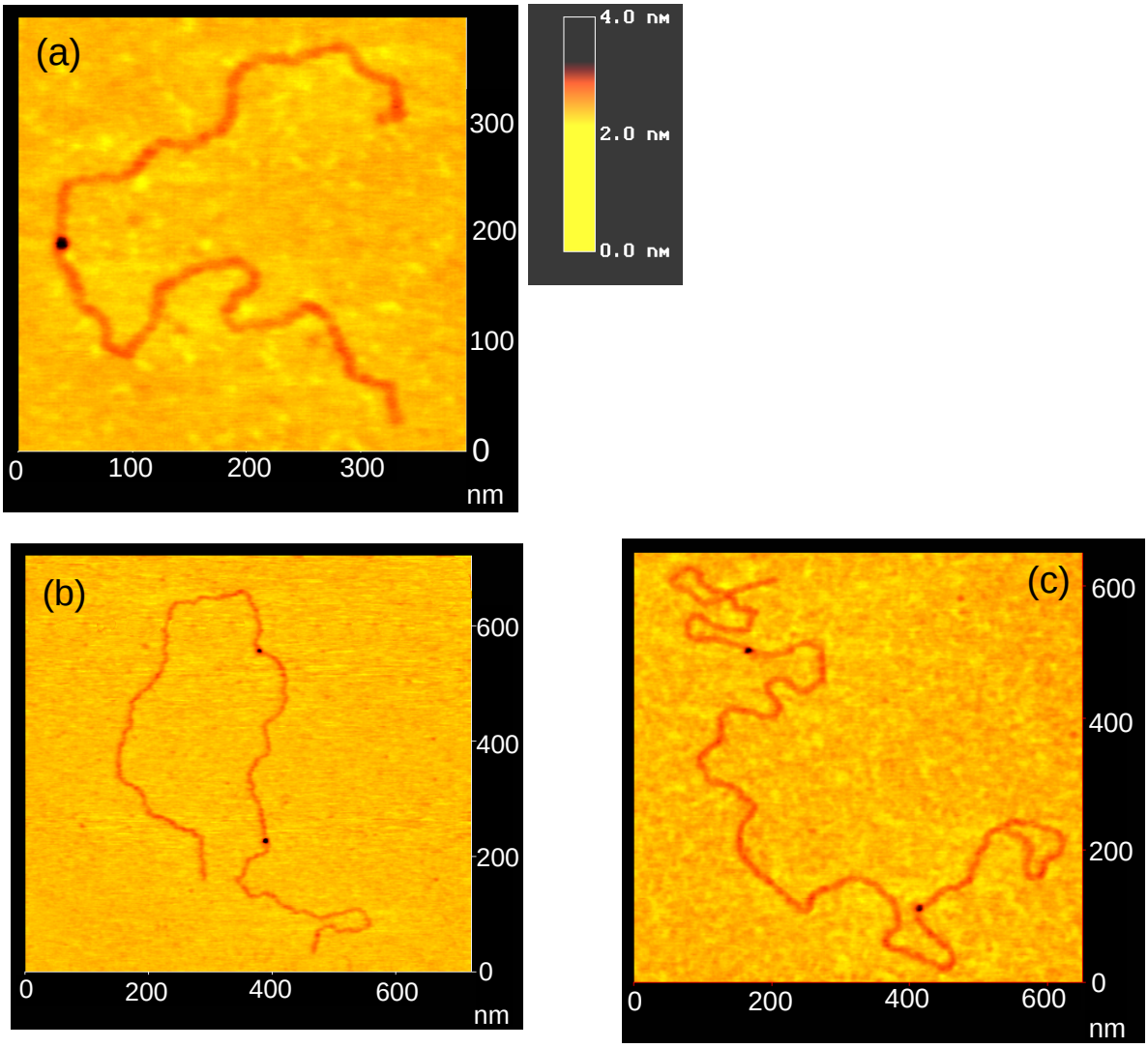

Figure 4-3. Images of pBS⁺, pGEM-*luc* and pSV-ß-galactosidase plasmids with Gln-111 mutant endonuclease bound to *Eco*RI sites. Images of pBS⁺ with one *Eco*RI site and pGEM-*luc* and pSV-ß-galactosidase each with two *Eco*RI sites are shown with mutant Gln-111 *Eco*RI endonuclease site-specifically bound to *Eco*RI restriction sites. In the figure (a) plasmid pBS⁺ with 3204 base pairs, (b) pGEM-*luc* 4933 base pairs and (c) pSV-ß-galactosidase 6821 base pairs, are shown imaged and mapped by AFM.

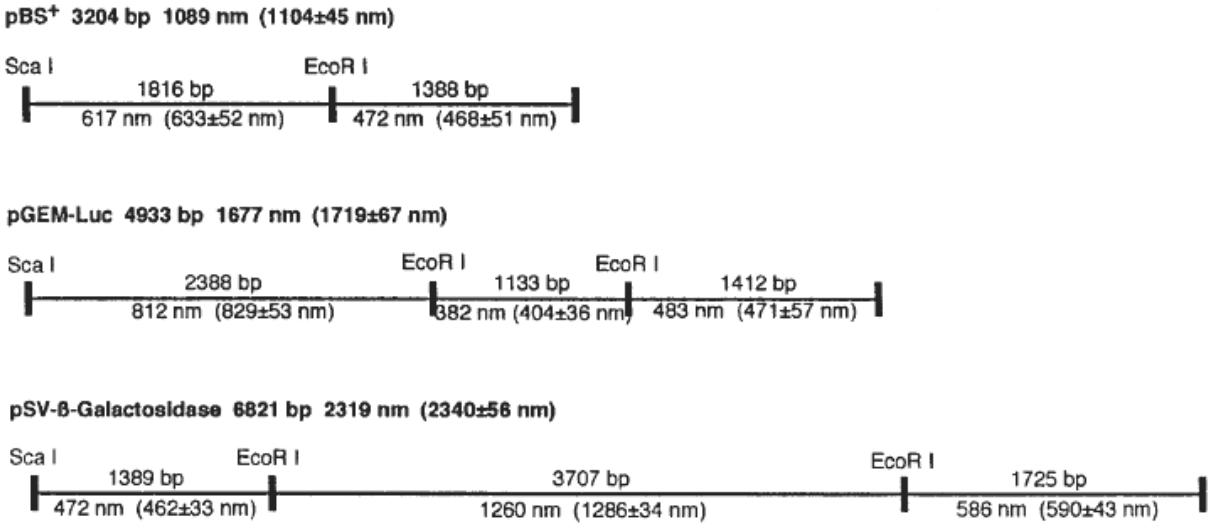

Figure 4-4. Plasmid maps of pBS$^+$, pGEM-*luc*, and pSV-ß-galactosidase. The maps of the plasmids cleaved with *Sca*I endonuclease are drawn to scale and show the position of *Eco*RI binding sites for each plasmid. Known map distances are given in both base pairs and in distances between *Eco*RI binding sites. The experimental data are presented in parenthesis with distances between *Eco*RI sites and standard deviation given in nm. The number of molecules measured to collect the data were 26 pBS$^+$, 24 pGEM-*luc* and 25 pSV-ß-galactosidase.

site-specific binding of the *Eco*RI Gln-111 mutant is accurate to about 100 base pairs. However, as can be seen from the results with all three of the plasmids, the actual figures are much more impressive.

Results: Mapping clone sized DNA by AFM imaging

AFM mapping lambda DNA

After demonstrating the utility of mapping plasmids with the Gln-111 enzyme site-specifically bound to plasmid DNA molecules, our next endeavor was to apply the technique to mapping larger clone-sized DNA molecules. Bacteriophage lambda served as a test for determining both the accuracy and resolution of the AFM mapping system. Lambda DNA was a logical choice since it was a cosmid-sized DNA molecule that had been sequenced with 48,502 base pairs and 5 characterized *Eco*RI restriction sites [Sanger 1982]. The protocol used to incubate the lambda DNA with the Gln-111 endonuclease was the identical protocol described earlier to map the *Eco*RI restriction sites on plasmid DNA molecules.

It is obvious from the image presented in Fig. 4-5 that all 5 *Eco*RI restriction sites are labeled with the Gln-111 mutant endonuclease. Due to tip convolution effects, AFM images of DNA molecules in air are typically imaged with widths of 9-15 nm as opposed to the known 2 nm known width of DNA [Vesenka 1992, Allen 1992, Thundat 1992]. However, tip convolution effects are an asset when imaging large DNA molecules: the imaging field must be decreased in order to image the entire molecule and the DNA molecules are much easier to see due to tip broadening effects. Since we did not need to use the horizontal effect of the bound Gln-111 to *Eco*RI sites in the plasmid experiments to identify binding, we used instead the differences in height. We also used height differentiation in the lambda DNA samples.

In the lambda DNA image the color scale is again set to a maximum Z range of 4 nm with the gradient from 0 to 4 nm with the surface being yellow and

Figure 4-5. Image of the entire length of lambda DNA with *Eco*RI sites identified. A contact AFM image of the entire length (48.5 kilobase pairs) of lambda DNA with all 5 *Eco*RI sites labeled with the Gln-111 mutant *Eco*RI restriction endonuclease. The width of the DNA molecule is imaged (due to tip convolution effects) as being 14 nm wide, instead of the 2 nm known width of DNA. This is an asset when imaging large molecules since it makes molecular resolution possible when the scan area must be extended to capture large molecules. By setting the color scale to 4 nm, the vertical component of the microscope is used to significant advantage since the extra height that the Gln-111 mutant contributes when bound to an *Eco*RI can clearly be identified.

progressing through red to black at the height of 4 nm. The image clearly shows the DNA molecule to be in the orange-red region and the 5 bound Gln-111 endonuclease molecules contributing additional height and appearing as black dots.

The accuracy with which *Eco*RI sites can be located on the lambda DNA molecules is shown in Fig. 4-6. The data collected in the figure came from measurements on 34 molecules. The measured mean molecular length of 15.4 μm of the 34 molecules was used to normalize the experimental data to 16.4 μm in order to reflect the B-form length of lambda DNA. This normalization was done to account for possible errors due to instrument calibration, structural variability in the DNA molecules and other experimental variability.

The experimental accuracy for mapping distances between two sites where the Gln-111 mutant enzyme is bound is clear from the data present in Fig. 4-6. These distances correspond to fragment lengths that would result if the wild type *Eco*RI endonuclease had been used to cleave the lambda DNA molecules. If at least 10 enzyme-to-enzyme distances are included in a data set, the standard deviation is about 3%, with the expected error of the mean being about 1%. Since bound endonuclease and therefore fragment lengths are recorded directly by AFM imaging, neither the number nor the size of the fragment affects the result. This is in contrast to conventional gel-based analysis where migration through the gel matrix does depend on the size of the fragments [Sambrook 1989]. For example, in the experiment to determine whether Gln-111 was bound to the lambda DNA molecules, gel electrophorsis that we used did not separate the 5804 and the 5643 fragments. In contrast, with AFM mapping this is easily accomplished and errors introduced by fragments of near equal size that are problematic in conventional gel-based mapping are eliminated.

Variable affinity of *Eco*RI sites

Although the cleavage site for *Eco*RI is the six nucleotide sequence GAATTC, there is a known problem with variability between individual sites [Thomas

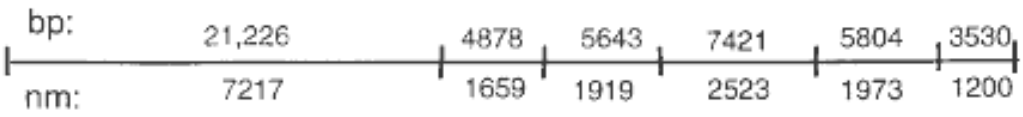

Section	Known Length (bp)	Known Length (nm)	Experimental Measured (nm)	Difference
1	21,226	7217	7153±253	0.9%
2	4878	1659	1666±55	0.4%
3	5643	1919	1905±74	0.7%
4	7421	2523	2521±102	0.1%
5	5804	1973	1969±86	0.2%
6	3530	1200	1194±58	0.5%

Figure 4-6. Lambda DNA map showing *Eco*RI sites. A lambda DNA map with the positions of *Eco*RI sites marked. Distances between *Eco*RI sites are presented in both base pairs and nanometer lengths. The experimental data was was collected and analyzed from images of over 30 lambda DNA molecules. Imaged *Eco*RI sites when compared with known values are located with better than 1% accuracy.

1975]. During our study with the multiple *Eco*RI sites on the lambda DNA molecule, it became apparent that there was also variability in the affinity of the individual sites to bind the Gln-111 mutant enzyme. Our results of the 34 lambda DNA molecules mapped showed that 11 out of 34 molecules had all six *Eco*RI sites labeled with Gln-111. However, our results indicated that three of the *Eco*RI sites bound the mutant endonuclease better than 90% of the time while two other sites were about 50% effective in binding the Gln-111 endonuclease. It is also noteworthy that in the lambda mapping experiments involving 34 mapped molecules, only 8 instances of nonspecific binding of the Gln-111 mutant were identified by AFM imaging.

AFM mapping cosmids

The demonstrated success with mapping well characterized plasmid and lambda DNA molecules with the Gln-111 mutant of *Eco*RI endonuclease was applied to mapping uncharacterized cosmid DNA. In these experiments cosmid clones from mouse chromosome 7 having exons of the *Gabrb3* gene were targeted for mapping by AFM imaging. In Fig. 4-7 the Gln-111 mutant endonuclease can be seen bound to six *Eco*RI restriction sites.

Although the more familiar topographic image is generally used to collect the experimental data, a surface plot where the attachment of the Gln111 mutant is more accentuated is shown in Fig. 4-8. As in the experiments with lambda and plasmid DNA molecules, the vertical component was used to identify the bound enzyme. The height component contributed by the bound endonuclease is especially accentuated in the surface image where the image plane is tilted and the bound enzymes appear as spikes on the DNA molecule.

Since the affinity for binding endonuclease differs between *Eco*RI binding sites, a number of cosmid molecules must be mapped in order to insure that sufficient data has been collected to identify all the binding sites. This is especially true when the data presented depends on measured distance between two bound enzymes and it is imperative that both of the enzymes are identified.

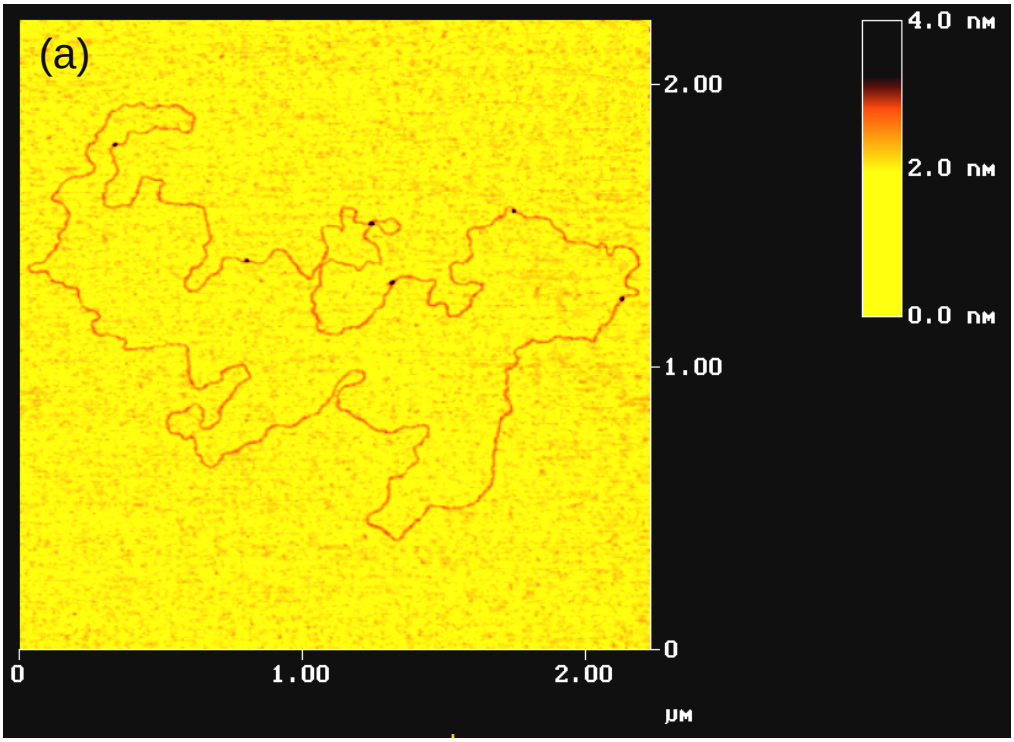

Figure 4-7. AFM image of 35 kilobase cosmid DNA from mouse chromosome 7. A topographic image of a 35 kilobase cosmid isolated from mouse chromosome 7. This had not been mapped by conventional techniques and was mapped by identifying the Gln-111 mutant *Eco*RI endonuclease site-specifically bound to all 6 *Eco*RI sites on the cosmid. Taking advantage of the gradient height scale set to a maximum of 4 nm allows easy identification of the bound enzyme.

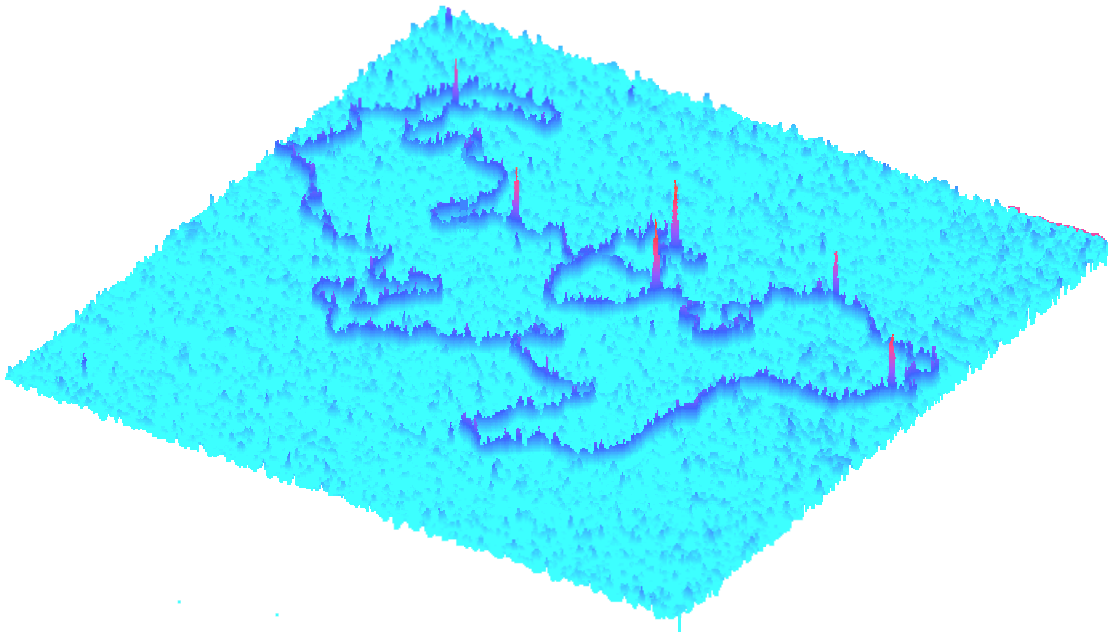

Figure 4-8. A surface plot image of the topographic image in Fig. 4-7. By tilting the topographic image presented in Fig. 4- a surface plot image is generated where height differences can be dramatically demonstrated. Perhaps future experiments will use this form of image presentation to identify two or more site-specifically bound proteins by differences in molecular weight and size.

For example, in the data presented in Fig.4-9 the two Gln-111 enzymes that define the 2297 and the 3126 base pair distances are present in 9 of 10 cosmid molecules imaged. However, at the other extreme, the two binding sites that define the 4118 and the 19,544 the distances bound enzymes are present respectively, in 3 and 2 of ten cosmids imaged. This process can be greatly facilitated if a wild type *Eco*RI digest of the cosmid is used in conjunction with gel electrophoresis to identify and size all of the fragments. In this way one can be insured that all of the distances between *Eco*RI sites on the cosmid, located by AFM, match the size and number of fragment lengths identified by gel electrophoresis.

The numerical data presented in Fig.4-9 is all experimental data since this is an uncharacterized cosmid molecule. The cosmid sample unlike the well characterized lambda DNA sample required the use of agarose (8%) gel analysis to confirm that all of the fragments had been identified. In Fig. 4-9 lane 3 the 19554, 4118, 3750, and 3126 are all identified as separate bands while the 2350 and the 2297 that differ by only 53 base pairs are not separated on the gel. In lane 4 the data also show the type of experiment used to determine the optimal binding conditions for the Gln-111 mutant enzyme where incubation of the mutant endonuclease with DNA is followed by incubation wild type *Eco*RI to determine the prophylactic effect of the mutant [Allison 1996].

Discussion

The results presented in this study have established that restriction mapping by AFM is a viable new approach to physically map cosmid-sized DNA clones. This has been accomplished by imaging a mutant, Gln-111, *Eco*RI endonuclease that preferentially binds to *Eco*RI sites with an affinity 1000 times greater than wild type *Eco*RI, but does not cleave the molecule. Imaging entire cosmid sized molecules, such as lambda DNA, site-specifically decorated with bound Gln-111 endonuclease has shown that distances between two bound enzymes, corresponding to fragment lengths, can be measured with 1% accuracy.

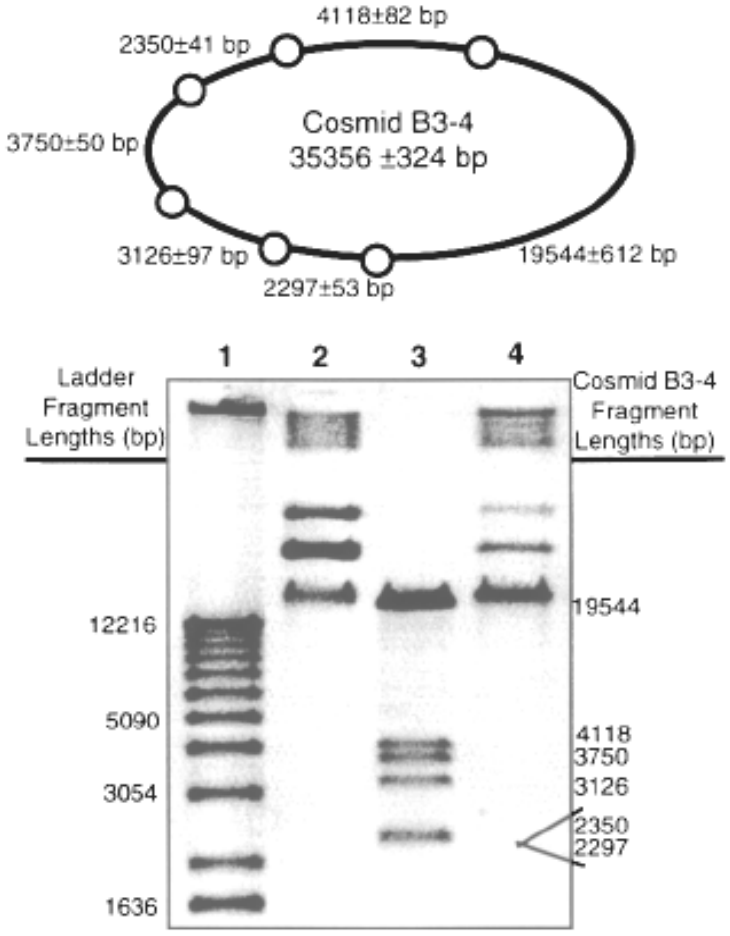

Figure 4-9 Agarose gel electrophoresis of cosmid from Figure 4-7. Agarose gel analysis and AFM mapping data are presented and used to confirm that all six *Eco*RI sites on the 35 kilobase cosmid (Fig. 4-7) have been identified. The experimental data is shown in the schematic where measured distances between *Eco*RI sites, identified by site-specific binding of the Gln-111 mutant *Eco*RI endonuclease, have been converted to base pairs. The 2350 and 2297 fragments were not identified on the gel, but could be easily identified by AFM mapping. Lane (1) is the 1 kilobase ladder, Lane (2) is mouse cosmid B3-4, Lane (3) is cosmid + wild type *Eco*RI, :ame (4) is cosmid + Gln-111 mutant followed by wild type *Eco*RI.

Differences in affinity for binding Gln-111 has been found to vary between *Eco*RI sites with some sites binding Gln-111 enzyme with 90% affinity while other sites have binding affinity as low as 20%. This has necessitated multiple imaging of cosmids in order to get statistically meaningful data.

Mapping Cosmids

In this study we have shown that AFM mapping can be used to map cosmid DNA molecules where the position of *Eco*RI sites are unknown. This was done using circular cosmids from mouse chromosome 7. Future efforts to map cosmids should be accomplished on linearized molecules. For example, a rare-cuttting endonuclease, one that identifies an 8 nucleotide sequence that would cleave DNA on the average every 64,000 base pairs, could be inserted into the cosmid vector together with an *Eco*RI site a known distance from the rare-cutting endonuclease. By identifying the inserted *Eco*RI site, occupied by Gln-111 a known distance from the end of the cleaved cosmid, would determine that the cosmid was cleaved at the vector and would determine the vector position in the linearized cosmid. Concurrently with AFM mapping studies, that will correctly identify the position of and the fragment length between *Eco*RI sites, gel electrophoresis should be done to identify and size all the fragments from a wild type *Eco*RI digest of the cosmid. This will insure that all of the *Eco*RI sites on the cosmid have been identified by AFM imaging when size and number of fragments agree between the two techniques.

AFM tip effects on images

AFM imaging of DNA molecules results in a broadening of the 2 nm DNA molecule to 9-15 nanometers. This is caused by the tip mounted on the end of the AFM cantilever touching the DNA molecule while imaging in contact mode. Image broadening is due to tip convolution, or more precisely the radius of curvature of the AFM tip. If just the end of the tip that contacts the DNA molecule is thought of as a hemisphere, the radius of the hemisphere is what you actually

image when you imaged the DNA. As the tip is scanned across the DNA molecule, first contact is made by the side of the hemispherical tip; as the tip rides up and over the molecule in contact with the DNA molecule the height information is being gained from this hemispherical tip and an image is formed. This broadening effect is an asset because it makes the larger lambda and cosmid molecules easier to image, and the lower resolution necessary to see molecules allows the entire molecule to be recorded in a single scan. Tip convolution only affects the lateral image and not the vertical since at the top of the DNA molecule only the very center of the tip is touching the molecule so the height is correct but width is not correct. In principal the DNA at this point should be 2 nm high and anything attached to the DNA such as the Gln-111 endonuclease would be contribuiting to additional height.

This height differential is what has been exploited in the identification of enzyme binding and is especially obvious in the surface image in Fig. 4-8, where the tilted surface plane allows the bound Gln-111 endonuclease to be imaged as spikes. The height of the bound enzyme might also be exploited as an estimate of molecular weight of the protein, or perhaps to differentiate between two or more bound proteins of different molecular weights, allowing for experiments with multiple enzymes.

Problems with identification of *Eco*RI sites

Fig. 4-10 is an image of a different 35 kilo base cosmid from mouse chromosome 7 and is included to point out that the *Eco*RI sites are well defined with bound Gln-111 endonuclease. Mapping this entire molecule at first glance would seem to be easy. However, on closer inspection there are four sites where one cannot determine which DNA strand is bound by the endonuclease. This problem could be solved by spreading the DNA molecule out in order to prevent places where the two DNA strands cross. Ideally this would be done on linear DNA molecules.

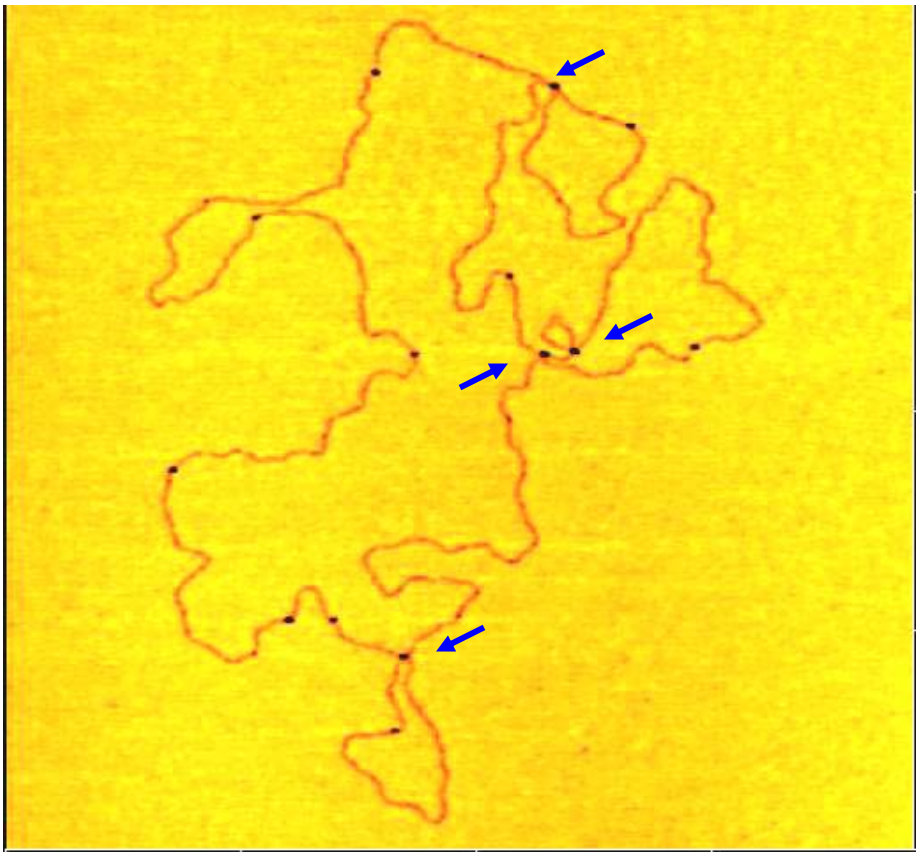

Figure 4- 10. 35 kilobase cosmid from mouse chromosome 7 with 14 *Eco*RI sites. This image is included to point out that multiple *Eco*RI sites can occur that greatly exceed the expected 6-7 *Eco*RI sites that would be expected in a 35 kilobase DNA molecule and to point out difficulties that arise when portions of the DNA molecule are close together. Assuming that DNA sequence is random the GAATTC sequence that identifies *Eco*RI endonuclease binding site should occur every 4096 base pairs and 6-7 sites would be expected on the cosmid instead of the 14 that is seen on this cosmid. Also, there are 4 sites (blue arrow) where difficulty arises as to which DNA strand is binding the Gln-111 enzyme.

It is also interesting to note that when we calculate the probability of an endonuclease that recognizes a six nucleotide sequence, including *Eco*RI that recognizes GAATTC, the enzyme should bind every 4096 base pairs on the average, assuming that nucleotide sequence in the DNA molecule is random. This does not always hold true since in the 35 kilobase cosmid in Fig. 4-10 shows 14 *Eco*RI sites when the expected would be 8, whereas the cosmid we mapped with 6 sites shows close to the expected average of 8. In Lambda DNA, which is a 48,502 base pair well characterized molecule, there are only 5 *Eco*RI sites, while there should be around 11 sites considering the size of the molecule.

Development of this technology as a practical mapping tool would require further work primarily by cleaving the plasmid at its vector site and by developing a method to straighten the molecule on the mounting surface. However, these results have established that our efforts have introduced a viable approach to mapping cosmid size clones that might be more accurate and perhaps much simpler to use than conventional techniques.

Chapter 5
Summary and future prospects

Summary

The work described in this thesis occurred during an exciting time for biological research. Newly invented scanning probe microscopes, such as the STM and the AFM, were becoming commercially available in 1987 and in 1989 respectively. At Oak Ridge National Laboratory our research group consisted of two physicists, Tom Ferrell and Bruce Warmack, who had built an STM in their lab; and a biologist, Dave Allison, who had worked with electron microscopes imaging biological samples. Our group started so early on scanning probe investigations that when the first commercial STM became available the one we purchased was labeled with serial number five. By today's standards these first instruments were primitive. For example, images produced by this first commercial STM were stored by photographing them: we either placed a Polaroid camera in a hood up against the STM computer screen, or we mounted a 35mm camera on a tripod in front of the screen to record the STM images.

At the time our group formed there were only thirteen papers published on the biological applications of scanning probe microscopes, and around thirty other papers related to instrument development and material science applications. Thus, our group found little foundation in scientific literature for designing biological experiments using the STM. Furthermore, our extensive experience with the electron microscopes could not be directly applied to the STM, a fundamentally different imaging instrument. The STM had no lenses, it operated in an ambient atmosphere, and standard EM techniques for specimen preparation did not apply. Under these challenging circumstances we designed and performed our first experiments to image tobacco mosaic virus and DNA.

The Department of Energy Human Genome Initiative

Our STM research fortunately coincided with the inauguration of the DOE human genome initiative. The general idea was to obtain libraries of overlapping cloned DNA from each of the chromosomes that would create the minimum tiling path to recreate the entire chromosome, ensuring a minimum sequencing effort by eliminating redundant sequencing. The genome project was an enormous undertaking and an underlying concern, with sequencing the 3 billion nucleotide bases in the human genome, was cost. In 1987, conventional sequencing methodology was expensive with estimates ranging from 2-3 dollars per base to sequence DNA. Any new technology that might cut sequencing costs or speed up the process was considered. Could the STM, capable of atomic resolution, be developed to sequence DNA or at least physically map cloned DNA? Our first step was to image DNA.

Imaging DNA with STM

Our group found itself in a race with other laboratories to publish images of DNA taken with the STM. Scanning required the DNA to be placed on an atomically flat surface such as crystalline gold or highly ordered pyrolitic graphite (HOPG). We published our first topographic STM images and STS images of DNA [Allison 1990] by simply adsorbing plasmid DNA to a graphite surface. Others also published images of DNA during this period [Travaglini 1987, Arscott 1989, Beebe 1989, Lee 1989, Keller 1989] using the same methodology. However, it became apparent that forces exerted by the STM tip during scanning removed DNA from these atomically flat mounting surfaces. DNA was being swept off the flat surface as it was imaged.

This led us to develop a technique for immobilizing DNA to the scanned surface. We used a self-assembled monolayer of 2-dimethylaminoethanethiol on a crystalline gold surface that allowed the positive charge on the amino group to attract and hold the negatively charged DNA on the surface [Allison 1992$_a$, Bottomley 1992]. This derivitized surface immobilized the DNA on the scanning

surface, and allowed us to produce the first STM images of entire genetically functional plasmid DNA [Allison 1992b, Bottomley 1992, Allison 1993].

Although our progress was encouraging, the poor conductivity of DNA was a roadblock to quick routine imaging with the STM. It was apparent that the STM was not suitable for the DOE genome sequencing effort. However, by this time the AFM had become commercially available, and was proving to be a more reliable scanning microscope for routine DNA imaging. Unlike STM that required conductivity for imaging AFM mechanically interacted with the surface and could be used to image both conductive and nonconductive samples. Accordingly, our group decided to develop a technology for mapping DNA with the AFM.

Mapping DNA with the AFM

Once commercial instruments became available, DNA imaging with the AFM advanced rapidly. The mounting surface for DNA imaging was freshly cleaved mica. A positive charge established on the mica surface immobilized the negatively charged DNA molecules for AFM imaging. This was accomplished by either including a divalent cation, such as Mg^{2+}, Ni^{2+}, or Co^{2+}, in the DNA solution applied to surface [Vesenka 1992, Thundat 1992b, Bezanilla 1994]; or by treating the mica surface with a silane compound with a positive head group, such as aminopropyltriethoxysilane (APTES), to immobilize the DNA molecules to the surface electrostatically [Lyubchenko 1992].

Our approach to physically mapping cloned DNA was to use AFM imaging to locate *Eco*RI restriction endonuclease sites on individual DNA molecules. Conventional restriction mapping was a well recognized method for physically locating either *Bam*HI or *Eco*RI restriction sites on DNA molecules. Basically, the DNA was cleaved with the endonuclease and various means were used to reorganize the fragments in the correct order. The time required to restriction map a clone was compromised by both the number of restriction sites and by sites that were slow to cleave. Our approach using AFM to directly identify

restriction sites on DNA molecules would not be compromised by the number of sites and would only be affected by differences in affinity for the *Eco*RI enzyme.

In proof-of-principle experiments on plasmid DNA we demonstrated that we could directly identify *Eco*RI restriction sites by AFM imaging [Allison 1996]. We used a mutant *Eco*RI endonuclease (Gln-111) that binds DNA with an affinity 1000 times greater than the wildtype endonuclease but does not cleave the molecule [Terry 1985, Wright 1989]. By evaluating various parameters (including buffers, concentrations of Mg^{2+} and NaCl in the buffer used, pH effects, and incubation times) we developed a protocol for optimizing the binding of Gln-111 to plasmid DNA molecules. Furthermore, we produced clean images of DNA unencumbered with contaminants by critical point drying the DNA to freshly cleaved mica. This eliminated contaminant binding that could be mistaken for the enzyme binding of the Gln-111 mutant to DNA.

Our group was the first to demonstrate that cosmid sized DNA molecules could be mapped by AFM imaging. We performed this on bacteriophage lambda DNA, that had been sequenced, thereby identifying all of the *Eco*RI sites. Our AFM images showed all five *Eco*RI sites on the molecule could be identified by imaging the site-specific binding of the Gln-111 mutant endonuclease . We also reported that measured distances between *Eco*RI sites (fragment lengths) were recorded with better than 1 % accuracy compared to known values. During the course of this study we also found that there were significant differences in the binding affinity between *Eco*RI sites, a problem that had also been reported by others [Thomas 1975]. We demonstrated further application of AFM by mapping cosmid clones from mouse chromosome seven.

Future prospects

Following the invention of the STM, there has been rapid growth in the field of scanning probe microscopy (SPM). Scanning microscopes capable of identifying surface properties related to capacitance [Williams 1989], magnetic

properties [Marttin 1987], ion conductance [Hansma 1989], electrochemical parameters [Bard 1991] and near-field optical properties [Pohl 1988] were reported in the literature. As the era of genomics expanded into the era of proteomics and nanotechnology, AFM images of proteins [Quist 1995, Radmacher 1994, Hallett 1995], DNA [Bustamante 1992, Thundat 1992abc, Hansma 1992, Lyubchenko1992], and even images whole living cells [Henderson 1992, Radmacher 1992] were published.

Scanning probe microscopy is now positioned at the forefront of 21st century biological research. SPMs capable of resolution at the nanoscale are in common use, and therefore I won't spend time describing established methods for imaging. A number of review articles and books serve this purpose and can be used as starting points for those who are interested [Bustamante 1996, Hansma 1997, Watanabe 2000, Bonnell 2000]. My objective here is to offer a brief overview of what I feel are key areas where scanning probe microscopes will play a significant role in the future.

Lithography and movement of the AFM tip

Most SPM have closed loop options for extremely accurate movement of the AFM cantilever tip in the XY domains. Researchers for various applications have exploited this capability, and companies that sell instruments have developed user interfaced software for operator-defined movement of the tip. Fig. 5-1 shows a simple demonstration of controlled tip movement. Our group needed a cover image for a conference program in Cancun, Mexico. So in about five minutes I used the AFM tip to plow the word CANCUN on a gelatin-coated mica surface. The letters are about 400 nm in height and the width of the plowed area is roughly 20 nm.

A more sophisticated application of this technique is dip-pen lithography. Here the cantilever tip is dipped into a solution of alkanethiol and used to write nanoscale patterns on crystalline gold surfaces [Piner 1999]. Additionally, the

Figure 5-1. Lithography and movement of the AFM tip. By incorporating closed loop feedback into the movement of the XY-piezo, the AFM tip can be precisely moved and returned to the same area. This has been recognized by manufactures of scanning probe microscopes to the extent that they include software applications that allow the operator to diagram tip movements. By designing a pattern on a template at normal size, that pattern can be translated and copied by the AFM tip at nanoscale resolution. In Fig. 5-1, I spelled out CANCUN as part of a conference program cover for a meeting in Cancun, Mexico. Using the cantilever tip dipped in an ink made of alkanethiol compounds, dip-pen lithography can be use to write nanoscale patterns on crystalline gold surfaces with compounds that can be functionalized for further applications.

alkanethiol can have a functional head group for binding other molecules, such as proteins, to the patterned surface.

A permutation of this technique is nanografting. A self-assembled monolayer of alkanethiol with a methyl terminated head group is patterned on a crystalline gold surface. The entire process is carried out in a liquid environment contained within a flow through wet cell that allows liquid exchange. Another alkanethiol with a functional head group is present in the wet cell solution. As the cantilever tip creates a pattern in the self-assembled monolayer, the pattern is filled in with the functionalized thiol. The system is then flushed out, and the patterned area with the functional thiol head group can then be used immobilize a biomolecule [Wadu-Mesthrige 1999]. By capitalizing on the precision of cantilever movement, and by repeatedly flushing the wet cell with functionalized alkanethiol and perhaps different biomolecules, it is not hard to envision building an enzymatic cascade at the nanoscale.

Force detection with the AFM cantilever

The AFM microcantilever is an extremely sensitive device otherwise forces exerted by the cantilever tip during scanning would likely destroy biological samples. Cantilever sensitivity to forces in the pico Newton range has been exploited in various ways to measure interaction forces between the cantilever tip and biological species. One prerequisite for measuring forces of any kind using the AFM cantilever is that one must determine the spring constant of the cantilever. This can be accomplished in a number of ways, with perhaps the thermal K method being the easiest [Butt 1995].

It is generally accepted that the first force measurement recorded with the AFM cantilever involved measuring the interaction between a silicon nitride cantilever tip and a glass surface [Hoh 1992]. The experiment was done in water, without scanning, by approaching the cantilever to the glass surface, making contact with the surface, and retracting the cantilever. This process could be followed in real time on the computer screen, and if there were an interaction

between the cantilever tip and the surface, a visible adhesion event would be recorded. This experiment, done in Paul Hansma's laboratory, showed a large adhesion peak at pH 5.0. At pH above 9.0, a repulsive interaction between the tip and surface was observed. Interestingly, at pH between 8.5 and 9.0, multiple discrete 12 pN adhesive interactions were observed. They proposed that these multiple interactions could result from either the rupture of individual hydrogen bonds between the tip and surface, or from the interactions with ordered water layers between the tip and surface.

Measuring forces between molecules

A number of experiments have been accomplished with a molecule immobilized on the scanning tip reacting with a molecule immobilized on a surface. This is accomplished in identical fashion as described above, and is illustrated in Fig. 5-2. In this figure I have immobilized biotin on the AFM tip via a polyethyleneglycol (PEG) linker molecule that is roughly 6 nm in length. The tip is then approached to a mica surface coated with avidin. When the tip is retracted, an interaction event occurs as the avidin-biotin bond ruptures. By knowing the spring constant of the cantilever, the rupture force can be calculated.

Similar experiments have been done with an adenine coated tip and a thymine coated surface; the force required to break a single A-T bond was found to be 54 pN [Boland 1995]. In a similar experiment both a gold-coated tip and surface were modified with 11-mercaptoundecanoic acid such that the (S-H groups) bound to the gold, and the carboxylic acid groups on the tip and surface were free to interact. In this experiment the force required to break a single hydrogen bond was found to be 16.6 pN [Han 1995], similar to what was reported by the Hansma group. The force to separate a single avidin-biotin interaction has been determined to be 160 pN [Ludwig 1995]. An experiment where oligonucleotides immobilized on the AFM tip annealed with complementary strands immobilized on a surface have shown that forces of 1.5 nN, 1.11 nN, and 0.83 nN were required

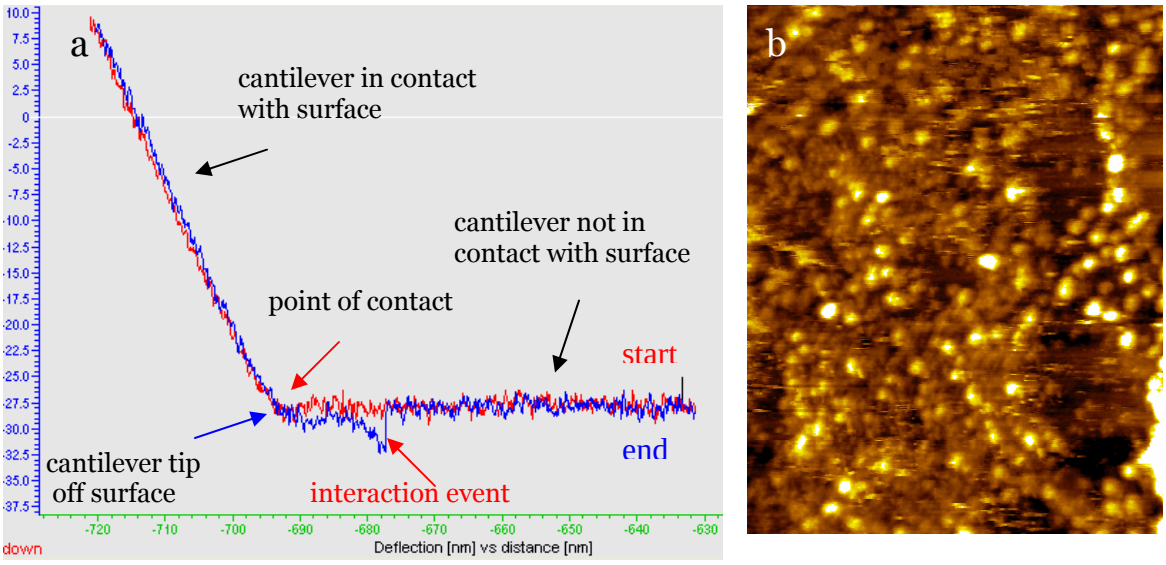

Figure 5-2. Measuring forces between molecules. Shown in Fig. 5-2a is a typical force curve without scanning. On the right side of the curve the cantilever is off the surface (start). By applying a voltage to the height Z-piezo, the cantilever was moved towards the surface, tracing leftward on the force curve (red line). The cantilever approach is shown on the X-axis in nanometers; on the Y-axis cantilever deflection voltage is shown but can be converted to display force. As the cantilever approached the surface, contact was made and the force curve rose left and up. As the cantilever was withdrawn from the surface (blue line) the tip leaves the surface and remains off the surface to the end.

In the experiment shown, Figure 5-2b is a topographic scanned image of an avidin-coated surface. Biotin was tethered to the cantilever tip with a PEG linker about 6 nm in length and allowed to interact with the avidin surface as the surface was approached and contacted. As the cantilever was retracted the interaction event at which the avidin-biotin bond ruptured in Fig. 5-2a was about 6 nm from the point the cantilever tip left the surface. The distance of the event was taken in nm off the Y-axis and the rupture force can be calculated from the known spring constant of the cantilever.

to rupture complementary molecules of 20, 16, and 12 base pairs, respectively [Lee 1994].

This application evaluates interactions between single molecules. In the area of proteomics, it has potential value for evaluating binding forces between proteins, between proteins and DNA, and between other bioentities in their native liquid environment.

Measuring forces within molecules

A force distance, more properly called a force extension curve, can be obtained by approaching a surface with the cantilever tip and retracting the tip from the surface. If there is interaction, there will be adhesion between the tip and the surface. At its simplest, when the tip is approached to a flat surface such as mica, the water layer on the tip contacts the water layer on the surface; an adhesion event can be measured when the tip is retracted. Such experiments have been done with proteins that have multiple folded domains, including structural proteins such as titin and elastin, and also with membrane proteins.

This type of experiment is illustrated in Fig. 5-3. Here a bacterial pore is removed from the hexagonally packed intermediate (HPI) layer of the bacterial cell envelope of *Deinococcus radiodurans*. In the figure, the six interaction peaks correspond to the forces required to remove each of the six protomers of the pore. In the topographic AFM image of the pore in Fig. 5-3a, the six protomers of several pores are clearly imaged. In the force extension curve in Fig 5-3b, the force required to remove each of the protomers ranges from 200 to 300 pN, while the inter-peak distance is averaged to be 7.3 nm. This represents the flexible link between protomers, and is in agreement with the known thickness of the HPI membrane [Müller 1999]. As can be seen from this single molecule experiment, this type of evaluation of membrane proteins could be extended to investigate membrane associated transporters and other membrane associated elements.

Studies of structural proteins have also been done at the single molecule level by simply bringing the AFM tip into contact with the protein and withdrawing the

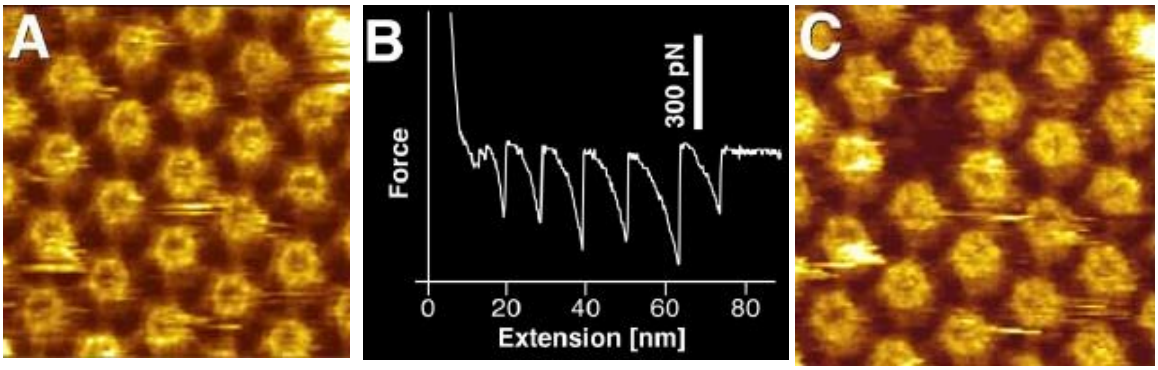

Daniel J. Muller, Wolfgang Baumeister,
And Andreas Engel PNAS (1999) 96: 13170

Figure 5-3. Measuring rupture forces within molecules. (A) A topographic image of bacterial pores from the in the HPI membrane layer of *Deinococcus radiodurans*. The cantilever tip was approached as described in Fig.5-2 to contact a single bacterial pore protein. (B) The force curve produced as the tip was retracted. The six protomers of the protein were sequentially withdrawn by forces estimated between 150 to 300 pN. The spaces between the peaks are averaged to be 7.3 nm which is the flexible link between protomers and corresponds to the thickness of the HPI layer. Note that in the first image before the tip contacted the surface all the pores are present in the image. (C) All the protomers were withdrawn by the cantilever tip from the vacated area.

Other experiments of this kind done with structural proteins having multiple domains, such as titin and elastin, show the same sort of saw tooth curve attributed to the force required to rupture individual domains in the protein.

tip. In a typical experiment the protein was adsorbed to a crystalline gold surface. The cantilever tip was then brought into contact with the surface with a force of a few nN and allowed to remain in contact for a period of 2-4 seconds. If a protein was contacted, a saw-tooth extension curve similar to that shown in Fig. 5-3b would be seen when the tip was withdrawn. To insure that what was observed was single molecule event, this experiment was done with a surface coverage of protein so sparse that 1 out of 20 approaches and retractions of the cantilever tip resulted in an interaction. Using titin as an example of this type of experiment, maximum force peaks have been found to vary between 150 to 300 pN with a periodicity between peaks of 25 to 28 nm. The expected length increase to unravel a single domain in titin was determined to be 31 nm [Rief 1997].

Genetically engineered proteins have been constructed with repeat domains that can be identified by force distance curves. Single molecule force studies have been extended to polysaccharides, alcohols, and DNA. Modifications have been made to the AFM to allow for either increasing force at a constant rate or maintaining a constant force in the retraction cycle. In addition, cantilevers have been constructed that allow fast force spectroscopy. This may facilitate studies where rate is important, such as in folding and unfolding experiments [Oberhauser 2001]. For those who are interested, a more detailed review of this material is referenced [Allison 2002].

Molecular recognition force microscopy

This application is similar to the earlier description of measurement of forces between molecules. Here, however, a probe immobilized on the cantilever tip was scanned over a surface and reacted with a target molecule on the surface. The original experiment was done with an antibody to lysozyme tethered to the cantilever tip and then scanned over immobilized lysozyme on a mica surface. The experiment was done in a liquid environment. When there was interaction with lysozyme, the image was distorted. If lysozyme was added to the solution, it bound to the antibody on the tip, and the image became clear [Raab 1999].

This work was extended so that a clear topographic image of the surface could be simultaneously recorded with a recognition image of the surface. Oscillating the AFM tip at its resonant frequency produces a sine wave. The topographic image was obtained by intermittent contact imagining as described in chapter 1 of this thesis; it was recorded from the bottom of the sine wave oscillation amplitude and produced height input for the image. The recognition image was produced by the tip reacting with the surface and affected the top of the sine wave oscillation amplitude. By splitting these two signals from the oscillating sine wave, simultaneous images of both topography and recognition can be recorded. Simultaneous single molecule topographic imaging with force recognition was first reported using antibody to lysozyme tethered to the cantilever to image lysozyme on the surface [Stroh 2004].

Often AFM applications are considered important enough by manufacturers that they acquire patent rights and incorporate the application into new instruments. For instance, Molecular Imaging, now part of Agilent Technologies, markets this capability with their microscope as PicoTrec. We have this application, and in Fig. 5-4 a simultaneously recorded topographic image of streptavidin-gold on the surface is shown with a recognition image caused by biotin tethered to the tip reacting with streptavidin on the surface. By attaching antibodies to specific membrane proteins to the AFM tip, we plan on using this methodology to study membrane transport proteins in bacteria.

Instrumentation Development

The research I have addressed to this point can be accomplished with equipment and techniques that are available today. The development of new SPM instrumentation can be expensive, and instruments may encounter limited marketability. For these reasons many innovative SPM instruments and new applications remain in the laboratories that have developed them.

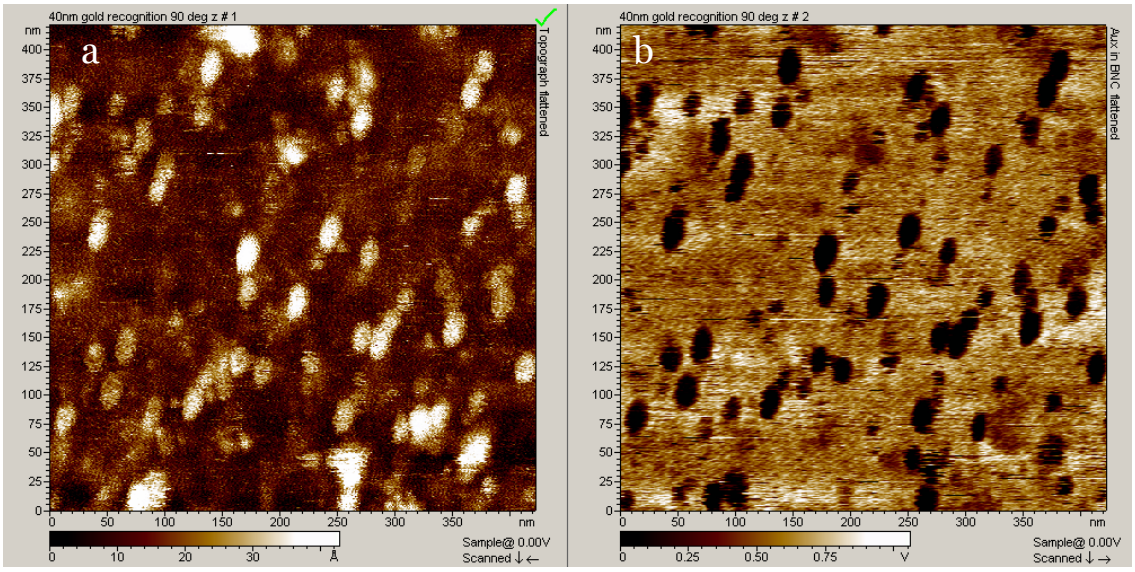

Figure 5-4. Molecular recognition force microscopy. Imaging in noncontact mode where the surface is sensed by dampening of the oscillation amplitude of the cantilever simultaneous topographic and force recognition images are made possible. This is accomplished by splitting the sine wave of the oscillating cantilever where the bottom of the wave that is dampened as the tip nears the surface is used to create the topographic image. If the tip interacts with the surface so that it has an interaction event this affects the top half of the sine wave and results in a recognition image.

In the In Fig. 5-4a the dampening of the bottom half of the since wave is used to identify proximity to the surface and generate a topographic image of streptavidin-labeled gold immobilized on a mica surface. In Fig.5-4b the top half of the oscillation amplitude sine wave is perturbed, in this instance by biotin tethered to the cantilever interacting with the streptavidin-labeled gold immobilized on a mica surface, resulting in a recognition image. This technique can be used to investigate how probes attached to the cantilever interact with specific target sites on cell surfaces.

Scanning electrochemical microscope

The scanning electrochemical microscope (SECM) developed by Bard's laboratory is a chemical microscope that is based on mass transfer and chemical reactions occurring at the sample surface and the scanning tip. A conducting tip serves as one of the electrodes in an electrochemical cell, which contains an electroactive species, a reference electrode, and an auxiliary electrode. The sample can but does not have to be one of the electrodes. The examination of a biological sample involves positioning it beneath the tip; scanning the tip over the surface allows for the detection of electro-active species on the surface. Bard's laboratory was the first to use this method to identify enzymatic activity in mitochondria at the micron level of resolution [Bard 1991].

This technology has been improved by the Mizaikoff laboratory by combining SECM with AFM. Placing an electrode above the contact point on the AFM tip allows for the simultaneous imaging and identification of electro-active species on surfaces. In this configuration the electrode is always the same distance from the surface; lateral resolution of the SECM is improved by the size of the electrode and degree to which the electrode can be placed proximal to the surface. Using this configuration, electroactive byproducts of enzymatic reactions can be recorded simultaneously with topographic images. In one experiment patches of horseradish peroxidase immobilized on gold surfaces were imaged by contact mode AFM in a solution containing ferroceniummethyl hydroxide. When H_2O_2 was added to the solution, simultaneous topographic and electrochemical images of horseradish peroxidase were recorded [Kranz 2004].

Scanning ion conductance microscope

A new adaptation of scanning probe microscopy called, scanning ion-conductance microscopy (SICM) was first demonstrated by Paul Hansma's laboratory. This new technique used a micropipette that had been pulled from capillary tubing so that only a small aperture (0.05 to 0.1 μm) existed at the tip. Both the pipette, mounted on a piezoelectric scanner configured to move in the

X,Y,Z directions, and a wet cell containing the sample had electrodes installed and were filled with 0.1 M NaCl. By applying a dc voltage to the electrode in the wet cell a dc current was established between the two electrodes. As the tip approaches and nears contact with the surface ion flow through the tip is partially blocked and there is a decrease in current flow. This decrease in current flow serves as the input for sensing near contact with the surface. By maintaining a constant current by applying voltages to the *Z* piazo through a feedback mechanism to raise or lower the tip as the tip is scanned over the surface and using this voltage as the height input, a topographic image of the surface of a was generated.

An alternative application of this technique was to scan the tip over a surface at a constant height and measure differences in ion currents coming off the surface. This was done using a tip with an inside diameter 50 to 100 nm and allowed for the identification of the 0.8 μm pores in a Nuclepore membrane. However, it was proposed that by using a tip with a smaller inside diameter would allow for the resolution of smaller ion channels [Hansma 1989]. This configuration was later improved by using pulled quartz instead of borosilicate glass tubing allowing the tip apertures of less than 50 nm thus improving resolution.

Instead of using ion conductance as the feedback mechanism the instrument was operated as an atomic force microscope in tapping mode where the oscillation of the quartz pipette was found to vary between 50 and 100 kHz. In this configuration the instrument was operaterated as a combination of AFM for imaging and SICM for sensing ion current [Proksch 1996]. Further improvement in the application of SICM has allowed for lower forces to be exerted on the specimen during imaging. We have already discussed how imaging with the AFM either in contact or intermittent contact mode does in fact exert significant force on the sample. The Korchev group has determined that when SICM is operated with maximum sensitivity, where the position of the probe is very close to the surface and strongly influences ion current, the tip is so close that the sides of the

tip will exert excessive force on neighboring structures on the sample. By developing a scanning algorithm where the setpoint is adjusted so that the tip distance from the surface is greater than the tip radius the tip does not contact the surface and minimal forces are exerted on the sample. This was demonstrated on living colon cancer cells where the imaging force was minimal and structures not normally seen by conventional AFM such as microvilli were readily imaged [Korchev 1997].

Fast scanning AFM

One of the obvious limitations of conventional AFM is the scan speed. Image acquisition time may range in length from roughly 30 seconds to as much as several minutes depending on the sample. There has been progress in this area that should eventually translate into new instrumentation. Ando's laboratory in Japan redesigned an AFM with the criterion that any component not capable of performing at high speed should be upgraded. They redesigned the scanning mechanism to be free of resonant vibrations up to 60 kHz, and used small cantilevers with high resonant frequencies in liquid (450-650 Khz) and with small spring constants (150-280 pN/nm). They also improved the deflection detection system by using an objective lens instead of mirrors to focus the laser beam on the very small cantilevers. Much of the electronics of the AFM, including movement of the Z-piezo, was redesigned for rapid scanning. The mounting stage was reconfigured to prevent feedback vibration. In the end they produced an AFM capable of 100 x 100 pixel sequential images of myosin movement on mica at 80 ms for each image [Ando, 2001,]. Others in this field are working on modifications that may lead to a marketable high-speed AFM.

Over the years the SPM has developed into a unique imaging tool for biological applications. This is primarily due to the fact that samples can be imaged in their native environment and since sample preparation does not require fixiation or staining viable samples can be imaged. However, SPM's are more that imaging tools as different modalities for sensing surfaces have been

developed. Nanometer scale control of the AFM tip has allowed construction at the nanoscale. Sensitivity of the AFM cantilever to forces as small as those required to rupture a single hydrogen bond have been demonstrated and force measurements on single molecules have been realized. The desire to image dynamic biological processes has initiated research to develop fast-scanning instrumentation. This technology is moving forward at a rapid pace, perhaps we are still in the formative years, and the future is still filled with some wonderful suprises.

References

Allen MJ, Balooch M, Subbiah S, Tench RJ, Siekhaus W, Balhorn R. Scanning tunneling microscope images of adenine and thymine at atomic resolution. *Scanning microsc.* 1991; 5: 625-630.

Allen MJ, Hud NV, Balooch M, Tench RJ, Siekhaus WJ, Balhorn R. Tip-radius-induced artifacts in AFM images of protamine-complexed DNA fibers. *Ultramicroscopy* 1992; 42-44: 1095-1100.

Allison DP, Thompson JR, Jacobson KB, Warmack RJ, Ferrell TL. Scanning tunneling microscopy and spectroscopy of plasmid DNA *Scanning Microsc.* 1990; 4: 517-522.

Allison DP, Warmack RJ, Bottomley LA, Thundat T, Brown GW, Woychick RP, Schrick JJ, Jacobson KB, Ferrell TL. Scanning tunneling microscopy of DNA: A novel technique using radiolabeled DNA to evaluate chemically mediated attachment of DNA to surfaces. *Ultramicroscopy* 1992_a; 42-44: 1088-1094.

Allison DP, Bottomley LA, Thundat T, Brown GM, Woychik RP, Schrick JJ, Jacobson KB, Warmack RJ. Immobilization of DNA for scanning probe microscopy. *Proc. Natl. Acad. Sci.* 1992_b; 89: 10129-10133.

Allison DP, Thundat T, Jacobson KB, Bottomley LA, Warmack RJ. Imaging entire genetically functional DNA molecules with the scanning tunneling microscope. *J.Vac. Sci. Technol.* A 1993; 11: 816-819.

Allison DP, Kerper PS, Doktycz MJ, Spain JA, Modrich P, Larimer FW, Thundat T, Warmack RJ. Direct atomic force microscope imaging of *Eco*RI endonuclease site specifically bound to plasmid DNA Molecules. *Proc. Natl. Acad. Sci.* 1996; 93: 8826-8829.

Allison DP, Kerper PS, Doktycz MJ, Thundat T, Modrich P, Larimer FW, Johnson DK, Hoyt PR, Mucenski ML, Warmack RJ. Mapping individual cosmid DNAs by direct AFM imaging. *Genomics* 1997; 41: 379-384.

Allison DP, Hinterdorfer P, Han W. Biomolecular force measurements and the atomic force microscope. *Current Opinion Biotech.* 2002; 13: 47-51.

Amerin M, Stasiak A Gross H, Stoll E, Traviglini G. Scanning tunneling microscopy of recA-DNA complexes coated with a conducting film. *Science* 1988; 240: 514-516.

Ando T. Kodera N, Takai E, Maruyama D, Saito K, Toda A. A high-speed atomic force microscope for studying biological macromolecules. *Proc. Natl. Acad. Sci.* 2001; 98: 12468-12472.

Arscott PG, Lee G, Bloomfield VA, Evans DF. Scanning tunneling microscopy of Z-DNA. *Nature* 1989; 339: 484-486.

Bain CD, Troughton EB, Tao YT, Evall J, Whitesides GM, Nuzzo RG. Formation of monolayer films by the spontaneous assembly of organic thiols from solution onto gold. *J. Am. Chem. Soc.* 1989_a; 111: 321-335.

Bard AJ, Fan FF, Pierce DT, Unwin PR, Wipe DO, Zhou F, Chemical imaging of surfaces with the scanning electrochemical microscope. *Science* 1991; 254: 68-74.

Baro AM, Miranda R, Alaman J, Garcia N, Binnig G, Rohrer H, Gerber Ch, Carrascosa JL. Determination of surface topographu of biological specimens at high resolution by STM. *Nature* 1985; 315: 253-254.

Becker RS, Golovchenko JA, Hamann DR, Swartzentruber BS. Real-space observation of surface states on Si (111) 7X7 with the tunneling microscope. *Phys. Rev. Lett.* 1985a; 55: 2032-2034.

Becker RS, Golovchenko JA, Swartzentruber BS. Electron interferometry at crystal surfaces. *Phys. Rev. Lett.* 1985b; 55: 987-990.

Beebe TP, Wilson TE, Ogletree DF, Katz JE, Balhorn R, Salmeron MB, Siekhause. Direct observation of native DNA structures with the scanning tunneling microscope. *Science* 1989; 243: 370-372.

Bendixen C, Besenbacher F, Laegsgaard E, Stensgaard I, Thomsen B, Westergaard O. Deoxyribonucleic-acid structures visualized by scanning tunneling microscopy. *J. Vac. Sci. Technol.* 1990; 8: 703-705.

Bezanilla M. Drake B, Nudler E, Kashlev M, Hansma PK, Hansma HG, Motion and enzymatic degradation of DNA in the atomic force microscope. *Biophys. J.* 1994; 67: 2454-2459.

Bibel DJ, Lawson JW. Scanning electron microscopy of L-phase streptococci. I. Development of thechique. *J. Microscopy* 1972; 95: 453-458.

Binnig G, Rohrer H. Scanning tunneling microscopy. *Helva Physica Acata* 1982; 55(6): 726-735.

Binnig G, Rohrer H, Gerber Ch, Weibel E. 7X7 reconstruction on Si 111 resolved in real space. *Phys. Rev. Lett.* 1983; 50: 120-123.

Binnig G, Rohrer H. *Trends in Physics* edited by J. Janta and J. Pantoflicek (European Physical Society, The Hague, 1984). P. 38.

Binnig G, Quate CF, Gerber C. Atomic force microscope. *Phys. Rev. Lett.* 1986_a; 56: 930-933.

Binnig G, Rohrer H. Scannning tunneling microscopy. *IBM j. Res. Dev*. 1986_b; 30: 355-369.

Boland T, Ratner BD. Direct measurement of hydrogen-bonding in DNA nucleotide bases by atomic force microwcopy. *Proc. Natl. Acad. Sci.* 1995; 92: 5297-5301.

Bonnell, D. *Scanning Probe Microscopy and Spectroscopy: Theory, Techniques, and Applications* 2nd Edition. (John Wiley & Sons Inc. New York, 2000).

Bottomley LA, Haseltine JN, Allison DP, Warmack RJ, Thundat T, Sachleben RA, Brown GM, Woychik RP, Jacobson KB, Ferrell TL. Scanning tunneling microscopy of DNA: the chemical modification of gold surfaces for immobilization of DNA. *J. Vac. Sci. Technol.* A 1992; 10: 591-595.

Brown GM, Allison DP, Warmack RJ, Jacobson KB, Larimer FW, Woychik RP, Carrier WL. Electrochemically induced adsorption of radiolabeled DNA on gold and HOPG substrates for STM investigations. *Ultramicroscopy* 1991; 38(3-4): 253-264.

Bustamante C, Rivetti C. Visualizing Protein-nucleic Acid Interactions on a Large Scale with the Scanning Force Microscope. *Annu. Rev. Bioph. Biom*. 1996; 25: 395-429.

Bustamante C, Vesenka J, Tang CL, Rees W, Guthold M, Keller R. Circular DNA molecules imaged in air by scanning force microscopy. *Biochemistry* 1992; 31: 22-26.

Butt HJ, Jaschke M. Calculation of Thermal Noise in Atomic-Force Microscopy. *Nanotechnology* 1995; 6: 1-7.

Coombs JH, Pethica JB. Properties of vacuum tunneling currents: anomalous barrier heights. *IBM J. Res. Develop.* 1986; 30: 455-459.

Cricenti A Selci S, Felici AC, Generosi R, Gori E, Djaczenko W, Charotti G. Molecular structure of DNA by scanning tunneling microscopy. *Science* 1989; 245: 1226-1227.

Cricenti A, Selci S, Chiarotti G, Amaldi F. Imaging of single-stranded-DNA with the scanning tunneling microscope. *J. Vac. Sci. Technol. B* 1991; 9: 1285-1288.

de Lozanne AL, Elrod SA, Quate CF. Spatial variations in the superconductivity of Nb_3Sn measured by low-temperature tunneling microscopy. *Phys. Rev. Lett.* 1985; 54: 2433-2436.

DeRose JA, Thundat T, Nagahara LA, Lindsay SM. Gold grown epitaxially on mica- conditions for larg area flat faces. *Surf. Sci.* 1991; 256: 102-108

Driscoll RJ, Youngquist MG, Baldeschwieler JD. Atomic-scale imaging of DNA using scanning tunneling microscopy. *Nature* 1990; 346: 294-296.

Dunlap DD, Bustamante C. Images of single-stranded nucleic-acids by scanning tunneling microscopy. *Nature* 1989; 342: 204-206.

Durig U, Gimzewski JK, Pohl DW. Experimental observations of forces acting during scanning tunneling microscopy. *Phys. Rev. Lett.* 1986; 57: 2403-2406.

Edstrom RD, Meinke MH, Yang XR, Yang R, Evans DF. Direct observation of phosphorylase-kinase and phosphorylase-B by scanning tunneling microscopy. *Biochemistry* 1989; 28: 4939-4942

Edstrom RD, Meinke MH, Yang XR, Yang R, Evans DF. Scanning tunneling microscopy of the enzymes of muscle glycogenolysis. *Ultramicroscopy* 1990; 33: 99-106.

Erie DA, Yang G, Schultz HC, Bustamante C. DNS bending by Cro protein in specific and nonspecific complexes: implications for protein site recognition and specificity. *Science* 1994; 266: 1562-1566.

Gooding GV, Herbert TT. A simple technique for purification of TMV in large quantities. *Phytopathology* 1967; 57: 1285.

Green PJ, Gupta M, Boyer HW, Brown WE, Rosenberg JM. Sequence-analysis of the DNA encoding the *Eco*RI endonuclease and methylase. *J. Biol. Chem.* 1981; 256: 2143-2153.

Gukenberger R, Heim M, Cevc G, Knapp HF, Wiegrabe W, Hildebrand A. Scanning tunneling microscopy of insulators and biological specimens based on lateral conductivity of ultrathin water films. *Science* 1994; 266: 1538-1530.

Hallett P, Offer G, Miles MJ, Atomic Force Microscopy of the Myosin Molecule. *Biophys. J.* 1995; 68: 1604-1606.

Han T, Williams JM, Beebe TP. Chemical-bonds studied with functionalized atomic force microscopy tips. *Anal. Chim. Acta* 1995; 307: 365-376.

Han W, Lindsay SM, Jing T, A magnetically driven oscillating probe microscope for operation in liquids. *Appl. Phys. Lett.* 1996; 69: 4111-4113.

Hansma HG, Vesenka J, Siegerist C, Kelderman G, Morrett H, Sinsheimer RL, Elings V, Bustamante C, Hansma PK. Reproducible Imaging and Dissection of Plasmid DNA Under Liquid with Atomic Force Microscope. *Science* 1992; 256: 1180-1184.

Hansma HG, Benzanilla M, Zenhausren F, Adrian M, Sinsheimer RL. Atomic force microscopy of DNA in aqueous solutions. *Nucleic Acids Res.* 1993; 21: 505-512.

Hansma HG, Kim KJ, Laney DE, Garcia RA, Argaman M, Allen MJ, Parsons SM. Properties of Biomolecules Measured From Atomic Force Microscope Images: A Review. *J. Struct. Biol.* 1997; 119: 99-108.

Hansma PK, Tersoff J, Scanning tunneling microscopy. *J. Appl. Phys.* 1987; 61: R-1-R23.

Hansma PK, Drake B, Marti O, Gould SAC, Prater CB, The scanning ion-conductance microscope. *Science* 1989; 243: 641-643.

Hansma PK, Cleveland JP, Radmacher M, Walters DA, Hillner PE, Bezanilla M, Fritz M, Vie D, Hansma HG, Prater CB, Massie J, Fukunaga L, Gurley J, Elings V, Tapping mode atomic force microscopy in liquids. *Appl. Phys. Lett.* 1994; 64: 1738-1740.

Henderson E, Haydon PG, Sakaguchi DS. Actin Filament Dynamics in Living Glial Cells Imaged by Atomic Force Microscopy. *Science* 1992; 257: 1944-1946.

Hoh JH, Cleveland JP, Prater CB, Revel J-P, Hansma PK. Quantized adhesion detected with the atomic force microscope. *J. Am. Chem. Soc.* 1992; 114: 4917-4918.

Keller D, Bustamante C, Keller RW. Imaging of single uncoated DNA-molecules by scanning tunneling microscopy *Proc. Natl. Acad. Sci.* 1989; 86: 5356-5360.

Klug A, Caspar DLD. *Advances in Virus Research* Edited by K. M. Smith and M. A. Lauffer (Academic Press, New York 1960) Vol. 7.

Kranz C, Kueng A, Lugstein A, Bertagnolli E, Mizaikoff B. Mapping of enzyme activity by detection of enzymatic products during AFM imaging with integrated SECM-AFM probes. *Ultramicroscopy* 2004; 100: 127-134.

Korchev YE, Bashford LC, Milovanovic M, Vodyanoy I, Lab MJ. Scanning ion conductance microscopy of living cells. *Biophys J.* 1997; 73: 653-658.

Lanz M, O'Shea SJ, Welland ME, Force microscopy imaging in liquids using ac techniques. *Appl. Phys. Lett.* 1994; 65: 409-411.

Lee GU, Arscott PG, Bloomfield VA, Evans DF. Scanning tunneling microscopy of nucleic acids. *Science* 1989; 244: 475-477.

Lee GU, Chrisey LS, Colton RJ. Direct measurement of the forces between complementary strands of DNA. *Science* 1994; 266: 771-773

Lindsay SM, Barris B. Imaging deoxyribose nucleic-acid molecules on a metal-surface under water by scanning tunneling microscopy *J. Vac. Sci. Technol.* 1988_a; 6: 544-547.

Lindsay SM, Thundat T, Nagahara L. Adsorbate deformation as a contrast mechanism in STM images of biopolymers in an aqueous environment: images of the unstained, hydrated DNA double helix. *J. Microsc.* 1988$_b$; 152: 213-220.

Lindsay SM, Thundat T, Nagahara L, Knipping U, Rill RL. Images of the DNA double helix in water *Science* 1989; 244: 1063-1064.

Lyubchenko YL, Lindsay SM, DeRose JA, Thundat T. A technique for stable adhesion of DNA to a modified graphite surface for imaging by scanning tunneling microscopy. *J. Vac. Sci. Technol B.* 1991; 9: 1288-1290.

Lyubchenko YL, Gall AA, Shlyakhtenko LS, Harrington RE, Jacobs BL, Oden PI, Lindsay SM. Atomic force microscopy imaging of double stranded DNA and RNA. *Biomol. Struct. Dyn.* 1992; 10: 589-606.

Mantovani JG, Allison DP, Warmack RJ, Ferrell TL, Ford JR, Manos RE, Thompson JR, Reddick BB, Jacobson KB. Scanning tunneling microscopy of tobacco mosaic virus on evaporated and sputter-coated palladium/gold substrates. *J. Microsc.* 1990; 158: 109-116.

Martin Y, Wickramasinghe HK. Magnetic imaging by force microscopy with 1000-A resolution. *Appl. Phys. Lett.* 1987; 50: 1455-1457.

McLarin JA, Frederick CA, Wang BC, Green P, Boyer HW, Grable J, Rosenberg JM. Structure of the DNA-*Eco*RI endonuclease recognition complex at 3 A resolution. *Science* 1986; 234: 1526-1541.

McMaster TJ, Carr H, Miles MJ, Cairns P, Morris VJ. Polypetide structures imaged by the scanning tunneling microscope. *J. Vac. Sci. Tech.* A 1990$_a$; 8: 648-651.

McMaster TJ, Carr H, Miles MJ, Cairns P, Morris VJ. Adsorption of liquid-crystals imaged using scanning tunneling microscopy. *J. Vac. Sci. Tech.* A 1990b; 8: 672-674.

Müller DJ, Baumeister W, Engel A. Controlled unzipping of a bacterial surface layer with atomic force microscopy. *Proc. Natl. Acad. Sci.* 1999; 96: 13170-13174.

Murray RW. *Electroanalytical Chemistry* Edited by A. J. Bard (Decker, New York, 1984) , Vol. 13.

Newman AK, Rubin RA, Kim SH, Modrich P. DNA-sequences of structural genes for EcoRI DNA restriction and modification enzymes. J. *Biol. Chem*. 1981; 256: 2131-2139.

Niu L, Shaiu WL, Vesenka J, Larson DD, Henderson E. Atomic force microscopy of DNA-collodial gold and DNA-protein compleses. *SPIE proc.* 1993; 1891: 71-77.

Oberhauser AF, Hansma PK, Carrion-Vazquez M, Fernandez JM. Stepwise unfolding of titin under force-clamp atomic force microscopy. *Proc. Natl. Acad. Sci.* 2001; 98: 468-472.

Piner RD, Zhu J, Xu F, Hong S, Mirkin CA. “Dip-Pen” Nanolithography. *Science* 1999; 283: 661-663.

Pohl DW, Fischer UC, Durig UT. Scanning near-field optical microscopy (SNOM). *J. Microsc.* 1988; 152(3): 853-861.

Proksch R, Lal R, Hansma PK, Morse D, Stucky G Imaging the internal and external pore structure of Membranes in fluid: Tapping mode scanning ion conductance microscopy. *Biophys J*. 1996; 71: 2155-2157.

Quist AP, Bjorck LP, Reimann CT, Oscarsson SO, Sundquist BUR. A Scanning Force Microscopy Study of Human Serum Albumin and Porcine Pancreas Trypsin Adsorption on Mica Surfaces. *Surface Sci*. 1995; 325: 406-412.

Rabb A, Han W, Badt B, Smith-Gill SJ, Lindsay SM, Schindler H, Hinterdorfer P. Antibody recognition imaging by force microscopy. *Nat. Biotechnol.* 1999; 17: 901-905.

Radmacher M, Tillmann RW, Fritz M, Gaub HE. From Molecules to Cells: Imaging Soft Samples with Atomic Force Microscope. *Science* 1992; 257: 1900-1905.

Radmacher M, Fritz M, Cleveland JP, Walters DR, Hansma PK. Imaging Adhesion Forces and Elasticity of Lysozume Adsorbed on Mica with the Atomic Force Microscope. *Langmuir* 1994; 10: 3809-3814.

Reddick BB. Isolation and partial characterization of tobacco mosaic virus from flowering dogwood in Tennessee. *Plant Disease* 1989; 73: 174-176.

Rief M, Gautel M, Osterhelt F Fernandez JM, Gaub HE. Reversible unfolding of individual titin immunoglobulin domains by AFM. *Science* 1997; 276: 1109-1112.

Sambrook J, Fritsch EF, Maniatis T. *Molecular Cloning*, 2 nd ed. (Cold Spring Harbor Press, Cold Spring Harbor, NY, 1989).

Sanger F, Coulson AR, Hong GF, Hill DF, Petersen GB. Nucleotide sequence of bacteriophage lambda DNA. *J. Mol. Biol.* 1982; 162: 729-773.

Sonnenfeld R, Hansma PK. Atomic-resolution microscopy in water. *Science* 1986; 232: 211-213.

Stroh CM, Ebner A, Geretschläger Freudenthaler G, Kienberger F, Kamruzzahan AMS, Smith-Gill SJ, Gruber HJ, Hinterdorfer P. Simultaneous topography and recognition imaging using force microscopy. *Biophys. J.* 2004; 87: 1981-1990.

Terry BJ, Jack WE, Modrich P, Facilitated diffusion during catalysis by *Eco*RI endonuclease. *J. Biol. Chem*. 1985; 260: 13130-13137.

Thomas M, Davis RW. Studies on the cleavage of bacteriophage lambda DNA with *Eco*RI restriction endonuclease. *J. Mol. Biol.* 1975; 91: 315-328.

Thundat T Allison DP, Warmack RJ, Ferrell TL. Imaging isolated strands of DNA molecules by atomic force microscopy. *Ultramicroscopy* 1992_a; 42-44: 1101-1106.

Thundat T, Warmack RJ, Allison DP, Bottomley LA, Lourenco AJ, Ferrell TL. Atomic force microscopy of deoxyribonucleic acid strands adsorbed on mica: the effect of humidity on apparent width and image contrast. *J. Vac. Sci. Technol.* A 1992_b; 10: 630-635.

Thundat T, Zeng XZ, Sharp SL, Allison DP, Warmack RJ. Callibration of atomic force microscope tips using biomolecules. *Scanning Microsc.* 1992_c; 6: 903-910.

Thundat T, Allison DP, Warmack Doktycz MJ, Jacobsen KB, Brown GM. Atomic force microscopy of single-stranded and double-stranded deoxyribonucleic acid *J. Vac. Sci. Technol.* A 1993; 11: 824-828.

Thundat T, Warmack RJ, Allison DP, Jacobson KB. Critical point mounting of kinetoplast DNA for atomic force microscopy. *Scanning Microsc.* 1994; 8: 23-30.

Travaglini G, Rohrer H, Amrein M. Gross H. Scanning tunneling microscopy on biological matter. *Surf. Sci.* 1987; 181: 380-390.

Traviglini G, Rohrer H, Stoll E, Amrein M, Stasiak A, Sogo j, Gross H. Scanning tunneling microscoy of recA-DNA complexes. *Physica Scripta* 1988; 38: 309-313.

Vesenka J, Guthold M, Tang CL, Keller D, Delaine E, Bustamante C. Substrate preparation for reliable imaging of DNA molecules with the scanning force microscope. *Ultramicroscopy* 1992; 42-44: 1243-1249.

Vogelstein B, Gillespie D. Preparative and analytical purification of DNA from agarose. *Proc. Natl. Acad. Sci.* 1979; 76: 615-619.

Wadu-Mesthrige K, Xu S, Amro NA, Liu GY, Fabrication and imaging of nanometer-sized protein patterns. *Langmuir* 1999; 15: 8580-8583.

Warmack RJ, Ferrell TL, Becker RS. Scanning tunneling microscopy of silver and gold islands on silicon. *Physica Scripta* 1988; 38: 159-161.

Watanabe Y, Sakurai T. *Advances in Scanning Probe Microscopy*. (Springer-Verlag, New York, 2000).

Watson JD, Hopkins NH, Roberts JW, Steitz JA, Weiner AM. *Molecular Biology of the Gene* 4 th ed. (Benjamin/Cummings, Menlo Park, CA, 1987).

Williams CC, Slinkman J, Hough WP, Wickramasinghe HK. Lateral dopant profiling with 200 nm resolution by scanning capacitance microscopy. *Appl. Phys. Lett.* 1989; 55: 1662-1664.

Wright DJ, King K, Modrich P. The negative charge of Glu-111 is required to activate the cleavage center of *Eco*RI endonuclease. *J. Biol. Chem*. 1989; 264: 11816-11821.

Zenhauseren F, Adrian M, Ten Hieggeler-Bordier B, Eng LM, Descouts P. DNA and RNA polymerase-DNA complexes imaged by scanning force microscopy. *Scanning* 1991; 14: 212-217.

Vita

David Post Allison was born in Waterloo, New York, October 20, 1936. He graduated from Waterloo Central High School in 1954 in the same building where he started his primary education. After spending four years in the United States Navy he attended Michigan State University where he received his undergraduate degree in Zoology in 1963. After coming to Tennessee for a job in the Biology Division of Oak Ridge National Laboratory he started taking courses and was accepted into the Department of Microbiology at the University of Tennessee where he received his Masters degree in 1970. He is currently enrolled in the Department of Microbiology at the University of Tennessee.